An Electromagnetic Pneumo Capsule System for Conveying Minerals and Mine Wastes

Final Report

Henry Liu and Charles W. Lenau
Freight Pipeline Company
2601 Maguire Blvd.
Columbia, Missouri 65201

March 1, 2005

DOE Award No.: DE-FG26-03NT41928
Project Duration: 09/30/03 - 12/31/04

Project sponsored by the U. S. Department of Energy under program "Ground Breaking Innovative Technology Concepts for Mining"

DOE Program Solicitation No. DE-PS26-03NT15757-1

DISCLAIMER

KEYWORDS

Capsule, Capsule Design, Capsule Pipeline, Conveying, Electromagnetic Pump, Linear Induction Motor, Minerals Transport, Mine Waste, Pneumatic capsule Pipeline, Railroad, Trucks

ACKNOWLEDGMENT

This research project was sponsored by the National Energy Technology Laboratory (NETL), U.S. Department of Energy (DOE). The DOE Program officers overseeing this project are Joseph Renk and Mike H. Mosser. DOE support of this project is highly appreciated.

ABSTRACT

The purpose of this project is to investigate the technical and economic feasibility of using a new and advanced pneumatic capsule pipeline (PCP) system for transporting minerals and mine wastes. The new system is different from conventional PCPs in two main respects: (1) it uses linear induction motors (LIMs) instead of blowers (fans) at the inlet of the pipeline to drive (pump) the capsules and the air through the pipeline; and (2) the capsules in the PCP have steel wheels running on steel rails as opposed to capsules in conventional systems, which use wheels with rubber tires running inside a pipe without rail. The advantage of using LIM pump instead of blower is that the former is non-intrusive and hence does not block the passage of capsules, enabling the system to run continuously without having to make the capsules bypass the pump. This not only simplifies the system but also enables the system to achieve much larger cargo throughput than that of PCPs using blowers, and use of LIMs as booster pumps which enables the system to have any length or to be used for transporting cargoes over practically any distance, say even one thousand kilometers or miles. An advantage of using steel wheels rolling on steel rails instead of using rubber tires rolling inside a pipeline is that the rolling friction coefficient and hence the use of energy is greatly reduced from that of conventional PCP systems. Moreover, rails enable easy control of capsule motion, such as switching capsules to a branch line by using railroad switching equipment.

The advanced PCP system studied under this project uses rectangular conduits instead of circular pipe, having cross-sectional areas of 1 m by 1 m approximately. The system can be used for various transportation distances, and it can transport up to 50 million tonnes (metric tons) of cargo annually-- the throughput of the largest mines in the world. Both an aboveground and an underground system were investigated and compared.

The technical feasibility of this new PCP system was determined by designing the details of the system and conducting a detail analysis of the system – both steady and unsteady analyses. Through the detailed design and analyses, it was found that no technical problem or hurdle exist that would otherwise prevent commercial use of the system today. Still, since it is a new technology, it will be prudent and advantageous to run a demonstration project before this technology is used – see **6.2. Recommendation.**

The energy intensiveness (EI) of this new PCP technology is analyzed in detail in Sec.4, which found that the system uses less than one-tenth of the energy used by trucks and less than one-fourth of the energy used by trains, to transport the same cargoes over the same distance. Therefore, it is a highly energy efficient system. In addition, the system uses electricity rather than diesel fuel, thereby reducing the consumption of foreign oil. Being enclosed and underground, the system is also much safer and more secure than trucks and trains for transporting minerals, mine wastes, and even nuclear wastes. Finally, use of this new system will reduce the need of using trucks for transporting minerals and solid wastes, thereby reducing air pollution and global warming caused by trucks. The system is the most environmentally-friendly, safe and secure method for transporting minerals and mine wastes.

The cost of the PCP system was studied using a sophisticated engineering life cycle cost analysis taking into consideration of many factors including inflation, interest rate, property and income taxes, depreciation, and a 15% above-inflation return-on-investment (ROI). The Excel-based cost model allows the determination of the **unit cost,** which is the cost of transporting each ton of cargo (mineral or waste) over the distance or length of the PCP, and

the **unit-distant cost**, which is the cost of transporting each ton of cargo over unit distance (i.e., 1 km). These costs were presented as a function of transportation distance and throughput, both in tables and graphs. It is seen from the cost analysis that when the throughput is high (say, above 10 MTY)[1], both the unit cost and the unit-distance cost are lower than those can be done by using trucks in most places in the world, especially in remove areas or mountainous regions where highways are in poor condition or tortuous -- conditions that often exist in mining. In such situations, using the PCP instead of trucks can produce huge cost savings in addition to environmental benefits. For throughputs smaller than 10 MTY, the PCP system can still be made economical if a single tube (conduit) is used for both delivering the cargo and the returning the empty capsules, and if the system is run periodically, say only 8 hours a day.

The cost model developed in this study -- a generic model -- can also be used in real cases when the site specific information is known. In such a case, using the same cost model supplied with site-specific cost data, the model can produce accurate unit cost and unit-distance cost, which can be used for comparison with the transportation costs charged by truck or other competing modes.

Based on the promising findings of this project and the need to demonstrate this new technology before using it commercially, it is recommended that the U.S. Department of Energy considers conducting or sponsoring a demonstration project, with participation from the mining industry, so that this new technology can be used to benefit the industry and the public as soon as the demonstration project is completed.

[1] MTY stands for million tonnes (metric tons) of cargo per year.

Table of Content

1. INTRODUCTION

Pneumatic capsule pipeline (PCP) is the modern version of the century old technology of "tube transport" or "pneumatic tubes", for transporting cargoes [1-3]. While the old tube transport systems used small-bore pipes or tubes of less than 1 ft (300 mm) in diameter, and used capsules without wheels to contain and transport the cargo through the pipe or tube, the new PCP technology uses large diameter pipes or rectangular conduits and use large capsules with wheels rolling through pipes or conduits driven by air. Japan is the country where PCP has been used most successfully [4-6]. The Japanese used PCPs of approximately 1 m diameter pipe, and 1m x 1m cross-section of rectangular conduits. Each capsule carries 1 to 2 tonnes (metric tons) of cargo. Figure 1 shows the two types of PCPs used in Japan – circular and rectangular types. They were used successfully for mining, for transporting raw materials to modern steel plants and cement plants, for construction of tunnels and highways, and for solid waste disposal. Detailed discussions of the use of PCPs in Japan are given in [7].

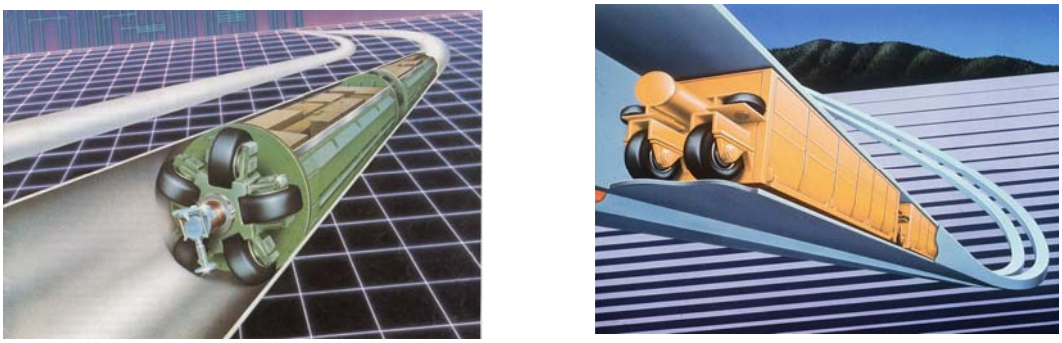

(a) Round (circular) PCP (b) Rectangular or square PCP

Figure 1. Pneumatic capsule pipeline (PCP) systems developed by and Used in Japan (Courtesy of Sumitomo Metal Industries, Ltd.)

Notwithstanding the success in using PCPs in Japan in recent years, the use of the technology has been limited throughout the world because the current system often could not compete with trucks and trains in terms of flexibility and low cost, and because most transportation providers do not know how to use or consider this new technology, in spite of the enormous environmental and safety benefits of using PCP instead of truck. For instance, PCP does not pollute air and does not cause traffic jam and accidents on highways as trucks do, etc. In the limited use of PCP in Japan, in each case a careful comparison of alternative transportation means were studied before PCP was selected, based not only on economics but also on environmental and safety considerations.

To enhance the attractiveness of PCP so that it will be used more widely, especially in the United States, the cost-effectiveness of PCP relative to other freight transport modes much be improved. This research seeks to improve the cost-effectiveness of PCP in two ways: (1) by using linear induction motor (LIM) instead of blowers (fans) to drive the system, and (2) using capsules with steel wheels that run on rails inside the PCP conduit.

LIM is the same technology used for the propulsion of magnetically-levitated high-speed trains, for accelerating and stopping roller coasters, and for many other existing commercial applications in which a large linear driving force is needed to propel vehicles or move objects. The advantage of using LIM instead of blowers to propel capsules through a conduit is that the LIM is a non-intrusive pump located at the inlet of the conduit. Capsules can move through the

LIM unhindered, deriving the driving force from the electromagnetic field of the LIM. With small clearance between the LIM and the capsules moving through it, the capsules not only accelerate but also behave as a piston pump, pushing the air through the entire length of the conduit, which propels the capsules in the entire length of the conduit. Thus the new system driven by LIM combines the advantage of LIM with the advantage of pneumatic conveying. For long-distance transport, LIMs also can be placed at intermediate stations along the long conduit, in the same way booster pumps work in ordinary long-distance oil and natural gas pipelines.

In any type of wheeled vehicles, there are two sources of drag force – the aerodynamic drag which increases with the speed of the vehicle, and the contact friction which is independent of speed but proportional to the rolling friction coefficient of the wheels. Thus, the smaller the rolling friction coefficient, the smaller the contact friction becomes, and hence the more energy efficient the vehicle becomes. The rolling friction coefficient of rubber-tired vehicles such as trucks is of the order of 0.01 (i.e., 1%). In contrast, for steel wheels rolling on steel rails, the coefficient is of the order of 0.002 or 0.2%, which is approximately five times smaller than that of trucks. For this reason, by using steel wheels instead of rubber tires for capsules, much energy can be saved, especially for vehicles that travel at low speed. The capsule speed used in this design, approximately 15 m/s, is regarded as low speed. At such speeds, much energy can be saved by using capsules fitted with steel wheels rolling on steel rails. This shows a main advantage of using rails for PCP. Another advantage of using rails is to offer good control of vehicles, in terms of the path of the vehicle and the ability to control the vehicle automatically, as for instance using standard rail switches for switching capsules to branches.

The new PCP system studied in this project combines the advantages of LIM with the advantages of rails, making it a super-performing and revolutionary advanced transportation system which is especially suitable for cargoes that do not require high speed, such as 20 m/s which is equivalent to 65.6 ft/s or approximately 45 mph. Such speed is more than adequate for transporting mineral or mine wastes.

The purpose of this project is to design and analyze such an advanced PCP-system for transporting large quantities of minerals and/or mine wastes. The system designed is of 1m x 1m rectangular cross-section. As will be shown later, such a system can transport up to 50 million tones of minerals per year, having enough capacity for the largest mines in the world. Small systems for small mines are not investigated here, for they may be difficult to compete with truck for low-cost transportation. Also, it is highly desirable that PCP systems be sufficiently large so that a worker can walk or crawl inside the conduit to inspect its interior whenever a need arises. This requires a minimum cross-section of 1m x 1m, approximately.

Section 1, Introduction, provides a general discussion of PCP and the related literature. Section 2, Rail-in-Tube System Design, provides the design of the rail, the tube, the capsules and the terminals (inlet-outlet stations). Section 3 is Analysis of System Operation. In Section 3.1, the steady-state analysis of the system is made. This involves the derivation and analysis of the fluid mechanic equations of the system, the derivation and analysis of the electromagnetic equations of the LIM in the system, the analysis of the system performance using both the fluid mechanic and electromagnetic equations, and the optimization of the system. Then, Section 3.2 presents the derivation and analysis of the unsteady (transient) equations governing the advanced PCP-LIM system.

Using the equations and analyses of Section 3, the energy efficiency of the system is assessed in Section 4. It can be seen that the advanced PCP system driven by LIM uses less than

one-tenth of the energy used by trucks and uses less than one-fourth of the energy used by trains, for transporting the same amount of cargoes over the same distance.

In Section 5 COST ANALYSIS, the capital cost, operation/maintenance cost, and the unit transportation costs (including both the ***unit cost*** and the ***unit distance cost***) are calculated. It shows that over a wide range of distances and throughputs, the unit transportation costs of the advanced PCP system are lower than that of trucks.

Details of the analyses and derivation of special equations can be found in the four appendices of this report.

2. RAIL-IN-TUBE SYSTEM DESIGN

2.1 Rail Design

Much of the information used in this study for designing the rails for PCP was derived from the book "Modern Railway Track," by C. Esveld [8].

(a) Size and gauge of rails

The size and gauge (i.e., spacing between rails) of the railroad in this study for application to PCP are smaller than the standard size and gauge for ordinary railroads.[1] Because the railroad track must fit inside a conduit of 1m x 1m cross section and because each capsule when fully loaded weighs only about 5 tons, the ASCE Standard 60-lb rail is used, which has a cross section as shown in Fig.2.1.1 [9]. The gage selected is 24 inches (0.610 m), which is the clearance between the flange heads of the two parallel rails as shown in the figure.

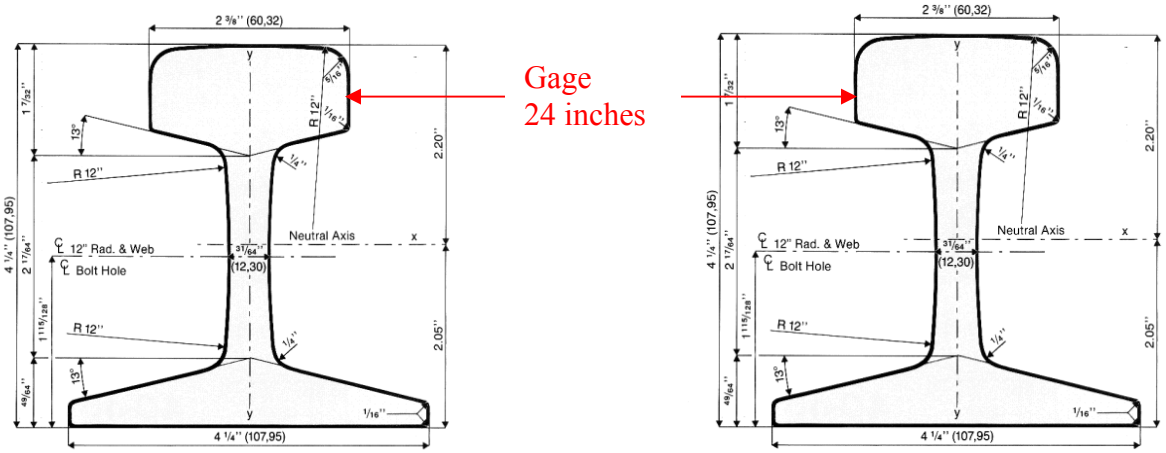

Figure 2.1.1 Standard ASCE 60-lb rail (gage=24 inches) [8]

(b) Rail curvature and slope

- **<u>Horizontal curvature:</u>**

Rails must have horizontal curves in order suit specific needs such as going around a hill or obstacles, or switching into a branch or another line. Careful design of each curvature is important in order to prevent possible derailment or damage to the track or wheels resulting from rail curvatures. Whenever a capsule or train moves around a curve, a centrifugal force F_c having a magnitude equal to mV^2/R_c is generated, where m is the mass of the capsule or train, V is the capsule speed, and R_c is the radius of curvature of the track centerline. The higher the speed V is, and/or the smaller the track radius R_c is, the larger becomes this force F_c. This centrifugal force, in the outward radial direction, generates both an overturning moment that can overturn the capsule, and an outward sliding force lateral (perpendicular) to the rails, which must be resisted by the rail and other components of the track. If the radius is sufficiently large for a given capsule of a given operational speed, the capsule can navigate the turn without reducing speed. For smaller radii, either a reduction in speed or superelevation of the track at the curves is required.

[1] The standard Amercian railroad gage, inherited from an old British standard, is 56.5 inches which is equivalent to 4 ft 8½ inches, or 1.435 m. Smaller gages are used for special railroads as in mining.

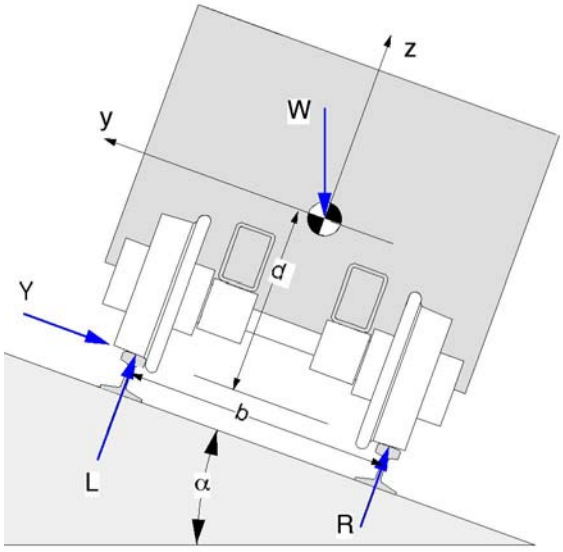

Figure 2.1.2 Superelevation around a railroad cure

A super-elevated track is shown in Figure 2.1.2. The center of the curve is to the right. To gradually change the superelevation angle, α, spirals are required at both ends of a curve. Track layout is complicated by superelevation of track because each track is at a different elevation adding additional dimensions to layout and maintain.

To determine the relationship between the superelevation angle α, the speed of the capsule V and the radius of the curve centerline, R_c, requires the determination of forces Y and L shown in Fig. 1. The force of the left rail on the left wheel flanges is Y, whereas the force of the left rail on the left wheel treads is L. Force Y is parallel and L is perpendicular to the surface of the inclined plane. Force R is perpendicular to the inclined plane and is equal to the force of the right rail on the right wheel. Force W is the weight of the capsule. Assuming that the capsule maintains a constant speed and both left wheel flanges maintain contact with the left rail, the centripetal acceleration of the center of mass will be horizontal and directed to the center of curvature. Summing forces in the horizontal and vertical directions separately yields:

$$\sum F_H = (L + R) \sin\alpha + Y \cos\alpha = m \frac{V^2}{r} \qquad (2.1.1)$$

$$\sum F_V = (L + R) \cos\alpha - Y \sin\alpha - W = 0 \qquad (2.1.2)$$

In Eq.2.1.1, **m** is the capsule mass, and **r** is the horizontal radius of curvature of the capsule mass. Coordinates **y** and **z** are designated in Fig.2.1.2. The x-coordinate is into the page, which is also the direction that the capsule is traveling. The origin of this coordinate system is located at the center of mass of the car. Summing up moments about the x-axis yields

$$\sum M_x = L \frac{b}{2} - R \frac{b}{2} - Y \frac{d}{2} = I_x \frac{d}{dt} (\omega_x) - (I_y - I_z) \omega_y \omega_z \qquad (2.1.3)$$

As shown in Fig.2.1.2, **b** is the lateral distance (span) between the two sets of wheels on the two sides of the track, and **d** is the distance from the center of mass of the capsule to the rail top. $\mathbf{I_x}$, $\mathbf{I_y}$ and $\mathbf{I_z}$ are the mass moments of inertia about the x, y and z axes. Terms $\boldsymbol{\omega_x}$, $\boldsymbol{\omega_y}$ and $\boldsymbol{\omega_z}$ are the three components of the angular velocity vector. For our problem the above equation reduces to

$$L\frac{b}{2} - R\frac{b}{2} - Y\frac{d}{2} = -(I_y - I_z)\left(\frac{V}{r}\right)^2 \sin\alpha\cos\alpha \qquad (2.1.4)$$

For our capsule, b and d are respectively 0.670 m and 0.482 m. The moments of inertia I_y and I_z are respectively 4,070 kg m^2 and 985 kg m^2. Note that one can select values of the angle α, the capsule speed V and the radius r, and then solve Eqs. 1, 2 and 4 simultaneously for forces L, R and Y.

A criterion to avoid derailing used by railroad industry is P/N < 1.2, where P is the force in the y direction and N is the force in the z direction of the rail on the wheel flange. This should be true for each individual wheel. Assuming the force Y to be carried by one of the two left wheels, and assuming the normal force on this wheel to be L/2, the criterion becomes Y/L < 0.6.

Based on this criterion, Fig. 2.1.3 was constructed. Values of V and α were selected. The radius r was calculated by trial until Y/L = 0.6.

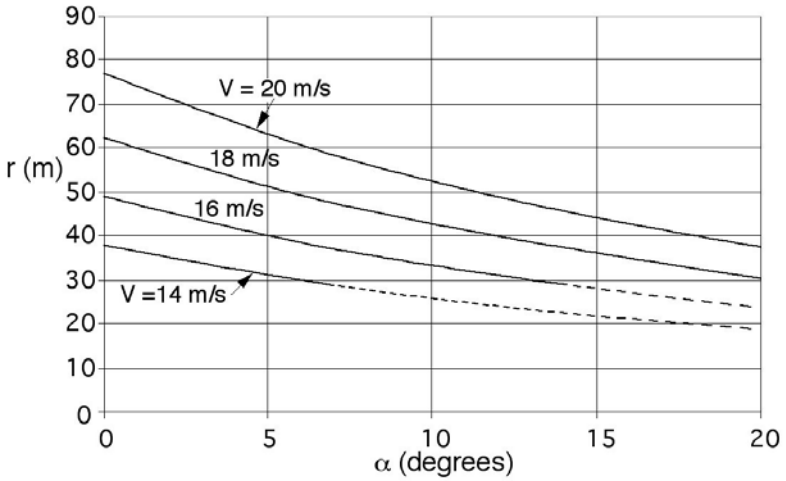

Figure 2.1.3 Determination of radius of curvature of rails in the PCP of this study

Figure 2.1.3 should be used with care. First and far most, the radius obtained is a minimum value. While larger values are satisfactory, small values may cause derailing. Secondly, the graph is based on Eqs. 2.1.1 through 2.1.4, along with the criteria Y/L = 0.6. It is possible that a radius obtained from the graph may be too small. The region that this happens is marked by dotted lines in Fig.2.1.3. For any set of wheels, rails, wheel gauge and rail gauge, there is a minimum curve radius independent of velocity. For the car described in this study this minimum curve radius is about 29 m. At this minimum radius, the flanges on the left and right wheels come in contact with the left and right rails. Thus, for any radius smaller than this minimum the wheels bind with the rail and derailing will occur when the capsule moves around the curve. To determine this minimum radius is difficult because it involves finding clearances between rail and wheel in three-dimensional space.

If small radius curves are necessary one should increase the track gauge around these curves. If the track gauge is increased too much however the wheel tread width must also be increased. Note that increasing the track gage may eliminate wheel binding but does not eliminate potential derailing due to car speed.

From Fig. 2.1.2, it can be seen that the relationship between the centerline radius, R_c, and r is given

$$R_c = r + (d + h)\sin\alpha \qquad (2.1.5)$$

where h is the rail height.

If a curve is to have no superelevation, then Fig. 2.1.3 can be replaced by the equation

$$r = 77.21\left(\frac{V}{20}\right)^2 \qquad (2.1.6)$$

in which V has units of m/s and r has units of m.

- **Vertical curvature:**

Because the centrifugal force due to vertical curvatures of any rail is in the vertical direction, it is resisted by gravity when there is a convex curvature, and resisted by the railbed when there is a concave curvature. At the kind of speed of capsules in PCP, approximately 20 m/s, it is seldom of concern. Therefore, under normal conditions the maximum vertical curvature, determined from the geometry and size of the wheels and the rails under static condition, should be adequate for the PCP rails.

- **Slope:**

Ordinary railroad slopes are limited to approximately 3^o so that locomotives can generate sufficient traction to pull the whole train of many cars up a sustained slope. However, the traction of PCP capsules is generated by the aerodynamic thrust of the air on each capsule traveling in the PCP. Because this thrust exists on every capsule in the PCP, the system can tolerate a much larger slope than that of ordinary railroads. By balancing the thrust with the wheel resistance and the gravitational force component along the slope, under steady-state motion we have the following:

$$\frac{C_D A\rho(V - V_c)^2}{2} = \mu W\cos\alpha + W\sin\alpha \qquad (2.1.7)$$

As will be shown later, for the 1m x 1m PCP system studied here, A= 1 m^2, ρ = 1.2 kg/m^3, μ = 0.002, and W = 4,971 kg = 48,766 N. Assuming that an air speed of V = 25 m/s is used to establish a capsule velocity of 20 m/s, from a calculation procedure to be discussed later, it can be shown that the capsule drag coefficient for this case is C_D = 292. Therefore, Eq.2.1.7 becomes

$$0.002\cos\alpha + \sin\alpha = 0.0891 \qquad (2.1.8)$$

Solving the above equation yields $\alpha = 5^o$ approximately. This means that if the air speed in the pipe is 25 m/s, in order to maintain a minimum speed of 20 m/s for capsules, any sustained slope in the PCP line must be limited to about 5^o. This however does not mean that the maximum rising slope of a PCP line is limited to 5^o. In fact, there is no such limit. By using larger values of V and/or smaller values of V_c, or using capsules of tighter seal plates which enhances the drag coefficient, the slope of the PCP line can be anything including vertical. This shows that there is no practical limit to the slope of PCPs. Also, it should be realized that the slope of PCP calculated from Eqs.2.1.7 and 2.1.8 is for sustained (long) slope. For slopes of short distances, much larger slopes than those predicted from the equations can be used. This is so because for short slopes, the capsules can be allowed to decelerate to a speed significantly lower than the speed in the horizontal part of the conduit. Due to the existence of large spacing between capsules, deceleration will simply bring capsules closer to each other without detrimental effect

on system operation. The designer should make sure, however, that the capsule speed is not so slow that will cause jamming, which happens when the spacing between neighboring capsules reduces to zero. When that happens, either the design speed V must be increased, or tighter seal plates must be used on capsules.

(c) Rail switching and turnouts

Turnout is the part of the railroad track that changes from one track to two or three tracks. It contains the ***switch*** or ***switches,*** which are the moving part of the turnout. A typical turnout that changes from one track to two tracks is shown in Figures 2.1.4. Figure 2.1.4(a) shows that when the left switchblade is closed, the train or capsule traveling from left to right is deflected to the right through the curved section of the track and exit the turnout traveling at an angle to its original direction of travel. Trains and capsules can also travel the same path in the reverse direction. Figure 1(b) shows the switch set so that trains or capsules traveling from left to right continue through the turnout without changing direction. Trains and capsules can also travel in the same path in the reverse direction.

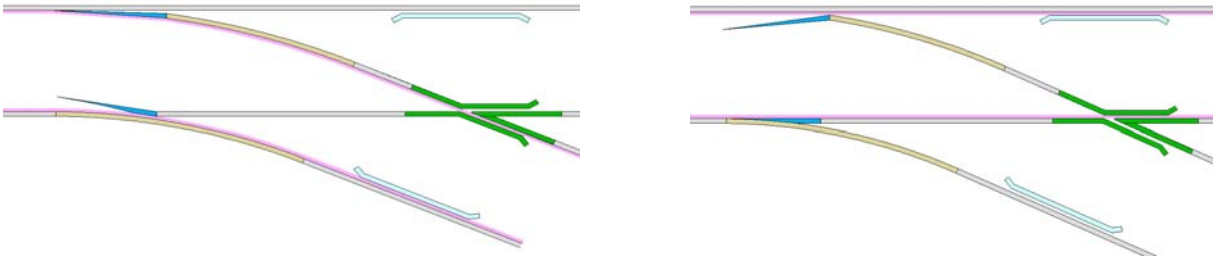

(a) Left switchblade closed (b) Left switchblade open

Figure 2.1.4 Turnabout and switches of railroads

The ***switchblades*** are shown in blue in the above figure. Switch blades are tapered steel members usually made from rail stock. Their geometry is complex due to milling the sides and top of the stock rail to form the blade. In addition, the switchblades that connect to curved rails (the top switchblade in the above figure) may be bent into an arc. The ***heel*** of a switchblade is the blunt end, which is attached to a rail via some sort of hinge about which it can rotate. Both blades along the same rail are linked together so that when one switch blade is open the other one is closed. The mechanism that moves the blades is not shown in the figure.

In Figure 2.1.4, the straight sections of the rails are gray (only the railheads are visible), and the curved rails are brown. The aqua objects are guardrails. The pink bands do not represent actual objects but represent flangeways. A ***flangeway*** is a region through which a wheel flanges can travel without impacting obstacles.

The green objects in Figure 2.1.4 are the ***frogs***, which allow one rail to cross another. Imagine a train or capsule entering the turnout from the left as shown in Figure 2.1.4(a). The left front wheel flange will be forced to following the left switchblade and then the curved section of rail. The right front wheel follows the curved rail because the left front wheel flange is being guided. The same thing happens with the left rear and right rear wheels. After the capsule travels a short distance on the curved rails, the right front wheel flange will enter the flangeway between the right guardrail and the straight section of rail. The purpose of this guard rail is to

control the position of the right wheel flange, thereby guiding the left front wheel flange into the proper flangeway of the frog. The same thing happens with the rear wheels. After passing both left wheels through the frog, the capsule leaves the turnout. A capsule entering the turnout from the left as shown in Figure 2.1.4(b) simply passes through the turnout continuing in a straight line. When the left wheel flange inters the narrow flangeway between the left guardrail and the rail, the right wheel flange is guided through the proper flangeway of the frog.

Shown in Figure 2.1.5 is a typical frog. The left portion of the frog is called the toe and the right portion is called the heel of the frog. As shown in the figure, the theoretical point of a frog is a knife edge point formed by the intersection of the two heel rails. The actual point is slightly blunted and is located to the right of the theoretical point. The width of this blunted edge is usually about 0.5 inches.

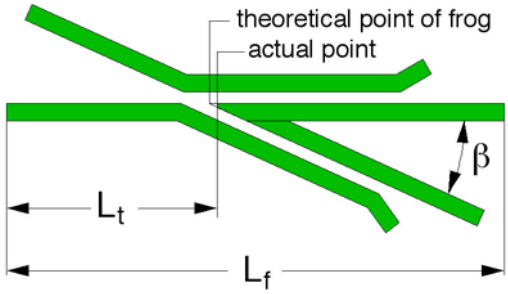

Figure 2.1.5 Schematic of a typical rail frog

Shown in Figure 3 is the frog angle β, which is related to the frog number, n, defined as follows:

$$2\tan(\frac{\beta}{2}) = \frac{1}{n} \qquad (2.1.9)$$

The available frog number range is $4 \le n \le 14$ with increment of 0.5. Hence $4.09^o \le \beta \le 14.25^o$. The frog length, L_f, and the frog toe length, L_t, depend upon the rails the frog is to be bolted to, the size of the flangeway needed, the frog number and the wheel loads of the cars. However L_f would probably be at least 2 m up to 5 m or more for large frog numbers. The toe length would probably be from 0.5 m up to 2 m or even longer.

The selection of a frog for a turnout has a great impact on the overall length of the turnout. Suppose the curve centerline radius, R_c, the rail and track gauge, g_{track}, have been select for a turnout design. The gauge lines are drawn as shown in Figure 2.1.6.

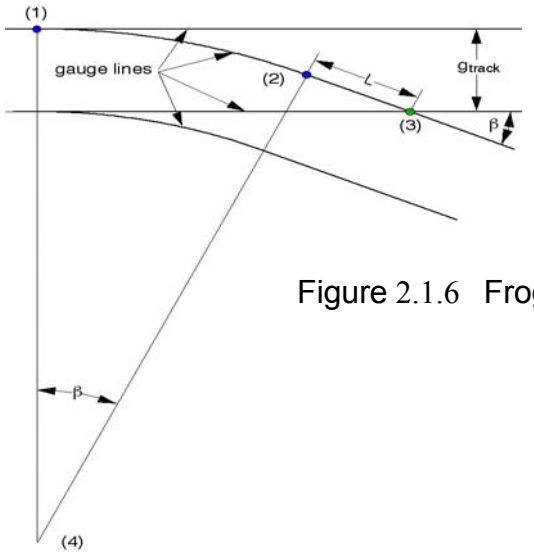

Figure 2.1.6 Frog placement

The curved line between points (1) and (2) is a circular arc with the center at point (4), and with a radius equal to

$$R = R_c + \frac{g_{track}}{2} \qquad (2.1.10)$$

This arc ends at (2) and the line (2) to (3) is straight with a length of L. Point (3) is the location of the theoretical point of the frog. The angle β is the frog angle. Once the frog angle is determined, the distance L shown in Fig. 2.1.6 can be calculated from the following equation:

$$L = \frac{g_{track} - (R_c + \frac{g_{track}}{2})(1 - \cos\beta)}{\sin\beta} \qquad (2.1.11)$$

If L is greater than or equal to the toe length of the frog, L_t, then the frog will work. If L is negative or less that the toe length of the frog, then the frog will not work.

Table 2.1 Frog data

n	Lf (m)	Lt (m)
4	1.803	0.635
5	1.956	0.635
6	2.235	0.889
7	2.477	0.889
8	2.718	0.889
9	2.972	0.889
10	3.467	1.143

Table 2.2 Calculation results

n	β	L (m)	Lt (m)
5	11.421°	-1.52	0.635
6	9.527°	-0.15	0.889
7	8.171°	1.000	0.889
8	7.153°	2.019	0.889

From example, suppose R_c is 45.72 m (150 feet) and the track gauge is 0.610 m (24 inches). Suppose also that the data shown in Table 2.1 is available from a supplier. Equations 2.1.9 and 2.1.11 are used to calculate the values in the first three columns of Table 2.2. The last column in Table 2.2 was obtained from Table 2.1. The results show that a frog number of 7 will work. Frog numbers 8, 9 and 10 will also work but will yield a longer turnout.

Formulas for calculating the minimum length of the left switchblade (the one to the left as we move from left to right in Fig.2.1.7) will now be given.

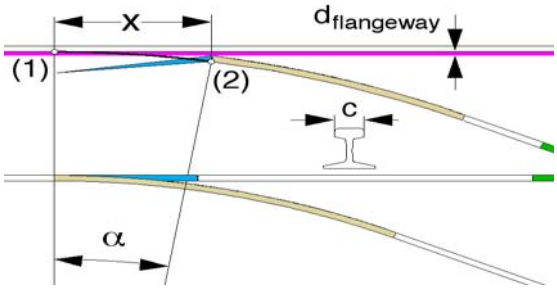

Figure 2.1.7 Left switchblade length

The minimum length, x, is determined from the flangeway width required, $d_{flangeway}$, the radius of the arc from point (1) to point (2), $R_c + g_{track}/2$, and the rail head width, c. The formulas are in two parts. First the angle α is calculated, and then the minimum length, x, is calculated.

$$\cos\alpha = \frac{R_c + \frac{g_{track}}{2} - d_{flangeway}}{R_c + \frac{g_{track}}{2} + c} \qquad (2.1.12)$$

$$x = \left(R_c + \frac{g_{track}}{2} \right) \sin\alpha \qquad (2.1.13)$$

For our previous example, R_c was 45.72 m and the track gauge was 0.610 m. If we add to the data a flangeway width of 0.0445 m (1.75 inches) and a railhead width of 0.0603 m (1.375 inches), we obtain from the above equations α = 3.865º and x = 3.102 m. Hence the left switchblade will have to be longer than 3.102 m.

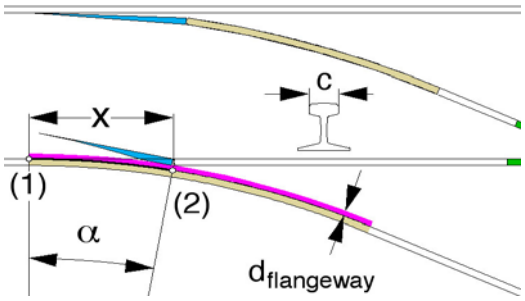

Figure 2.1.8 Right switchblade length

For the minimum length of the right switch blade, use the two equations shown below.

$$\cos\alpha = \frac{R_c - \frac{g_{track}}{2} - c}{R_c - \frac{g_{track}}{2} + d_{flangeway}} \qquad (2.1.14)$$

$$x = \left(R_c - \frac{g_{track}}{2} \right) \sin\alpha \qquad (2.1.15)$$

Using the data used before for the left switchblade, the above two equations yield α = 3.891º and x = 3.082 m. Hence, we take both switchblade length to be 3.20 m.

The final design parameters for the turnout in the foregoing example are shown in Figure 2.1.9.

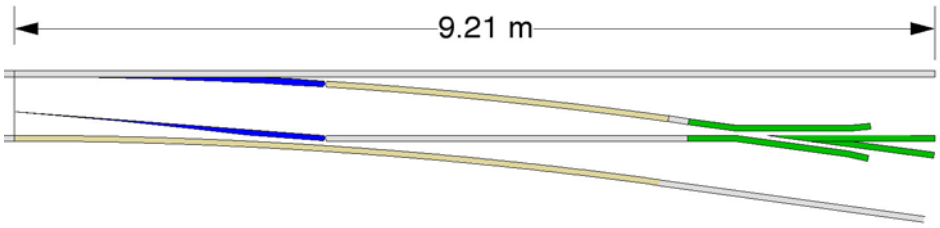

Figure 2.1.9 Turnout design parameters
(Frog number = 7, R_c = 45.72 m, $d_{flangeway}$ = 0.044 m, c = 0.0603 m, switchblade lengths = 3.20 m, overall length of turnout = 9.21 m.)

The turnout design shown in Figure 2.1.9 can be used to bifurcate a single track into three or more parallel tracks. An example of three parallel tracks is shown in Figure 2.1.10. The overall length of this arrangement is 24.86 m.

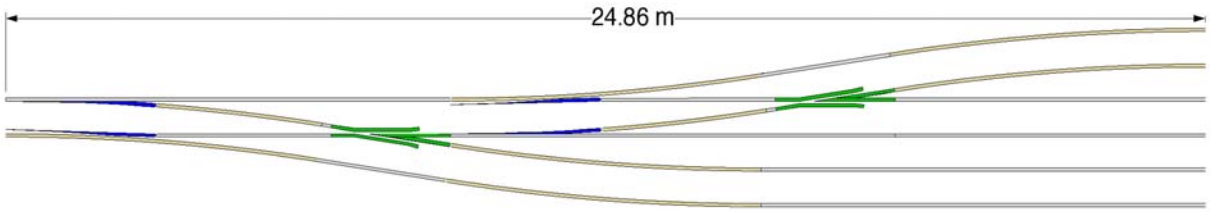

Figure 2.1.10 Bifurcating from one track to three parallel tracks

(d) Base of rail

A typical conventional railroad consists of a set of two parallel steel rails anchored by steel fasteners to the top of a set of ***ties*** (***sleepers***) made of wood, which in turn are imbedded in a layer of crashed rocks or crashed gravels of about 12-inch (30-inch) thick, called the ***ballast bed***. Immediately beneath the ballast bed is the ***sub-ballast***, which is a layer of crushed rocks of a finer size of about 4-inch (10 cm) thick. Finally, beneath the sub-ballast is the ***subgrade,*** which is the compacted soil of sufficient bearing capacity, so that the ballasts and the rails will not settle, or will settle very little, less than 1 cm. The top of the ballast bed must be at least 18 inches aboveground in order to maintain good drainage characteristics.

A newer railroad system, used for high-speed trains and urban mass transit, replaces the ballast layer with a concrete slab. The slab track is preferred to ballast track in that it costs less to build, is stronger and more stable, and has less maintenance problems than ballasted tracks. For these reasons, the railroad inside the PCP conduit will use concrete slab instead of ballast. For best result, the rails will be mounted on concrete sleepers, which in turn are imbedded in a 6-inch

layer of concrete. A profile of such a system is shown in the next section dealing with the tube (conduit) design.

2.2 Tube Design

Depending on individual cases, the PCP tube (conduit) for transporting minerals or mine wastes may be either aboveground or underground. In some cases, it may also have part of the tube underground and part of it aboveground. For best results, the aboveground tube should use a steel structure, whereas the underground tube should use a concrete structure. They are separately discussed next.

(a) Aboveground tube

- **Straight track region**

Steel modules make up the aboveground PCP conduit or tube. These modules can be constructed at a fabrication factory and transported by truck to the construction site for installation. A 3-D view of the module is shown in Figure 2.2.1.

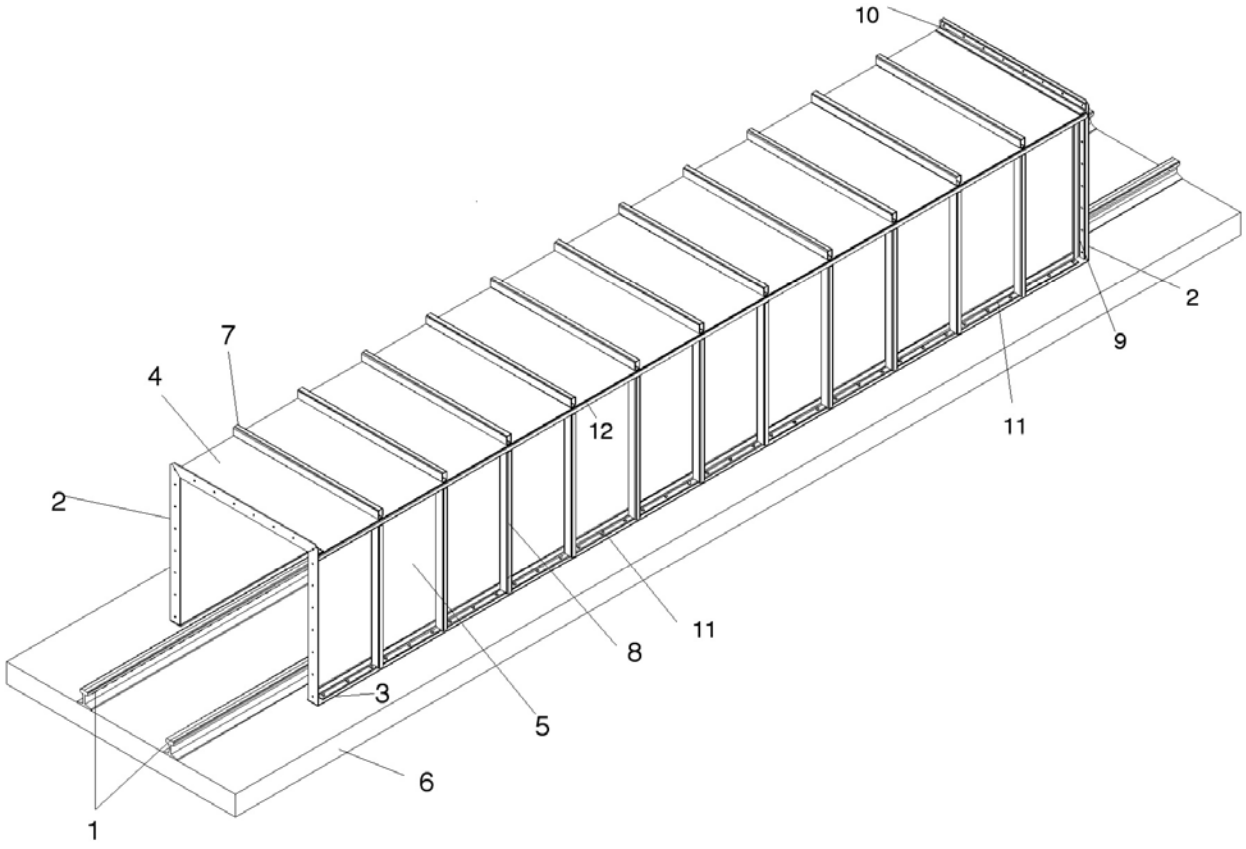

Figure 2.2.1- Orthogonal (3-D) view of PCP tube module

The overall length of each module is 19 feet 8 1/4 inches or 6.00 m. The inside dimensions of the tube are 1 m by 1 m. The entire module is constructed from 1/4 inch steel plate stiffened by ribs made of rectangular 1.5-inch by 2.5-inch structural tubing with a wall thickness of 1/4

inch. Also used are stiffeners made of 2-inch by 2-inch angle of 1/4-inch thickness. The use of materials with equal wall thickness will facilitate welding.

Referring to Fig.2.2.1, the concrete slab 6, poured on site, serves as the foundation for both the rails 1 and the tube module. Each end of the module has a flange 2, which allows it to be bolted to adjacent modules. Rubber gaskets will be used to keep the flange hermetic. There is also flanges 3 on the bottom of the module which enables bolting and sealing the module against the slab.

The side plates 5 are 39 1/8 inches by 235 3/4 inches. They are reinforced by vertical stiffeners 8 constructed from structural tubing 37 5/8 inches long. These stiffeners are spaced every 19 11/16 inches along the module except at the module ends. At the ends, the flanges 2 are stiffened by angles 9 and 10. The dimensions in inches of the flange plates are shown in Figure 2.2.2.

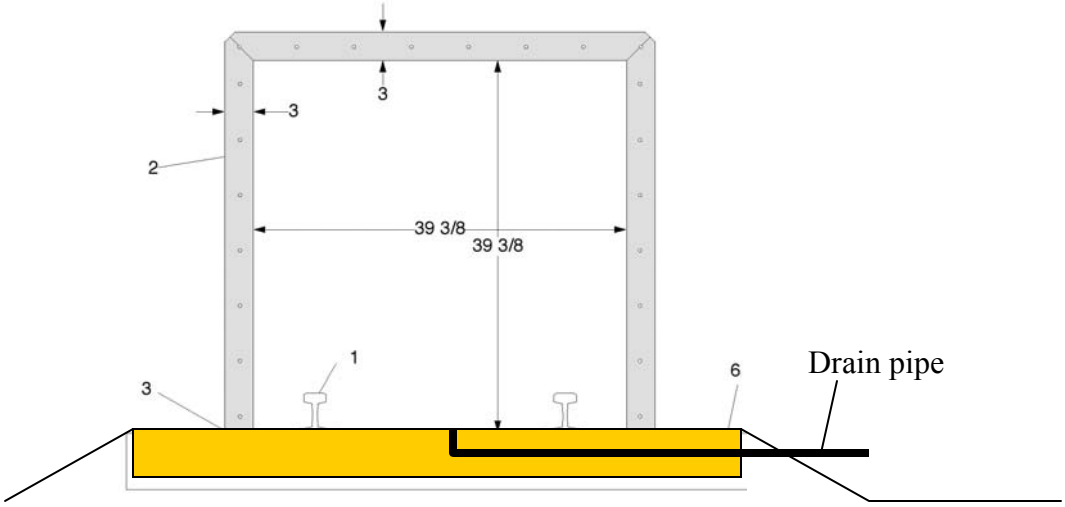

Figure 2.2.2 End View of module

The top plate 4 is 44 9/16 inches by 235 3/4 inches. It overhangs the two side plates 5 by approximately 2 1/2 inches on each side. The overhang regions are reinforced with stiffeners 12 constructed from structural tubing. These stiffeners tie the top plate 4 to the side plates 5 and to the side plate stiffeners 8. The top plate 4 is also reinforced by structural tubing stiffeners 7 which are 44 9/16 inches long and spaced every 19 11/16 inches.

The two bottom flanges 3 consist of two plates each 3 1/4 by 236 1/4 inches. Each plate is welded to a side plate on the inside of the tube. The plates are reinforced on the outside of the tube by angles 11.

- **Curved Track Region:**

The terrain may make it necessary to curve the track. It is assumed here that curve radius R_c is large enough that super elevate of the track is not required.

Clearance between the wall of the conveyance tube and the car is more complicated around a curve. To determine how much clearance is needed between the car and the tube wall it is necessary to know those critical dimensions of the car and track shown in Figure 2.2.3. The

length and width of the box are L and b. The wheelbase is L_w , the wheel gauge is g_w, and the track gage is g_{track}. Terms r and b_H are dimensions of the wheel hubs and do affect clearance but have little other significance. The endplate has width b_d and is located at a distance L_d in front of the front wheel axial. Figure 2.2.4 gives another view of the wheel and track gage. The track gage is the distance between the railheads measure a small distance (1/4 to 1/2 inch depending upon standard used) down from the top of the rail. The wheel gage is basically the distance between the outside of the flanges. As one views a wheel profile as seen in Figure 2.2.4, there is a curve that connects the wheel tread to the flange. This curve is concave near the tread and convex near the flange. The distance between the points where the curvature reverses for the two wheels is the wheel gauge.

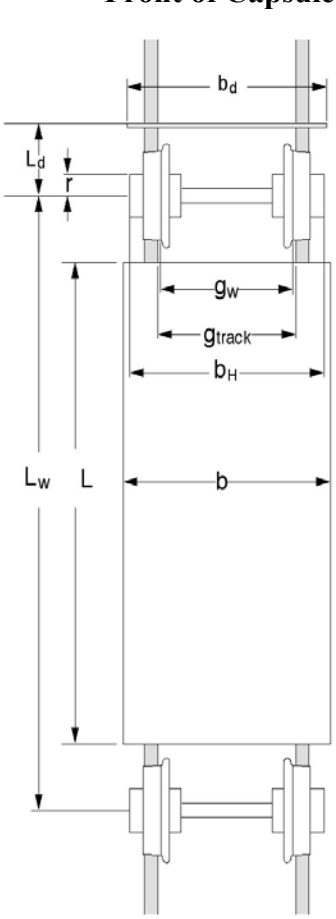

Figure 2.2.3 Critical dimensions of the capsule

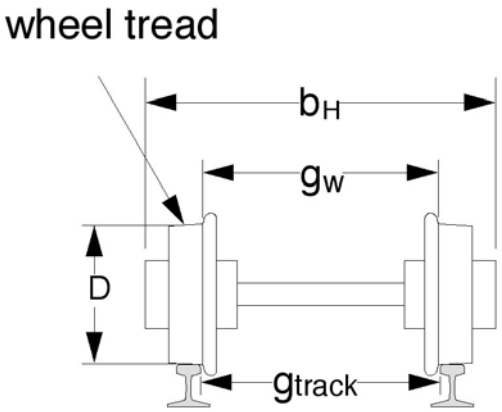

Figure 2.2.4 Track and wheel gauge

The wheel tread is a conical surface with the maximum diameter next to the wheel flange. The nominal wheel diameter, D, is measured in the center of the tread.

When the capsule enters a curve to the right, the left front wheel flange will come in contact with the left rail. The increase in drag due to this contact may cause the car to rotate slightly so that the right rear wheel flange will also come in contact with the right rail. Thereafter the motion becomes complicated due to small rotations back and forth. In so far as clearance

between the car and the tube wall is concerned, there are three configurations that should be considered. For configuration 1, shown in Figure 2.2.5, the left front and left rear wheel flanges are in contact with the left rail.

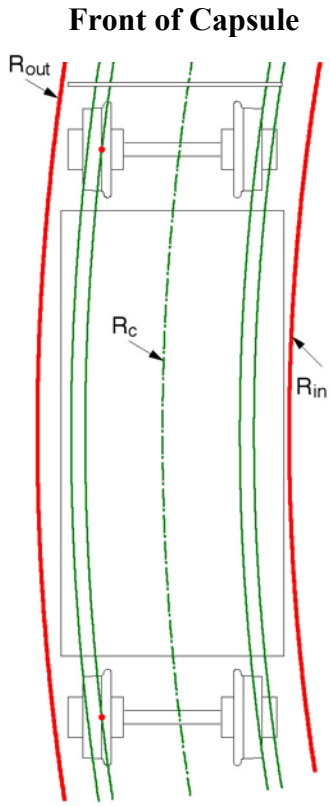

Figure 2.2.5 Capsule and rail for configuration 1

In Fig. 2.2.5, the track gauge is exaggerated to show the points (red dots) where the wheel flanges contact the railhead. The solid green lines in Figure 2.2.5 are the sides of the rail heads and the dotted line is the centerline that has a radius R_c. The two red lines represent an imaginary boundary that the vertical walls of the conveyance tube should not penetrate. For configuration 2 (not shown), the left front wheel flange is in contact with the left rail and the right rear wheel flange is in contact with the right rail. Both configurations 1 and 2 should be considered when determining the clearance needed between the capsule and the left wall. For configuration 3 (not shown), both right wheel flanges are in contact with the right rail. This configuration should be considered to determining the clearance needed between the right wall and the car.

Configuration 1 leads to Eqs. 2.2.1 through 2.2.4, which can be used for calculating the minimum outer radius R_{out}. Term δ is the minimum clearance desired. One should use the largest of the three values of R_{out}.

$$R = -\frac{b}{2} - \frac{g_w}{2} + \sqrt{\left(R_c + \frac{g_{track}}{2}\right)^2 - \frac{L_w^2}{4}} \qquad (2.2.1)$$

$$R_{out} = \sqrt{(R + b)^2 + \frac{L^2}{4}} + \delta \tag{2.2.2}$$

$$R_{out} = \sqrt{\left(R + \frac{b}{2} + \frac{b_H}{2}\right)^2 + \left(\frac{L_w}{2} + r\right)^2} + \delta \tag{2.2.3}$$

$$R_{out} = \sqrt{\left(R + \frac{b}{2} + \frac{b_d}{2}\right)^2 + \left(\frac{L_w}{2} + L_d\right)^2} + \delta \tag{2.2.4}$$

Configuration 2 is geometrically more complicated, and a sequence of calculations is required as follows:

$$\alpha = \sin^{-1}\left(\frac{L_w}{2\left(R_c + \frac{g_w}{2}\right)}\right) \tag{2.2.5}$$

$$\theta = \cos^{-1}\left(\frac{g_w}{\sqrt{L_w^2 + g_w^2}}\right) \tag{2.2.6}$$

$$\beta = \cos^{-1}\left(\frac{2 R_c g_{track} + g_w^2 + L_w^2}{2\sqrt{g_w^2 + L_w^2}\left(R_c + \frac{g_{track}}{2}\right)}\right) \tag{2.2.7}$$

$$\varepsilon = \theta - \alpha - \beta \tag{2.2.8}$$

$$x1 = \sqrt{\left(R_c + \frac{g_{track}}{2}\right)^2 - \frac{L_w^2}{4}} \tag{2.2.9}$$

$$y1 = \frac{L_w}{2} \tag{2.2.10}$$

$$x = x1 + \left(\frac{b_H}{2} - \frac{g_w}{2}\right)\cos\varepsilon + r\sin\varepsilon \tag{2.2.11}$$

$$y = y1 - \left(\frac{b_H}{2} - \frac{g_w}{2}\right)\sin\varepsilon + r\cos\varepsilon \tag{2.2.12}$$

$$R_{out} = \sqrt{x^2 + y^2} + \delta \tag{2.2.13}$$

$$x2 = x1 + \left(\frac{b_d}{2} - \frac{g_w}{2}\right)\cos(\varepsilon) + r\sin(\varepsilon) \qquad (2.2.14)$$

$$y2 = y1 - \left(\frac{b_d}{2} - \frac{g_w}{2}\right)\sin(\varepsilon) + L_d\cos(\varepsilon) \qquad (2.2.15)$$

$$R_{out} = \sqrt{(x2)^2 + (y2)^2} + \delta \qquad (2.2.16)$$

After a value for R_{out} is obtained, it should be compared with the value obtained from configuration 1 equations (i.e., equations 2.2.1 through 2.2.4), and the smaller value discarded.

The configuration 3 equation is

$$R_{in} = -\frac{b}{2} + \frac{g_w}{2} + \sqrt{\left(R_c - \frac{g_{track}}{2}\right)^2 - \frac{L_w^2}{4}} - \delta \qquad (2.2.13)$$

Once R_{out} and R_{in} have been calculated, it is possible to design a conveyance tube module for the curve. The design for the steel modules for straight reaches of track discussed earlier can be adapted to curved regions in at least two different ways. Suppose as an example we have a curve with a radius of 33 ft 4 inches. This radius is smaller than the capsule can negotiate at least for the track gauge and the tread width to be discussed in the next section. However, this radius distorts the geometry, so that the effects of curvature are apparent. For our calculation, we use the data listed in Table 2.3 for capsules without end plate.

Table 2.3 Data for the example

Item	Length (inches)
L	75.0
b	37.38
g_{track}	24
g_w	23.5
L_w	96.63
B_H	35.0
r	3.38

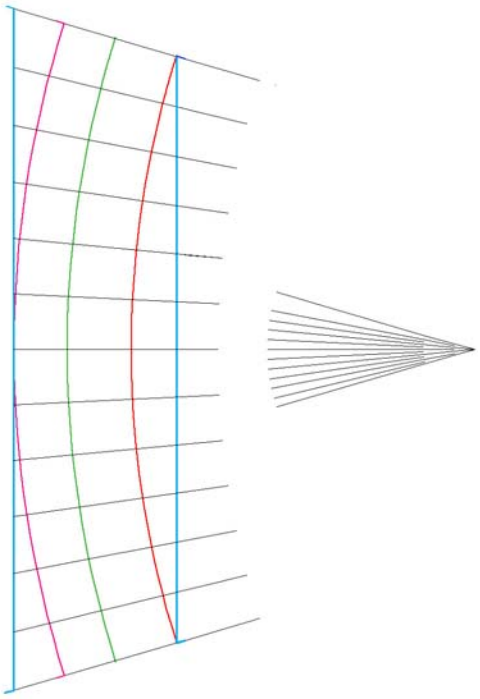

Figure 2.2.6 Example conveyance tube module for curved track

Based on these data, R_{out} turns out to be 419.13 inches and R_{in} is equal to 377.04 inches. These two radii are shown in Figure 2.2.6 as the two red lines. The centerline radius of 400 inches is shown in green. The rails are not shown. The centerline length has been selected to be 236.22 inches, making it the same as the straight track sections previously discussed. The center of the arcs is shown in Figure 2.2.6 although not in its correct geometric position. Two radial lines can be drawn from this center to the ends of the centerline arc. These two lines fix the miter angles for the module-end flanges. The sides of the conveyance tube can be curved and placed just outside the red lines. If this is done the module design can mimic the one for straight track except that two pieces of rectangular structural tubing would have to be bent, and the angle stiffeners between the bottom flange and the tube wall would have to be bend or segmented somehow. A curved conveyance tube module has the advantage of minimizing the maximum clearance in the module. However, it may be difficult and expensive to construct. The other option is to have several segments (modules) of straight tubes connected to each other at an angle to form a curve. For our example the two module walls are the blue lines shown in Figure 2.2.6. Clearly this option requires a wider tube than the curved option. However, construction would be easier because each module would be the same as for straight track except for being wider and mitered at the ends. Moreover, the wasted space can be reduced greatly by decreasing the length of each module. Remember that the radius selected for this example is only about 25% of radii likely to be used in actual applications.

Whichever module design is selected, one can place the side wall stiffeners and the top stiffeners along radial lines equally spaced along the centerline. Shown in Figure 2.2.7 is an orthogonal view of a curved section of the PCP tube made of straight modules.

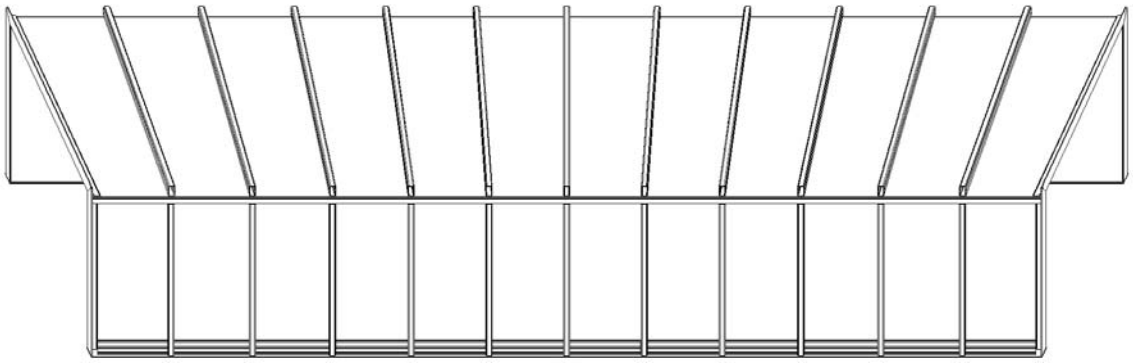

Figure 2.2.7 Orthogonal view of a curved tube made of short straight modules

(b) Underground tube

The recommended underground tube (conduit) of the PCP for mining is a reinforced concrete structure – the same as the box culvert used in waterworks as shown in Fig.2.2.8. A concrete slab is laid on the bottom of the conduit to support the rails.

Figure 2.2.8 Large box culvert made of reinforced concrete that can be used for constructing large rectangular conduits for PCP using the open-cut construction method. (Photo reprinted from the web page of the Hanson Pipe & Products, Inc. [10])

2.3 Capsule Design

The capsule design is similar to that of a railroad car except for some modifications to suit the special need of this system, such as a bottom gate to discharge the cargo (minerals or mine wastes) by gravity, gadgets to activate the brake automatically, and a double-layer wall (steel inside and aluminum outside) to enable the capsule to receive the thrust of the LIM (linear induction motor) in an efficient manner. More details of the design are discussed as follows:

(a) Capsule body

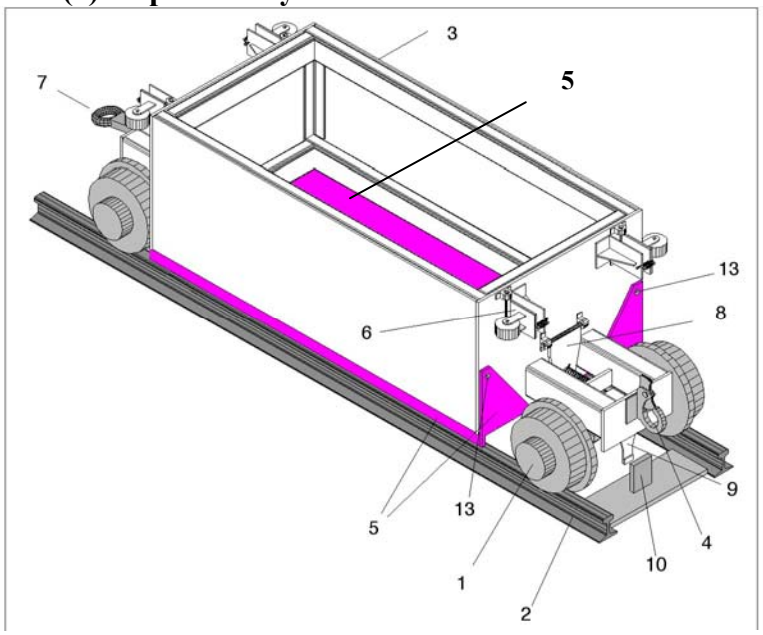

1. Wheel
2. Rail
3. Box
4. Latch (for capsule linkage)
5. Gate
6. Guide wheel assembly
7. Drawbar (to match latch)
8. Front latch assembly (for bottom gates)
9. Trigger
10. Front barrier plate
11. Rear latch assembly
13. Gate hinge

Figure 2.3.1 Capsule design (front 3-D siometric view)

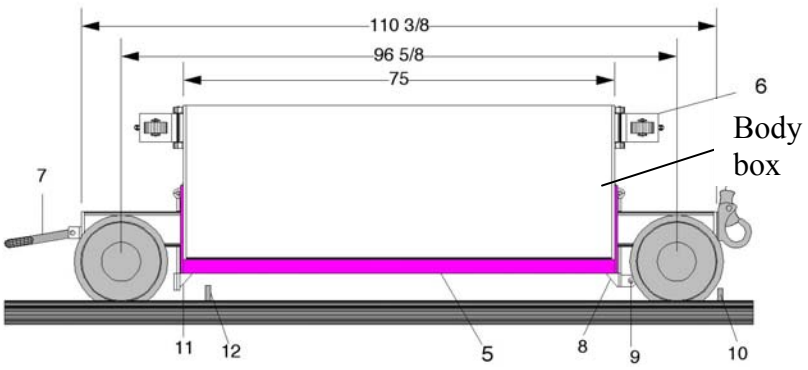

3. Box
4. Latch (for capsule link)
5. Gate (bottom open)
6. Guide wheel assembly
7. Drawbar (to match latch)
8. Front latch assembly (for bottom gates)
9. Trigger
10. Front barrier
11. Rear latch assembly
12. Rear twin barrier

Figure 2.3.2 Capsule side view

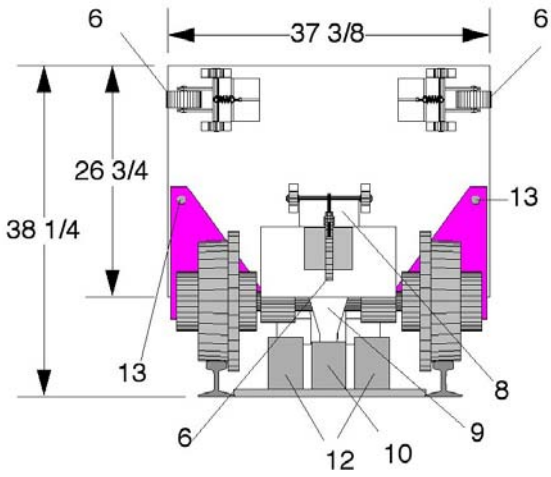

3. Box
6. Guide wheel assembly
8. Front latch assembly
9. Trigger
10. Front barrier
12. Rear twin barriers
13. Gate hinge

Figure 2.3.3 Capsule front view

A front isometric 3-D view of the capsule is shown in Fig. 2.3.1. Figures 2.3.2 and 2.3.3 show a side and front view of the capsule. As shown in Figs. 2.3.2 and 2.3.3, box 3 of the car has a length of 75 in (1905 mm), a width of 37 3/8 in (949 mm) and a height of 26 3/4 in (679 mm). The maximum volume of the box, when filled with cargoes to within about 2 inches (50 mm) from the top, is about 40 ft^3 (1.133 m^3). The weight of the empty capsule is about 2,960 lb (1,343 kg). Assuming that the maximum unit weight of the cargo is 200 lb/ ft^3 (3,201 kg/m^3), the maximum cargo weight (payload) will be 8,000 lbs (3,628 kg), and the maximum gross weight of the loaded capsule will be 10,960 lb (4,971 kg) or 2.74 ton (2.485 tonnes) per axle.

As shown in Figure 2.3.3, the height of the capsule measured from the base of the rail to the top of the box is 38 1/4 in (972 mm), and the maximum width of the capsule excluding the guide wheels is 37 3/8 in (949 mm). This allows approximately 1 in (25 mm) of clearance between the top and each side of the capsule and the conveyance tube.

Figure 2.3.4 shows the double-layer wall design – an aluminum outer wall backed by a steel inner wall. While the aluminum outer walls are where the eddy current and the thrust of the linear induction motor (LIM) are generated in, the steel walls serve two functions: (1) as the structural walls to contain the materials contained inside the capsule, and (2) as the ferrous material to complete the magnetic circuit generated by the LIM though the aluminum conductor. Without the ferrous (steel) inner walls, not much magnetic force (thrust) can be generated on the capsule by the LIM.

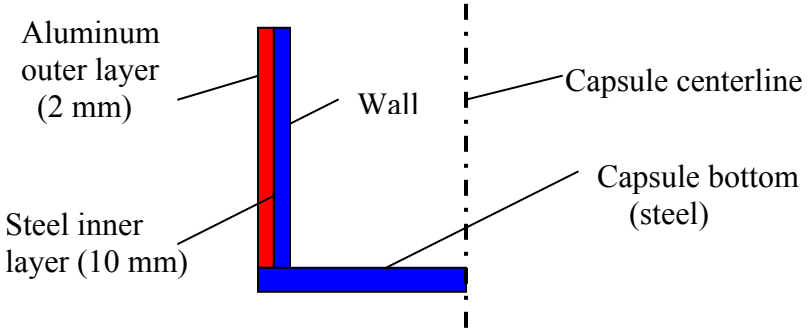

Figure 2.3.4 Capsule side walls. (Note that only one of the two sidewalls is shown).

(b) Wheels

As shown in Fig.2.3.2, the wheel base (i.e., the distance between the two axels) is 96 5/8 in (2.454 m), and the overall length of the car excluding the coupling 4 and drawbar 7 is 110 3/8 in (2.804). The wheels 1 have an average tread diameter of 14 in (356 mm) and a tread width of 3 1/2 in (89 mm). The wheel gage is about 23.5 in and the track gage is 24 in. As discussed in Sec. 3.1 (a), the track rail 2 is 60 lb. ASCE.

The capsule has four guide wheel assemblies, 6. Each assembly supports a guide wheel that protrudes beyond the sides of the box to provide lateral support while the capsule is in the LIM portion of the conveyance tube. This prevents the capsule walls from contacting the LIM when the LIM exhibits an attractive rather than repulsive force on the LIM, in addition to the longitudinal thrust which moves the capsule forwards. The guide wheels also prevent the capsule wall from contacting the outer radius of the tube in bends when the radius of curvature of the rails is insufficient to prevent the capsules from tipping at high speed, due to the overturning moment generated by the centrifugal force at the bend. These guide-wheel assemblies can be adjusted as the guide wheels wear.

(c) Brakes

For controlling capsule motion, standard railroad train brakes are to be used. The standard brakes use compressed air to activate the brakes of each car, with each car carrying a compressed air tank to supply the energy for activating the brakes. This will be the same for capsules. However, in ordinary trains the brakes and the air tank on each car are activated by a person in the locomotive. In contrast, because capsules have no locomotives and no drivers, their bricks must be triggered and controlled remotely. This will be done by having each capsule train carry a

radio frequency identification (RFID) tag, the same as used at current toll booths on highways. When the train is approaching the outlet, the receiver of the RFID signals, located at the PCP tube outlet, will send a command signal via a PLC (programmable Logic Controller) to each capsule in the train in order to activate the brakes and to bring the capsule train to a slow stop. The brakes will remain stopped until the capsules have received a new command radio signal, ordering the brakes to be released.

The brake system for each capsule is shown in the Figure 2.3.5. The system has two air cylinders (28), a compressed air tank (29), two brake blocks (30), two brake arms (31), and two fix axles (32). The air tank (29) supplies the compressed air needed for activating the brake. The air cylinder (28) uses the compressed air to move linearly in order to activate the brake arm (31). Each air cylinder is attached to the brake arms via clevises. Each brake arm, pivoted about a fix axle (32), applies the frictional force on a wheel to slow down the capsule. The brake blocks (30) are attached to the arms and serves the same purpose as brake pads in an automobile.

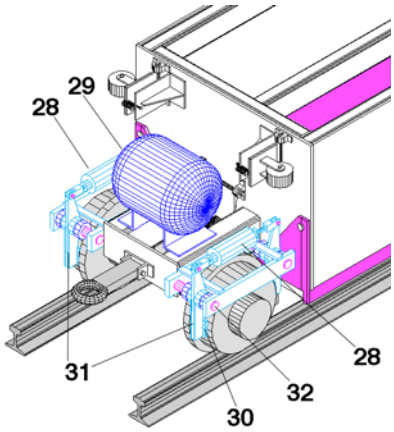

Figure 2.3.5 Brake assembly for capsules

Each air cylinder has a 3-inch bore, a 2-inch stroke and is double activating. The brakes are applied when the air cylinders are in the extended position and removed when the air cylinder is in the contracted position. The air cylinders are controlled by means of a 4-way 2-position solenoid air control valve. The air is supplied by the air tank (29) which can carry an air pressure of up to 600 psi (pound per square inch), and holds about 7 gallons. Due to this high pressure, a pressure control valve will be needed between the air tank and the control valve to reduce the pressure to about 80 psi. The air contained in a fully charged air tank should be capable of about 150 brake and brake release cycles. Periodic refilling of the air tank is needed, which can be done in the short time when the capsule is parked during cargo loading.

A 12-volt lead acid battery supplies the electric current needed for operating the solenoid control valve. The solenoid control valve can be set up so that current is needed only during braking at which time the current drawn is about 50 mA. Hence a small fully-charged, lead-acid battery should last for days. These batteries will be recharged periodically. Due to the slowness in charging batteries, the batteries will be recharged off-line. While they are being recharged off-line in the battery house of the PCP inlet station, replacement batteries will be used to keep the capsules running. Switching of the batteries can be done during the short time when a train is stopped for reloading. An RFID receiver responding to a remote signal controls the current that

operates the solenoid control valve. The solenoid control valve, pressure control valve and the RFID receiver are not shown in Figure 2.3.5. They are commercially available standard equipment.

Assuming that brakes are mounted on all wheels, in a straight horizontal track with negligible air resistance the stopping distance, Δx, for a car with an initial velocity V_o can be calculated from the following equation:

$$\Delta x = \frac{\frac{1}{2} m V_o^2 + \frac{4}{2} m_w V_o^2 + \frac{4}{2} I_w \frac{V_o^2}{r^2}}{8 \mu P} \qquad (2.3.1)$$

in which m_w is the mass of one wheel, I_w is the mass moment of inertia of one wheel, r is the rolling radius of the wheels (about 7 inches), and m is the total mass of the car excluding the mass of the four wheels. Term P and μ are respectively the normal force and the contact friction coefficient between the brake blocks and the wheel treads. For our cars, m_w = 5.21 slug, I_w = 0.95 slug/ ft^2, and m = 313 slug.

Assuming that the air pressure in each air cylinder is 80 psi, the force developed by each cylinder would be 565 pounds. The mechanical advantage (leverage) is about 1.01, so P = 571 pounds. Assuming μ = 0.5, the stopping distance Δx for a capsule train traveling at 20 m/s is 324 feet or about 99 m. This same brake force, when applied to all the four wheels of each capsule, will also allow fully-loaded trains to park on a track of maximum slope of 12^o, and to allow empty trains to park on a slope as large as 50^o.

(d) Dumping mechanism

The capsule is designed for transporting crushed minerals or mine wastes of less than 6-inch (152 mm) size, approximately. The cargo (minerals or mine wastes) are loaded into the capsules through their open top. Experience in Japan in using a 1m-diameter PCP for transporting crushed limestone [4] indicates that it is not necessary for each capsule to have a lid. Should a lid be needed, it can be easily added into the design of the capsule shown before. When a loaded capsule reaches its destination, it goes over a horizontal truss above a pit and dumps the cargo into the pit. The bottom dump is accomplished through two symmetric gates 5 --shown in purple color in the three foregoing figures. The gate rotates about shafts 13 while opening to discharge load -- see Fig. 2.3.6. As shown in Figs. 2.3.7 and 2.3.8, the gates are held closed by latch assemblies 8 and 11. As shown in Figs. 2.3.6 and 2.3.7 the latch assembly 8 is held in position by spring 14 and can be rotated about hinge 23. Similarly, Figs. 2.3.8 and 2.3.9 show that the latch assembly 11 is held in position by spring 15 and can be rotated about 24. Spring stops 18 (Fig.2.3.7) and 19 (Fig.2.3.8) are fixed to the capsule and do not move.

The latches are opened at the dumpsite by the center barrier 10 and the off-center twin barriers 12, which are both fixed to the rail track—compare the location of barrier 10 in Fig. 2.3.6 with that of the twin barriers 12 in Fig. 2.3.9. Barrier 10 releases the front latch 8 and barrier 12 releases the rear latch 11. Figures 2.3.6 and 2.3.7 give details about how barrier 10 releases latch 8. The latch trigger 9 is made up of a plate assembly 17 which rotates clockwise about hinge 26 when it strikes barrier 10. The linkage 16 rotates counterclockwise pulling latch

8 to the right, rotating the latch assembly counterclockwise about the front-latch hinge 23, thereby opening the latch.

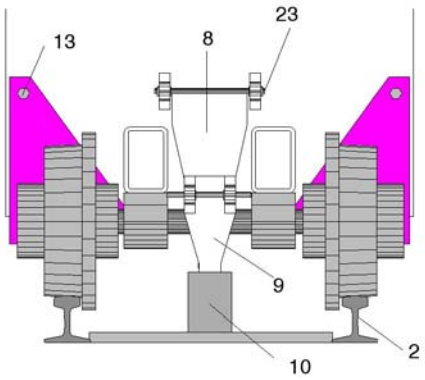

2. Rail
8. Front latch assembly
9. Trigger
10. Front barrier
13. Shaft (for gate)
23. Front-latch hinge

Figure 2.3.6 Cutaway front view of front assembly

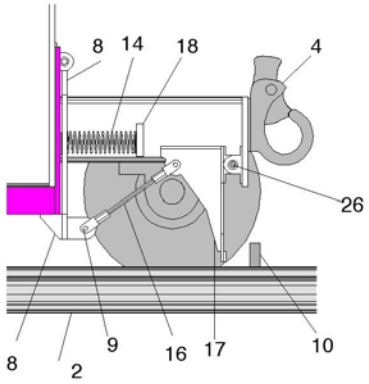

2. Rail
4. Latch (for capsule link)
8. Front latch assembly
9. Trigger
10. Front barrier
14. Front-latch spring
16. Linkage (for front trigger)
17. Plate assembly
18. Front-latch spring stop
26. Trigger hinge

Figure 2.3.7 Cutaway side view of rear assembly

Figures 2.3.8 and 2.3.9 give details about how barriers 12 release latch 11. As the capsule move to the right in Figure 2.3.8, latch release 9 does not strike twin barriers 12. However, the configuration of latch 11 is such that the twin barriers12 does strike latch 11, thereby rotating the latch about hinge 24 and opening the latch. After the capsule dumps it load and continues to move, barrier 10 strikes latch 11. This impact between barrier 10 and latch 11 serves no useful purpose but does not cause a problem.

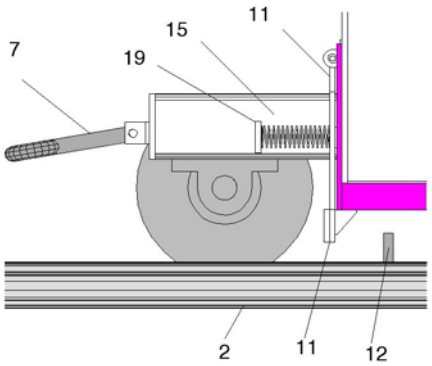

2. Rail
7. Draw bar
11. Rear latch assembly
12. Rear twin barriers
15. Rear-latch spring
19. Rear-latch spring stop

Figure 2.3.8 Cutaway side view of rear assembly

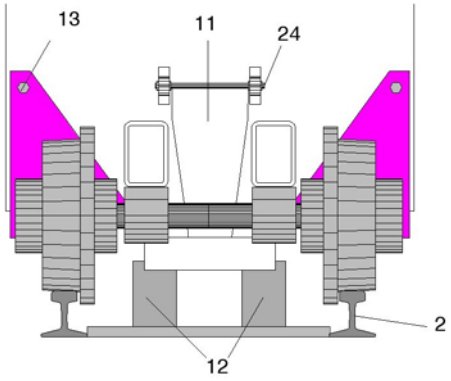

2. Rail
11. Rear latch assembly
12. Rear twin barriers
13. Shaft (for gate)
24. Rear-latch hinge

Figure 2.3.9 Cutaway rear view of rear assembly

After the capsule passes both barriers, gates 5 can be re-latched. This is carried out by two gate-closing sets 20 located at the latching station on both sides of the track. As shown in Fig. 3.2.10, the gates protrude from the side of the capsule when they are open. The arm 25 of each gate-closing set 20 is in a vertical position with the stud bearing 21 in close proximity of the open gate. The push-pull air cylinder 22 is controlled by an air solenoid (not shown). At an appropriate time the air cylinder is activated via the air solenoid and the arm 25 rotates toward the capsule, thereby pushing the gates closed as shown in Fig. 2.3.11. After the gates are pushed closed, latch 8 and 11 latch the gates in place. After the gates are closed the air solenoid is activated again and the air cylinder returning the arm to a vertical position.

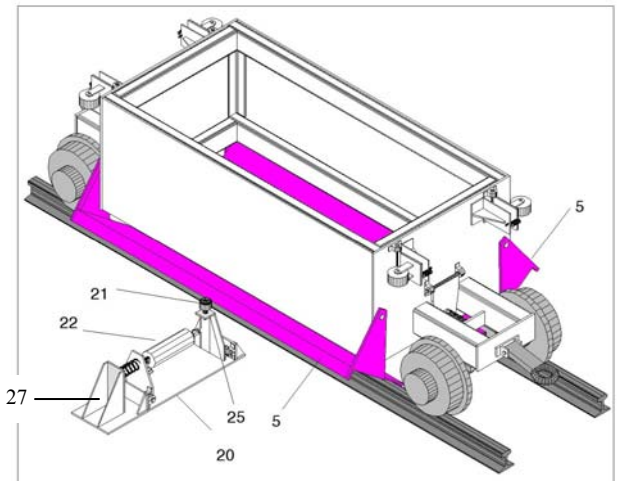

5. Gates (unlatched)
20. Gate-closing set
21. Stud bearing
22. Pneumatic cylinder
25. Gate-closing arm
27. Cylinder buttress

Figure 2.3.10 Capsule with gates unlatched

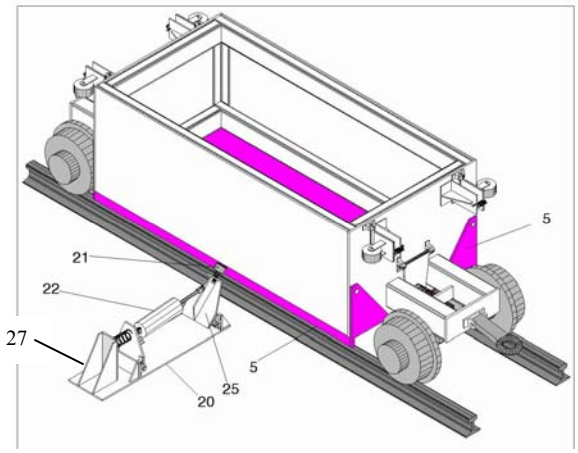

5. Gate (latched)
20. Gate-closing set
21. Stud bearing
22. Pneumatic cylinder
25. Gate-closing arm
27. Cylinder buttress

Figure 2.3.11 Capsule with gates latched

.

2.4 Inlet/Outlet Stations Design

(a) General Layout

The general layout of the LIM-driven PCP system is shown in Fig. 2.4.1. The system consists of three main parts: an inlet station, an outlet station, and the dual conduits between the two stations, one is the ***delivery line*** and the other the ***return lin***e. While the delivery line carries the loaded capsules to the outlet station, the return line carries the empty capsules back to the inlet station. Depending on the topography and other factors, the conduits can be either aboveground or underground, following more or less the surface elevation of the ground along the route between the inlet and the outlet.

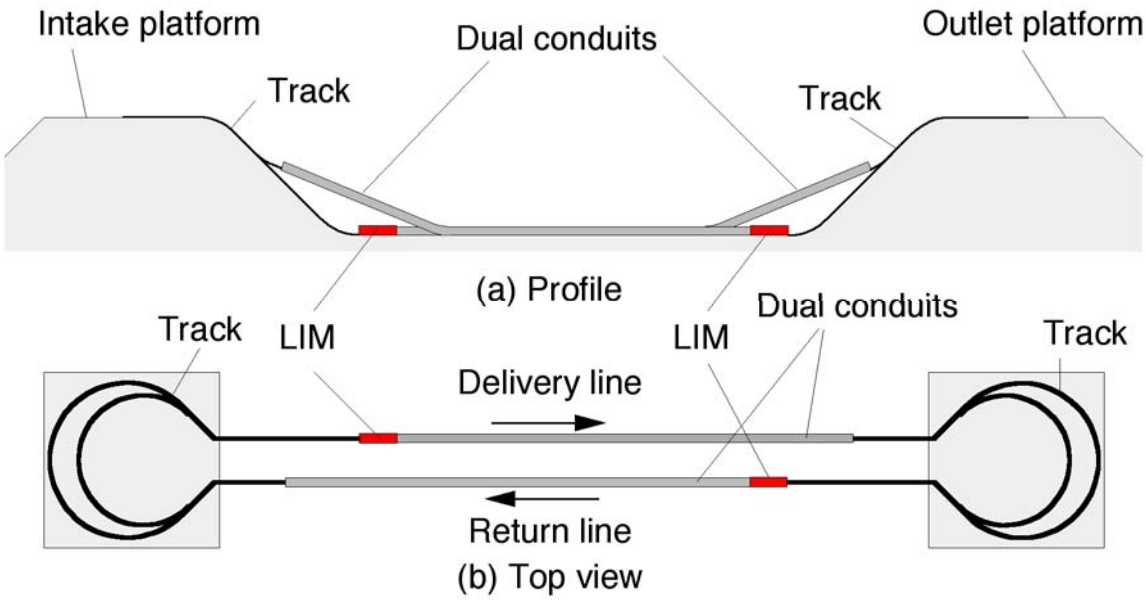

Figure 2.4.1 General layout of a LIM-driven PCP for mining use

Both the inlet and the outlet will be constructed on elevated platforms. The inlet platform must be elevated to about 22 m above the LIM at the inlet of the delivery line, so that capsules loaded with cargo on the inlet platform, with an initial speed of 2 m/s on the platform, can be accelerated by gravity to approximately 20 m/s before they enter the LIM. As will be discussed in the section on steady-state analysis, 20 m/s is the capsule speed in the LIM to achieve maximum efficiency. Once the capsule train has passed the LIM, the train speed will reduce to 15 m/s approximately for the entire journey through the conduit. At the other end of the conduit (i.e., near the outlet platform), the platform also must be elevated in order to decelerate the capsules from about 15 m/s to about 2 m/s when capsules reach the outlet platform. This requires an elevation difference of 10 m approximately, between the outlet of the conduit, and the outlet platform. For simplicity, the two platforms are drawn in Fig.2.4.1 as being at equal elevation, and the conduits between the stations to be horizontal. In reality, depending on topography, the inlet elevation and the outlet elevation can be quite different, and the dual conduits must follow more or less the ground level along the route between the two stations. The design of the conduit has been discussed in Sec.2.2. More about the inlet and outlet will be considered next.

(b) Inlet layout and operation

The layout of the inlet station (platform) is shown in Fig. 2.4.2. The platform is a flat rectangular area of 100 m x 115 m approximately. Because capsules on the platform must move much slower than in the conduits, multiple tracks may be needed on the platform when the throughput rate is high. As an example, a 4-track system is shown in the figure. For the maximum annual throughput of 50 million tonnes of cargo (minerals or mine waste), assuming around-the-clock operation for 360 days a year, the number of capsules that must be launched or handled per second is 0.443. If each train contains 5 capsules, the number of capsule trains that

must be handled in a second is 0.0886. This means that the time to launch and load each train is 11.3 seconds.

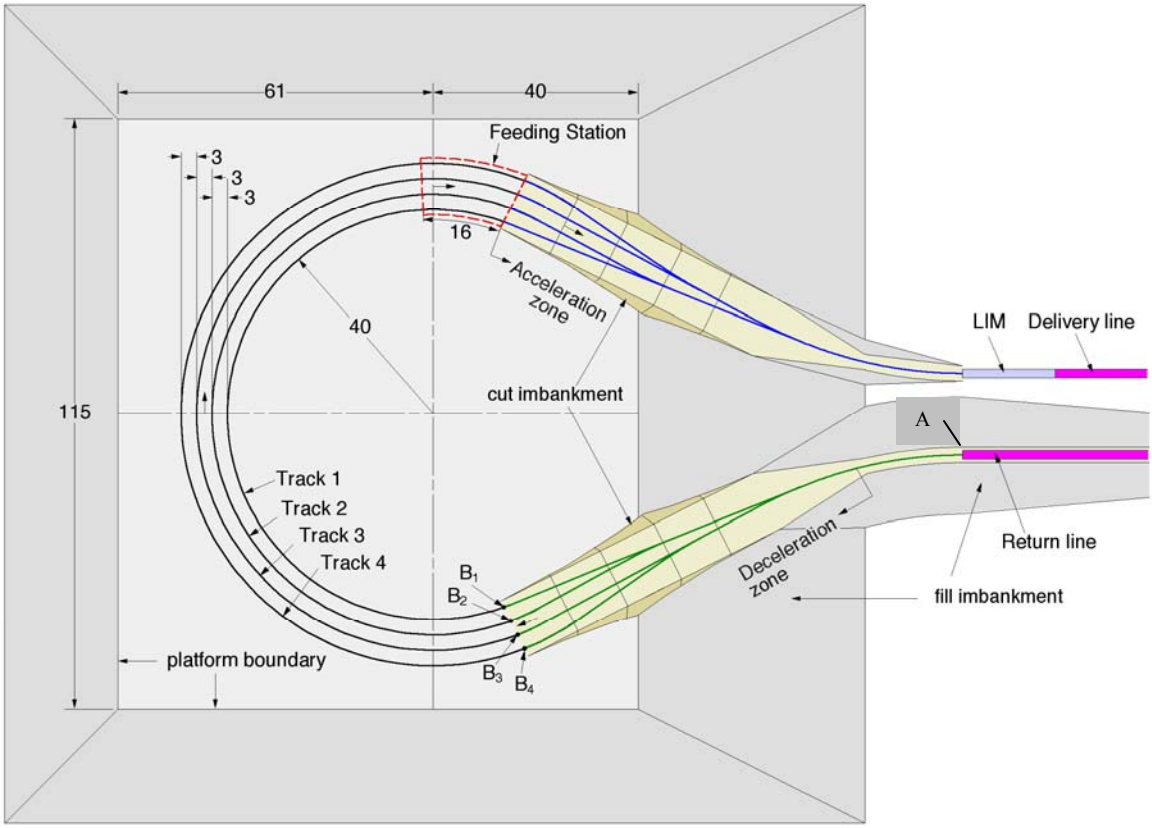

Figure 2.4.2 Layout of the inlet station (platform)

The linefill rate, α, is the linear distance in the PCP conduit occupied by the capsules divided by the total distance of the conduit. It can be calculated from

$$\alpha = \frac{L_t}{TV_c} \qquad (2.4.1)$$

where L_t is the capsule train length, T is the time interval of train injection at the inlet, and V_c is the steady-state velocity (speed) of the capsule train moving through the conduit.

The train length, L_t, used in this system design is 16.2 m. For the maximum throughput of 50 million tones per year, T = 11.3 s, and V_c = 15 m/s. Substituting these values into Eq.2.4.1 yields α = 0.0956 or 9.56 %. This means the linefill in the conduit is 9.56 %. As any capsule train reaches the platforms of the inlet/outlet stations, the train speed must be reduced for ease in loading/unloading. If the train speed on the platform is reduced to 2 m/s, from Eq.2.4.1, the linefill will rise to 71.7%, which means that the capsule trains will follow each other on the platform with small spacing (clearance) between neighboring trains, of the order of 4.5 m. Note that the theoretical maximum linefill rate at any location, corresponding to zero clearance, is 100%.

Referring to Fig. 2.4.2, when an empty capsule train in the return line reaches point A where the conduit ends, the speed of the train is still 15 m/s as in the remaining parts of the conduit. However, as soon as the front part of the train has passed point A and starts to rise on the slope (bank) of the platform, the train starts to slow down as it rises and enters one of the 4 tracks. When the entire train has arrived on the platform at any of the B points (say B_1 for track 1), the train speed is decreased by gravity to 2 m/s. From engineering calculation, the elevation difference needed to accomplish this speed decrease by gravity is about 10 m. The time that it takes the train to slow down from 15 m/s (at A) to 2 m/s (at any of the Bs) is approximately 2.6 seconds. Note that trains will arrive at B_1, B_2, B_3 and B_4 successively at an interval of 11.3 seconds. (track). For each track, the time interval between successive trains is 11.3n, where n is the number of tracks. For instance, if 4 tracks are used, the time interval between successive trains arriving at any point along the track is 4 x 11.3 = 45.2 seconds. Therefore, if the train must be stopped to load the mineral or mine waste, it should not be stopped for more than 45.2 second, or else collision will happen. In reality, due to the need of about 2 seconds to stop the empty capsule train from the speed of 2 m/s, and another 5 second to accelerate it to 2 m/s after stoppage and loading, the loading time for each train (5 capsules) should be no more than 38 seconds. This is not a problem at all with gravity feeding, if 5 feeders are used simultaneously to feed the 5 capsules in each train.

It is expected that the feeding time for each capsule or train can be as short as 20 seconds. This means no more than three tracks are really needed at each time to transport 50 million tones of ores annually. Therefore, only 3 of the 4 tracks will be running at any given time; the 4th will be used as a spare, which will be activated only when one the three tracks being used breaks down, or when tracks need to be taken out of service one at a time for maintenance.

With 4 tracks, a total of 20 feeders will be needed, one for each capsule. The feeding station can be anywhere along the semi-circular part of tracks, preferably near the end of the tracks as shown in Fig.2.4.2, so that as soon as the trains are loaded, they can enter the delivery line.

Once a capsule train is on the platform, it will be pushed to move at a constant speed of 2 m/s either by an overhead crane system built along the circular track, or by a long horizontal arm of 40 to 50 m length, which is supported by and rotates around a central pivoting shaft at the center of the platform, as shown in Fig.2.4.3.

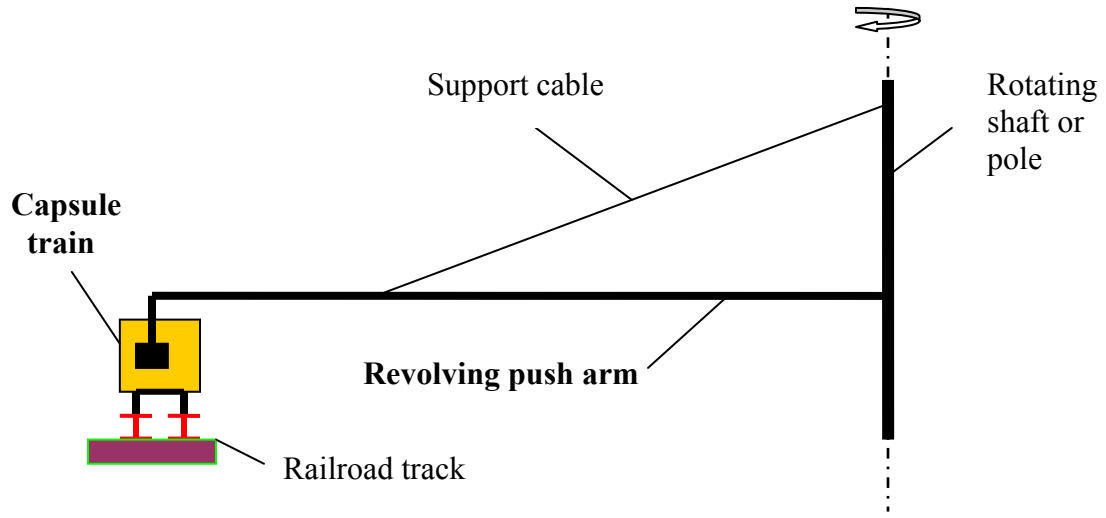

Figure 2.4.3 Rotary push arm to move capsule trains along a circular track

(c) Outlet Station design

The arrangement for the outlet station (i.e., the station at the destination of the ore or waste to be transported by the PCP) is similar to that of the inlet station, except for the fact that the outlet station has unloading rather than loading equipment. Capsules arriving at the unloading station do not need to stop in order to dump the load. They move on parallel tracks at the constant speed of 2 m/s throughout the entire course on the outlet platform. Load dumping is accomplished through opening the twin gates on the bottom of each capsule as the capsule train crosses a bridge built over the stockpile of the transported minerals or wastes– see Fig.2.4.4. The dumping mechanism is discussed in more details in Sec.2.3(d). Upon load dumping, the empty capsules go around a circular track as in Fig.2.4.2 and re-enter the PCP tube nonstop.

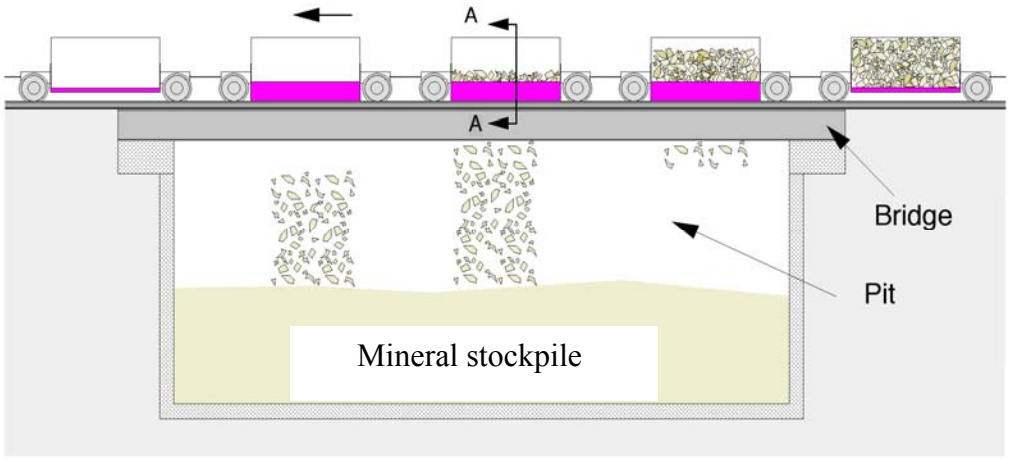

Figure 2.4.4 Method for unloading capsule train while it is moving

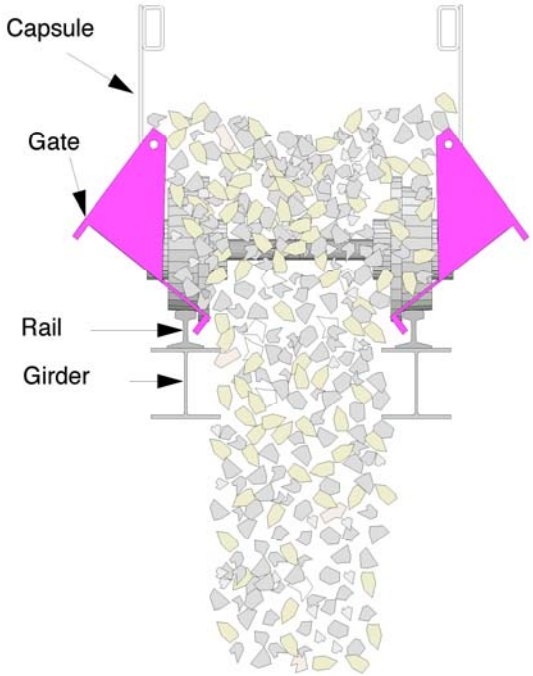

Section A-A

3. ANALYSIS OF SYTEM OPERATION

3.1 Introduction

The purpose of this section is to analyze the LIM-driven PCP system design in Section 2, in order to determine its operational characteristics, and to optimize the system design and operation. First, the system equations, both for the steady and the unsteady cases, will be derived. Then, they will be used to analyze the system performance. Through the analysis, how to optimize the design and the operation will be pointed out.

3.2 Operational Mode of a PCP Driven by LIMs

Before meaningful operational analyses can be made on a PCP driven by LIMs, the system and its mode of operation must be understood. They are described as follows:

A PCP driven by LIMs consists of a pipeline, tube or conduit of either circular or rectangular cross section, with at least one LIM located near the inlet of the pipe. When the pipeline is long, additional LIMs may be needed along the pipe at suitable intervals; they are called "booster LIMs."

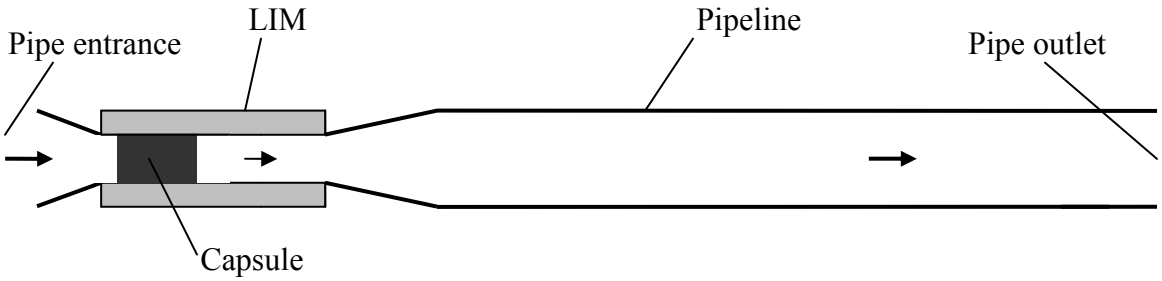

Figure 3.2.1 A PCP driven by a LIM. (Note that an exaggerated lateral scale is used. Besides, the real pipeline is much longer than the LIM as shown here.)

Figure 3.2.1 is the schematic of a PCP with a single LIM placed near the inlet of the pipeline. Note that the inner diameter of the LIM is slightly (a few percent) smaller than the inner diameter of the pipe. This is necessary in order to keep the air gap (i.e., the air-filled gap between the LIM and the capsule passing through the LIM) a minimum, which is necessary for effective and efficient use of LIM. A smooth transition is needed between the LIM and the slightly-larger-diameter pipe, making the LIM to look like a venture meter. Capsules are fed into the pipe one at a time at the inlet. Assume that at the beginning of operation ($t = 0$), the first capsule is fed into the LIM. As soon as the capsule has entered the LIM, it encounters an electromagnetic force (thrust) produced by the LIM, causing the capsule to accelerate through the LIM. This makes the capsule in the LIM to move faster than the air in the LIM, causing the air to accelerate due to transfer of momentum and energy from the capsule to the air. The acceleration of the capsule and the air in the LIM continues until the capsule reaches the end (exit) of the LIM. Thereafter, the capsule is outside the LIM, no electromagnetic force remains on the capsule, and both the capsule and the air in the pipe start to slow down or decelerate due to contact friction and flow resistance. Before the capsule is slowed down significantly, another capsule must be fed into the pipe entrance to keep the air and the capsule moving. The electromagnetic thrust on the second capsule in the LIM will impart additional energy into the airflow, which in turn will transfer

energy to the first capsule which is now in the pipeline downstream at a distance from the LIM exit. By feeding more and more capsules into the pipe in this manner, a more or less steady state can be reached in which the entire pipeline is now occupied by capsules spaced at more or less equal intervals, and there will be as many capsules exiting the pipe as being fed into the pipe. This will be the normal or steady-state operational condition of the PCP. Should the length of the pipeline be too long for a single LIM, additional LIMs can be placed along the pipe at approximately constant intervals, in the same manner booster pumps are normally used for long-distance pipelines that transport liquids or natural gas.

For the LIM pump to work, each capsule must be made of metal with a two-layer sidewall: an outer layer made of a good conductor such as aluminum of 2 to 3 millimeter thick, and a much thicker inner layer (say, 10 mm thick) made of a good ferromagnetic material such as steel. The steel layer also provides the structural strength to the capsule, keeping the capsule body rigid and wear-resistant.

For ordinary PCPs driven by blowers instead of LIMs, the body of each capsule usually contains either one or two disks (for cylindrical PCP) or plates (for rectangular PCPs) at the capsule ends, called "end disks", or "end plates", respectively. The end disks or end plates, fitted with a rubber rim around their peripheries, have a diameter (or cross section) larger than the capsule diameter (or cross-section) but only slightly smaller than the inner diameter (or cross section) of the pipe. They restrict air from passing over the capsule, thereby creating a seal to allow the capsule to develop a large drag which is needed for efficient energy transfer from air to capsule. Figure 3.2.2 shows a set of three capsules with end plates linked together to form a train in a rectangular pipe. For PCPs driven by LIMs instead of blowers, the end-plate diameter, D_e, must be only slightly smaller than the LIM bore or inner diameter, D,' in order to achieve good efficiency.

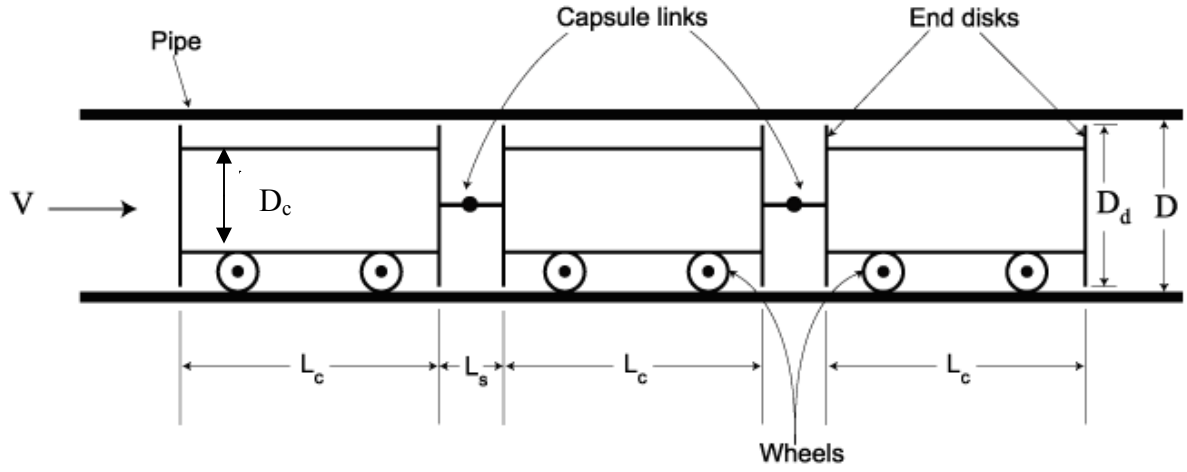

Figure 3.2.2 Capsule train in a rectangular conduit. (Note that although two end plates are shown for each capsule, in most cases one plate is sufficient for each capsule.)

3.3 System Eqations

3.3.1 Fluid Mechanics Equations for Steady-State Analysis

(a) Problem statement and assumptions

Based on the foregoing discussion, the operation of a LIM-driven PCP during steady-state operation can be analyzed by using the simplifying assumption that the pipe is horizontal, the fluid is incompressible, and the flow is steady with capsules of equal spacing traveling through the pipe at a constant velocity. The incompressible flow assumption limits the validity of the analysis to relatively short pipelines. In long pipelines, the air density varies significantly along the pipe, and the flow must be considered as compressible.

Figure 3.2.3 consists of the same pipeline and the same LIM shown in Fig. 3.2.1, except that the flow has reached steady state with the entire pipeline or conduit filled with capsules with approximately equal spaces (clearances) between neighboring capsules. This condition is established after many capsules have been feed into the pipe at the entrance, and the rate of capsules exiting the pipe is equal to that entering the pipe. During such a steady state, assume that the average spacing between neighboring capsules in the pipe and in the LIM are respectively L_s, and L_s'. In this study, primed quantities refer to quantities inside the LIM, whereas unprimed quantities pertain to those outside the LIM and inside the pipeline. For instance, the inner diameters of the pipe and the LIM are D and D', respectively, and the capsule velocities in the pipe and the LIM are V_c and V_c', respectively. Quantities that are the same in the pipe as in the LIM, such as the capsule length L_c, will be written without prime even if it is in the LIM.

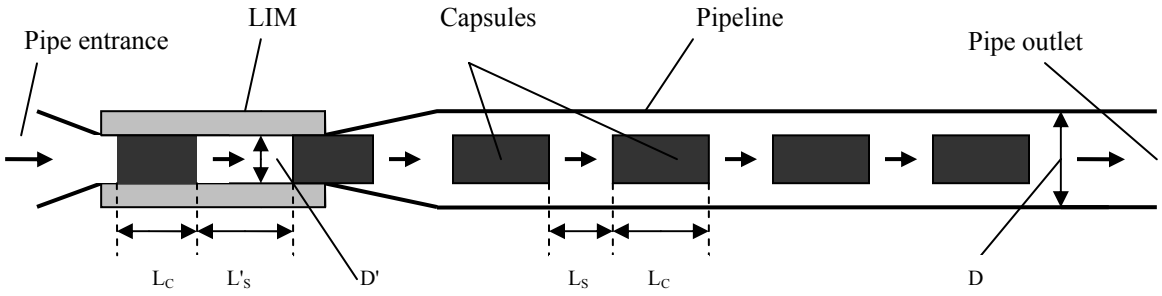

Figure 3.2.3 Steady flow of capsules in a PCP driven by a LIM. (Note that an exaggerated lateral scale is used.)

(b) Derivation of equations

The behavior (operational properties) of a LIM-driven PCP system can be analyzed and predicted from a set of engineering equations known in the fields of mechanics (fluid and solid mechanics) and electromagnetic theory (especially motor theory). Because the mechanical equations are mainly from fluid mechanics, both the fluid mechanics equations and solid mechanics equations are to be referred to as the "fluid mechanics equations." In what follows, the fluid mechanics equations will be derived. The derivation of the electromagnetic equations governing the behavior of LIM will be derived later in Sec.3.3. Now the derivation of the fluid mechanics equations:

If the capsule launching interval at the pipeline entrance is T (in seconds), under steady-state condition the number of capsules in the pipeline (outside the LIM), N, and the number of capsules in the LIM, N', can be calculated from:

$$N = \frac{L}{TV_c} \qquad \text{and} \qquad N' = \frac{L'}{TV_c'} \qquad \ldots\ldots\ldots\ldots\ldots\ldots\ldots\ldots \quad (3.3.1)$$

From Eq.3.3.1, the capsule injection rate into the PCP (which is the same as the number of capsules transported through the pipeline under steady-state condition) is

$$n = \frac{1}{T} = \frac{NV_c}{L} = \frac{N'V_c'}{L'} \qquad \ldots\ldots\ldots\ldots\ldots\ldots\ldots\ldots\ldots\ldots \quad (3.3.2)$$

The linefill rate, α, is defined as the total length of capsules in the pipeline, NL_c, divided by the total pipe length, L, namely,

$$\alpha = \frac{NL_c}{L} = \frac{L_c}{TV_c} \qquad \text{and} \qquad \alpha' = \frac{N'L_c}{L'} = \frac{L_c}{TV_c'} \qquad \ldots\ldots\ldots\ldots\ldots\ldots \quad (3.3.3)$$

From the assumption of steady incompressible flow,

$$\alpha V_c = \alpha' V_c' \qquad \ldots\ldots\ldots\ldots\ldots\ldots\ldots\ldots\ldots\ldots\ldots\ldots \quad (3.3.4)$$

$$V' = V\frac{A}{A'} \qquad \ldots\ldots\ldots\ldots\ldots\ldots\ldots\ldots\ldots\ldots\ldots\ldots \quad (3.3.5)$$

The contact friction between each capsule and the pipe is

$$F_C = \eta W_c \qquad \ldots\ldots\ldots\ldots\ldots\ldots\ldots\ldots\ldots\ldots\ldots\ldots\ldots\ldots \quad (3.3.6)$$

where W_c is the weight of the capsule, and η is the contact friction between the capsule and the pipe. Since large PCPs used wheeled capsules, η is the rolling friction coefficient of the wheels of the capsules.

Likewise, the contact friction between each capsule and the LIM is

$$F_C' = \eta' W_c \qquad \ldots\ldots\ldots\ldots\ldots\ldots\ldots\ldots\ldots\ldots\ldots\ldots\ldots\ldots \quad (3.3.7)$$

where η' is the rolling friction of the capsule wheels in the LIM. Depending on the surface conditions of the pipe and LIM, η' may or may not be the same as η. Both F_c and F_c' are in the opposite direction of the capsule motion.

The aerodynamic drag force on any capsule by the flow in the pipe is

$$F_D = A_c C_D \frac{\rho(V - V_c)^2}{2} \qquad \text{(capsule } \underline{\textbf{without}} \text{ end disk)} \ldots\ldots \quad (3.3.8)$$

$$F_D = A_d C_D \frac{\rho(V - V_c)^2}{2} \qquad \text{(capsule } \underline{\textbf{with}} \text{ end disks) ……} \quad (3.3.9)$$

where A_c is the cross-sectional area of the capsule, A_d is the cross-sectional area of each end disk, C_D is the drag coefficient of the capsule inside the pipe, and ρ is the density of the air inside the pipe, which is treated as a constant throughout the pipe and the LIM based on the assumption of incompressible flow.

Likewise, the corresponding drag in the LIM is

$$F'_D = A_c C'_D \frac{\rho(V'_c - V')^2}{2} \qquad \text{(capsule } \underline{\textbf{without}} \text{ end disk)....} \quad (3.3.10)$$

$$F'_D = A_d C'_D \frac{\rho(V'_c - V')^2}{2} \qquad \text{(capsule } \underline{\textbf{with}} \text{ end disks)…….} \quad (3.3.11)$$

where C'_D is the drag coefficient of the capsule in the LIM.

When capsules are in the pipe, the fluid velocity is higher than the air velocity, namely, $V>V_c$. In contrast, when capsules are in the LIM under the influence of an electromagnetic force created by the LIM, the capsule velocity is higher than the fluid velocity, namely, $V'_c > V'$. While the drag on the capsule in the pipe, F_D, is in the flow direction because V is greater than V_c, the drag on the capsule in the LIM, F'_D, is in the opposite direction of the flow because V' is smaller than V'_c. This means that the energy transfer in the pipe is from the fluid (air) to the capsules, whereas the energy transfer in the LIM is from the capsules to the fluid.

Because in this part of the analysis the capsules are assumed to have no acceleration, considering the balance of forces on a capsule in the pipe under steady state yields

$$F_D = F_C \qquad \text{.. ..……} \quad (3.3.12)$$

Likewise, considering the balance of forces on a capsule in the LIM yields

$$F'_D + F'_C = F_e \qquad \text{……} \quad (3.3.13)$$

where F_e is the electromagnetic thrust force generated by the LIM on the capsule.

Substituting Eqs. 3.3.6, 3.3.8 and 3.3.9 into Eq.3.3.12 yields

$$V = V_c + \sqrt{\frac{2\eta W_c}{C_D A_c \rho}} \qquad \text{(capsule } \underline{\textbf{without}} \text{ end disk)……} \quad (3.3.14)$$

$$V = V_c + \sqrt{\frac{2\eta W_c}{C_D A_d \rho}} \qquad \text{(capsule } \underline{\textbf{with}} \text{ end disk)……} \quad (3.3.15)$$

Likewise, substituting Eqs.3.3.7, 3.3.10 and 3.3.11 into Eq.3.3.13 yields

$$V_c' = V' + \sqrt{\frac{2(F_e - \eta' W_c')}{A_c C_D' \rho}} \quad \text{(capsule } \underline{\textbf{without}} \text{ end disk)}\ldots\ldots \quad (3.3.16)$$

$$V_c' = V' + \sqrt{\frac{2(F_e - \eta' W_c')}{A_d C_D' \rho}} \quad \text{(capsule } \underline{\textbf{with}} \text{ end disk)}\ldots\ldots\ldots \quad (3.3.17)$$

or,

$$F_e = \eta' W_c' + \frac{A_c C_D' \rho (V_c' - V')^2}{2} \quad (\underline{\textbf{without}} \text{ end disk})\ldots \quad (3.3.18)$$

$$F_e = \eta' W_c' + \frac{A_d C_D' \rho (V_c' - V')^2}{2} \quad (\underline{\textbf{with}} \text{ end disk})\ldots\ldots \quad (3.3.19)$$

To solve the foregoing set of equations, the drag coefficients C_D and C_D' must be determined. In ordinary PCPs driven by blowers, the drag coefficient C_D is usually determined from the following equation by Kosugi [7]:

$$C_D = \frac{4k_d^4}{(1-k_d^2)^2} \quad \text{(capsule } \underline{\textbf{with two end disks}}\text{)} \ \ldots\ldots \quad (3.3.20)$$

Note that the above equation is valid only for a stationary capsule with two end disks. If only one end disk exists, the factor 4 in the equation should be changed to 2. Also, Eq.3.3.20 was derived from the assumption that the flow passing through the small gap between the end disks and the pipe behaves like an orifice flow. This assumes that all the drag on the capsule is generated by the pressure difference across the two ends of the disk, and the drag due to shear on the capsule wall (i.e., the skin drag) is neglected. This assumption holds only when the capsule body diameter, D_c, is significantly smaller (at least 5% smaller) than the pipe diameter, D, or when the gap between the capsule and the pipe is relatively large – say, $(D-D_c)>0.05D$. Furthermore, Eq.3.3.20 was derived for the case of stationary capsule. When the capsule is moving, it is anticipated that the value of C_D will differ somewhat from that given by the above equation, depending on the velocity ratio V_c/V and the cross-sectional area ratio A_c/A . Moreover, when the capsule has no end disk, the drag coefficient is also expected to be significantly different from that given by the above equation. As will be shown in **Appendix I**, by using a combination of continuity, momentum and energy equations, the drag coefficients C_D and C'_D for any capsule with or without end disks can be found. Therefore, for the analysis of the LIM-driven PCP capsules in this study, the approach used in Appendix I is used for determining a more accurate drag and drag coefficient given by Eq.3.3.20.

Assuming steady-state condition and using momentum equation of fluid mechanics, the pressure drop across each capsule is $\eta W_c/A$. Thus, the pressure drop due to having N capsules in the pipeline is $\Delta p_c = N\eta W_c/A$. From Darcy-Weisbach formula, the pressure drop in the capsule-free space along the pipeline is $\Delta p_f = f\,(L-NL_c)\rho V^2/(2D)$. Summing the two yields the total pressure drop along the PCP as:

$$\Delta p = \Delta p_c + \Delta p_f = \frac{N\eta W_c}{A} + f\frac{(L-NL_c)}{D}\frac{\rho V^2}{2} \ldots\ldots\ldots\ldots\ldots \quad (3.3.21)$$

By the same token, the cumulative pressure rise in the LIM caused by N' capsules moving through the LIM at high velocity V'_c is:

$$\Delta p' = \Delta p'_c + \Delta p'_f = \frac{N'(F_e - \eta' W_c)}{A'} - f' \frac{(L' - N'L_c)}{D'} \frac{\rho V'^2}{2} \quad \ldots\ldots\ldots\ldots \quad (3.3.22)$$

Note that Eqs.3.3.21 and 3.3.22 are written for round pipe of diameter D, and round LIM of diameter D'. For rectangular pipe (conduit) using rectangular LIM, the diameters D and D' should be changed to $4R_H$ and $4R'_H$ respectively, where R_H and R'_H are the hydraulic radius of the pipe and LIM, respectfully.

Under steady-state equilibrium, the cumulative pressure drop in the pipe, Δp, is compensated by the cumulative pressure rise in the LIM, Δp', namely,

$$\Delta p' = \Delta p \quad \ldots\ldots\ldots\ldots\ldots\ldots\ldots\ldots\ldots\ldots \quad (3.3.23)$$

Note that Eq.3.3.23 is correct only for long PCPs of which the pressure drop along the pipeline or conduit is large. Otherwise, a correction term to take into account of the momentum change across the LIM is needed. This correction for short PCP systems is discussed in **Appendix II**.

Substituting Eqs.3.3.21 and 3.3.22 into Eq. 3.3.23 and solving for F_e yields

$$F_e = (\eta' + \frac{NA'}{N'A}\eta) W_c + [f \frac{(L - NL_c)}{D} + f' \frac{(L' - N'L_c)}{D'} \frac{A^2}{A'^2}] \frac{\rho V^2}{2} \frac{A'}{N'} \ldots\ldots \quad (3.3.24)$$

Note that the friction factors f and f ' can be determined either from the Moody diagram or from the Colebrook equation given in Appendix I. The Reynolds numbers used should be:

$$R = \frac{DV}{\nu} \quad \text{(for f in the pipe)} \quad \ldots\ldots\ldots\ldots\ldots \quad (3.3.25)$$

$$R' = \frac{D'V'}{\nu} \quad \text{(for f ' in the LIM)} \quad \ldots\ldots\ldots\ldots\ldots \quad (3.3.26)$$

The relative roughness used should be

$$\varepsilon = \frac{e}{D} \quad \text{and} \quad \varepsilon' = \frac{e'}{D'} \quad \ldots\ldots\ldots\ldots \quad (3.3.27)$$

Knowing that the total pressure drop along a PCP is Δp (see Eq.3.3.21), the power consumed by the motion of air and capsules in the PCP (i.e., the flow power or the power output of the pump) is

$$P = Q\Delta p = VA\Delta p \quad \ldots\ldots\ldots\ldots\ldots\ldots\ldots\ldots\ldots\ldots\ldots\ldots \quad (3.3.28)$$

The cargo throughput of the PCP in terms of weight of cargo transported per second is

$$T_h = nW \quad \ldots\ldots\ldots\ldots\ldots\ldots\ldots\ldots\ldots\ldots\ldots\ldots\ldots\ldots \quad (3.3.29)$$

in which n is the number of capsules transported through the pipe per second (see Eq.3.3.2), and W is the weight of the cargo carried by each capsule.

Note that the power P in Eq.3.3.28 is equal to the output power of the LIM pump. The input power of the pump, also called "***brakepower***," is given by

$$(P_i)_P = N' F_e V_c' \qquad \text{……..} \qquad (3.3.30)$$

where N' is the number of capsules in the LIM, which is determined from Eq.3.3.1. Therefore, the **pump efficiency** in this case is

$$E_P = \frac{VA\Delta p}{N' F_e V_c'} \qquad \text{……} \qquad (3.3.31)$$

On the other hand, the electric power consumed by the LIM, P_e, is the input power to the motor (LIM). It can be calculated from

$$P_e = \sqrt{3} I V_o \cos\theta \qquad \text{……..} \qquad (3.3.32)$$

where I is the input current in amp, V_O is the input voltage in volts, and θ is the phase angle between the alternating current I and the the alternating voltage V_o. The factor $\cos\theta$ is called the "***power factor***." Note that the quantity $\sqrt{3}$ in the equation is for the 3-phase current.

From Eqs.3.3.30 and Eq.3.3.32, the efficiency of the motor (i.e., the LIM efficiency or motor efficiency) is

$$E_L = \frac{(P_i)_P}{P_e} = \frac{N' A \Delta p}{\sqrt{3} I V_o \cos\theta} \qquad \text{……..} \qquad (3.3.33)$$

From Eq.3.3.31 and Eq.3.3.33, the total system efficiency of a LIM-driven PCP is

$$E_{sys} = E_L E_P = \frac{VA\Delta p}{\sqrt{3} I V_o \cos\theta} \qquad \text{…….} \qquad (3.3.34)$$

(c) Calculation procedure

The foregoing steady-state equations can be used to design a PCP system using the following procedure:

1. Specify the key properties of the system. For instance, specify the pipe geometry (whether rectangular or round) and dimensions, such as diameter and length. Also specifies the geometry and the dimensions of the LIM and each capsule, and the capsule weight. Determine the surface roughness of the pipe interior, LIM interior, and capsule exterior, and determine the rolling friction coefficient of the capsule wheels rolling through the pipeline and the LIM.
2. Specify the desired average speed of the capsules in the pipe, V_c.
3. Use the equations in Appendix I to calculate the airflow speed in the pipe V, the drag on each capsule in the pipe F_D, and the drag coefficient C_D.
4. Specify the capsule injection interval T, such as 10 seconds (T = 10). Use Eq.3.3.1 to calculate the number of capsules in the pipe, N.
5. Use Eq.3.3.3 to calculate the linefill rate in the pipe α.

6. Use Eq.3.3.4 to calculate the air velocity in the LIM, V', from the air velocity in the pipe, V.
7. Select a desirable capsule velocity in the LIM, V'_c. As a start, select V'_c to be twice the value of V_c (namely, $V'_c = 2\ V_c$).
8. Use Eq.3.3.4 to calculate the linefill in the LIM, α'.
9. Set the value of N' equal to 1.5. This will yield the minimum length of the LIM to be designed.
10. Use Eq.3.3.3 to calculate the minimum length of the LIM that must be used, L'.
11. Calculate the total pressure drop along the PCP by using Eq.3.3.21.
12. The power consumed by the flow in the PCP can be calculated from Eq.3.3.28.
13. Use of Eq.3.3.29 to calculate the cargo throughput of the PCP system. This cargo throughput must match the need (demand) for the system. If the cargo throughput does not match the need, the design must be adjusted to do meet the need.
14. Use Eq.3.3.24 to calculate the electromagnetic force (thrust) needed on each capsule going through the LIM.
15. The remaining work involves the design of a LIM that can create the calculated force F_e needed on each capsule at velocity V'_c and the efficiency at this capsule velocity. Try to make a design that can generate F_e at V'_c with high efficiency. Try to have the synchronous speed of the LIM selected to be 2% to 5% higher than V'_c, which usually yields maximum efficiency. The LIM design equations will be discussed after considering the following example to illustrate the use of the above design procedures.
16. After the LIM is designed, the power of the flow, the brakepower, the input power to the motor, the pump efficiency, the motor efficiency, and the overall efficiency of the system can be obtained respectively from Eqs.3.3.28, 30, 32, 31, 33 and 34.

(d) Example

A LIM-driven PCP has a squared cross section of 1 m x 1 m dimensions, and a length of 5 km. A LIM of 0.92 m x 0.92 m cross section is used; the LIM should be less than 100 m long. The capsules are box shaped of 0.90 m width x 0.90 m height x 4 m length. Each capsule weighs 5 tonnes of which 3 tonnes are cargo (limestone) and 2 tonnes are the deadload. The capsules use steel wheels rolling on steel rails in the pipe, having a rolling friction coefficient of $\eta = 0.002$. The PCP system is to be designed for a capsule speed of 15 m/s in the pipe. The capsule injection rate (launching interval) at the inlet is one capsule in every 10 seconds. Calculate the key system properties of the PCP-LIM by following the steps outlined above.

[Solution] In each of the following steps, two determinations will be made, one for the **delivery** pipe with capsules full of cargoes weighing 5 tonnes each, and the other for the **return** pipe bringing empty capsule back. Both pipes are of the same length and cross-sectional area, but they need different LIMs—the LIM for the return pipe need not be as powerful because the returning capsules are empty and weigh less.

Step 1: Specify or calculate key parameters of pipe, LIM and capsule.

Delivery Pipe: A = 1m x 1m = 1 m^2, A' = 0.92m x 0.92m = 0.8464 m^2, A_c = 0.9m x 0.9m = 0.81 m^2, L = 5 km, L_c = 4 m, M_c = 5000 kg, V_c = 15 m/s, $\rho_c = M_c/(A_cL_c)$ = 1543 kg/m^3, ρ = 1.23 kg/m^3, $S = \rho_c/\rho$ = 1543.2/1.23 = 1255, $\nu = 1.46 \times 10^{-5}$ m^2/s, and $\eta = 0.002$, $C_L = 0$, $C_p = 0.8$, and g = 9.81 m/s^2.

Return Pipe: Same as delivery pipe except that M_c = 2000 kg, ρ_c = 617.3 kg/m^3, S = ρ_c/ρ = 501.9.

Step 2: Specify V_c.

V_c is specified to be 15 m/s for both the **delivery** and the **return** pipes.

Step 3: Use the equations in the Appendix to find V, F_D and C_D.

Delivery Pipe: From Eqs. I-5, I-6 and I-7 in Appendix I, we have respectively k = 0.9, b = 5.263, and a = 3.94. Therefore, Eqs. I-2, I-3 and I-4 yield, respectively,

$C_{21} = 27.5 + 574.4\ f_c$ ….…… (a)
$C_{22} = 516.9\ f_p$ …….. (b)
$C_{23} = 201.7$ …… (c)

Substituting (a), (b) and (c) into Eq. I-1 yields

$$(27.5 + 574.4\ f_c)\ (V - 15)^2 + (516.9\ f_p)\ (V-12.15)^2 = 201.7 \ldots. \text{(d)}$$

Since f_c and f_p are both functions of V, the above equation (d) can be solved by iteration as follows:

Iteration No. 1:

Assuming $f_c = f_p = 0.012$, equation (d) yields V = 16.54 m/s. Using this value of V in Eqs. I-8 and I-9 yields respectively $R_c = 6.26 \times 10^5$ and $R_p = 1.79 \times 10^5$. Then, assuming the roughness of the capsule wall surface and the roughness of the pipe interior are the same as the roughness of ordinary commercial steel pipe, Eqs. I-10 and I-11 yield respectively $\varepsilon_c = \varepsilon_p = 0.0004$. Therefore, from the Moody diagram in fluid mechanics, $f_c = 0.017$ and $f_p = 0.019$.

Iteration No. 2:

During this iteration, the values of f_c and f_p obtained at the end of the previous iteration are used, namely, $f_c = 0.017$ and $f_p = 0.019$. Substituting these values into (d) yields V = 16.12 m/s. Following the same approach in the previous iteration and using Moody diagram yields approximately the same f_c and f_p as obtained from the first iteration. Thus, it is clear from only two iterations that $f_c = 0.017$, $f_p = 0.019$ and V = 16.12 m/s.

In this problem, a = 3.94, b = 5.263, k = 0.9, A_c = 0.81, C_p = 0.8, $(V-V_c)$ = 1.12, and $(V-k^2V_c)$ = 3.97. Substituting these values into Eq. I-13 yields F_D = 100.4 N. Finally, Eq. I-14 yields C_D = 160.7.

To check the correctness of the above calculations, let's use C_D = 160.7 and V_c = 15 m/s to determine V from Eq.3.3.14. The result is:
$V = 15 + \sqrt{(2 \times 0.002 \times 5000 \times 9.81)/(160.7 \times 0.81 \times 1.23)} = 15 + 1.11 = 16.11$ m/s. The result is consistent with the solution of Eq.I-1 which is 16.12 m/s.

It may be of interest to compare the C_D value calculated above, 160.7, with the C_D calculated from Eq.3.3.20 for a capsule with two end disks, each having a value of k_d equal to 0.90. From Eq.3.3.20, C_D = 72.7, which shows that the correct drag coefficient for capsules

without end disks cannot be determined accurately from Eq.3.3.20, which is for capsules with end disks.

Return Pipe: For the return pipe, the results are the same except that C_{23} =80.58, and equation (d) becomes:

$$(27.5 + 574.4\ f_c)\ (V - 15)^2 + (516.9\ f_p)\ (V\text{-}12.15)^2 = 80.58\ldots.\ \text{(d)}$$

Assuming that $f_c = 0.017$ and $f_p = 0.019$ as in the delivery pipe, the above equation yields V =

Step 4: Specify T and calculate N.

Choosing T to be 10 seconds, Eq.3.3.1 yields $N = L/(TV_c) = 5000/(10 \times 15) = 33.3$. This means that under steady-state operation, there is an average of 33.3 capsules in the pipeline of 5 km length.

Step 5: Calculate the linefill rate α.

From Eq.3.3.3, the linefill rate is $\alpha = L_c/TV_c = 4/(10 \times 15) = 0.0267 = 2.67\%$. If T and V_c remains the same, by linking five capsules into a train the linefill will be increased five times to yield $\alpha = 0.1333 = 13.33\%$. This shows that the linefill can be increased significantly by linking capsules into a train and by injecting capsule trains instead of individual capsules.

Step 6: Calculate V' .

From Eq.3.3.5, $V' = AV/A' = (1\times1)\times16.11/(0.92\times0.92) = 19.03$ m/s.

Step 7: Select V'_c.

Somewhat arbitrarily, we select $V'_c = 2\ V_c = 2 \times 15 = 30$ m/s.

Step 8: Determine α'.

From Eq.3.3.3, $\alpha' = L_c/(TV'_c) = 4/(10\times30) = 0.01333 = 1.333\%$.

Step 9: Assume N'.

Assume that N' = 1.5. This means that on the average there will be 1.5 capsules in the LIM at any given time.

Step 10: Determine the length of the LIM, L'.

From Eq. 3.3.3, $L' = N'L_c/\alpha' = 1.5\times4.0/0.01333 = 450$ m. Since this is unacceptably long, it should be reduced by using capsule trains. By using trains of 5 capsules, the length of the LIM can be reduced by 5 times to L' = 450/5 = 90 m. To further reduce the LIM length, either the train length must be increased, or the injection interval of 10 seconds must be reduced, or both.

Step 11: Determine the total pressure drop along the PCP.

Under steady-state condition and the injection rate of one capsule in every 10 seconds, the total pressure drop along the 5-km-length PCP can be calculated as follows:
$\eta = 0.002$, N = 33.3, A= 1×1 = 1.0 m^2, D = 1.0 m, L = 5000 m, L_c = 4 m, $\rho = 1.23$ kg/m^3, V = 16.11 m/s, $R = DV/\nu = 1\times16.11/(1.46\times10^{-5}) = 1.10\times10^6$, $\varepsilon = 0.000046$. From Moody diagram, f = 0.0125. Thus, from Eq.3.3.21 the total pressure along the PCP is $\Delta p = 3270 + 9709 = 12{,}979$ Pa = 271 psf = 1.88 psi. Since this pressure drop is less than 14% of one atmospheric pressure, the assumption of incompressible flow used herein is accurate and permissible.

If the capsule injection rate is increased to one capsule train (of 5 capsules) per ten seconds, with the five times increase in capsules in the pipe and the LIM, the alternate results are: N = 166.7, and Eq.3.3.21 yields: $\Delta p = 16{,}350 + 8{,}645 = 25{,}000$ Pa = 522 psf = 3.62 psi. Since this is less than 25% of the atmospheric pressure, the incompressible flow assumption used in the calculations is still acceptable.

Step 12: Calculate the power consumed by the capsule-air flow through the PCP.

Using Eq.3.3.28, the power consumed by the capsule-air flow is $P = VA\Delta p = 16.11\times1.0\times12{,}979 = 209{,}100$ w = 209.1 kw. This is for the case of 1 capsule every 10 second. For the case of one train per 10 second (or 5 capsules in 10 seconds), $P = 16.11\times1.0\times25{,}000 = 402{,}750$ w = 402.8 kw.

Step 13: Calculate cargo throughput.

From Eq.3.3.2, for the case of injecting one capsule in every 10 seconds, n = 1/10 = 0.1. Then, from Eq.3.3.29 the cargo throughput is $T_h = nW = 0.1\times3000 = 300$ kg/s = 0.3 tonne/s = 1080 tones/hr = 25,920 tonnes/day = 9,331,000 tonnes/year-- based on 360 operating days per year. If, on the other hand, 5-capsule trains are injected at the rate of one train per 10 seconds, then the cargo throughput will be increased by 5 times, reaching 46.7 million tonnes/year, which is a huge throughput, bigger than produced at the largest mine in the world. Thus, using one capsule train per 10 seconds should be the upper limit for the cargo throughput of PCP-LIMs to be analyzed herein.

Step 14: Determine the thrust generated by the LIM on each capsule under steady-state operation.

Under steady-state condition and the injection rate of one capsule in every 10 seconds, the thrust generated by the LIM on each capsule, F_e, can be calculated from Eq.3.3.24 as follows: $\eta = \eta' = 0.002$, N = 33.3, N' = 1.5, $A = 1\times1 = 1.0$ m^2, $A' = 0.92\times0.92 = 0.8464$ m^2, D = 1.0 m, D' = 0.92 m, $\rho = 1.23$ kg/m^3, V = 16.11 m/s, $R = DV/\nu = 1\times16.11/(1.46\times10^{-5}) = 1.10\times10^6$, $R' = 19.03\times0.92/(1.46\times10^{-5}) = 1.20\times10^6$, $\varepsilon = 0.000046$, $\varepsilon' = 0.000050$, f = 0.0125, f ' = 0.0126. Thus, from Eq.3.3.24, $F_e = 8{,}064$ N, of which 1941 N is to overcome contact friction (wheel friction) and 6123 N is to overcome fluid resistance. The fluid resistance is much larger than the wheel friction due to the high velocity of the air (16.11 m/s in the pipe and 19.03 m/s in the LIM), and the low linefill rate (2.67%).

If the capsule injection rate is increased to one capsule train (of 5 capsules) per ten seconds, with the five times increase in capsules in the pipe and the LIM, the alternate results are: N = 166.7, N' = 7.5, and from Eq.3.3.24 $F_e = 2{,}934$ N, of which 1941 N is to overcome contact friction (wheel friction) and 993 N is to overcome fluid resistance. Note that this alternative of using 5-capsule trains is far better than the case of using single capsules in terms of LIM length, cargo throughput, energy efficiency for freight transport, and unit cost (namely, cost per ton of cargoes transported by this PCP). This ends the discussion of Example 1.

Step 15 & 16: Design a LIM that can generate the thrust force F_e on each capsule going through the LIM, and can generate the capsule velocity V_c in the pipe. Determine the Power and the efficiency of the LIM, and the efficiency of the overall system.

This part of the computation is described in Appendix III dealing with LIM design.

3.3.2. Electromagnetic Equations for LIM

The electromagnetic equations governing the design of the LIM used in PCP are derived in Appendix III. The Appendix also shows through an example how to use the equations to analyze the performance of the LIM such as the thrust, power and efficiency that the LIM can generate as a function of capsule speed going through the LIM, and the effect of the tooth-width-to-tooth-spacing ratio of the LIM on the LIM performance. These equations along with the fluid mechanics equations presented in the previous subsection will then be used together to predict the performance of the special PCP system for transporting minerals and mine wastes designed in Section 2 Rail-in-Tube System Design. General literature on LIM is given in [11-13]; specific technical literature on designing LIMs for PCP is given in [14-19].

3.4 Prediction of Steady-State Behavior of PCP System Driven by LIM

The LIM-driven PCP system to be analyzed here is the same system designed in Sec. 2, using tubes (rectangular conduits) of 1m x 1m cross-section, capsules of 1.905m length, 0.949m width, 0.679m height, and ASCE 60-lb rails of gage 24. The system parameters used in the design are summarized in Table 3.1. In all cases, there are 5 capsules per train, and unless otherwise specified, the pipe length is 10,000 m. Note that the behavior of the LIM-driven PCP system includes both a delivery line containing loaded capsules, and a returning line containing empty capsules. The two lines must be analyzed separately.

Table 3.1-Assumed parameters in the PCP system analysis

item	symbol	value	units
pipe cross–sectional area	A	0.992	m^2
LIM cross–sectional area	A'	0.932	m^2
wall roughness	e	4.57×10^{-5}	m
capsule payload volume		1.133	m^3
unit weight of payload	γ	31,420	N/m^3
empty weight of capsule		13,167	N
capsule cross–sectional area	A_c	0.705	m^2
end disk area in LIM	A'_d	0.900	m^2
end disk area in pipe	A_d	0.918	m^2
capsule rolling friction	η	0.002	
air density	ρ	1.23	kg/m^3
kinematics viscosity	ν	1.46×10^{-5}	m^2/s

(a) Delivery line with loaded capsules

As a practical matter, the LIM-driven PCP system was analyzed for the throughput range between 2 MTY (million tonnes per year) and 50 MTY. The lower limit of 2 MTY corresponds to the lowest throughput that this size of conduit, capsule and rails should be used. At any throughput smaller than this value, one should use a smaller conduit, smaller capsules and smaller rails if any, to be more practical (economical). The highest throughput of 50 MTY is not limited by the capability of the PCP system because the system can handle much larger than 50 MTY if necessary. This higher limit is used because it corresponds to the largest single-mine throughput in the world. It seems pointless to make any analysis at present for operating this

system at throughputs beyond what is needed by even the largest single mine in the world, such as the largest coal mine in the Powder-River Basin of Wyoming. Should there ever be a need for using a single PCP system to transport coal (or another mineral) from a cluster of largest mines in lieu of using an ordinary railroad system to do the same, the analysis made in this report can easily be extended to transport more than 50 MTY, or even 100 MTY. This is so because even at 100 MTY this PCP system will be operating at only about 20% linefill.

Most of the graphs presented in this section are for a pipe length, L, of 10,000 m, and for LIM length, L', of 100, 200, 300, 400 and 500 m. These values corresponds to L'/ L = 0.01, 0.02, 0.03, 0.04 and 0.05. Unless otherwise specified, L = 10,000 m or 10 km.

Given the parameters in Table 3.1, L'/ L, L, throughput, and a value for V_c, it is possible to calculate the capsule velocity in the LIM, V_c', the LIM force (thrust) per capsule, F_e, the power output of the LIM (given by Eq.3.3.30), and the LIM-pump efficiency, E_P. All these can be done without designing the LIM. Fortunately, V_c can have a range of acceptable values and hence can be used as a variable to investigate its effects on, F_e, E_P, etc. Calculations have shown that the E_P increases with increasing V_c until a maximum is reached. Thereafter, E_P decreases as V_c continues to increase. However, for a throughput greater than about 13.4 MTY (million tonnes per year), the maximum pump efficiency E_P occurs at V_c greater than 15 m/s. Practical considerations of the rail system suggest that V_c should be restricted to 15 m/s. With this restriction, the maximum LIM-pump efficiency E_P sometimes occurs for V_c < 15 m/s but, for large throughput it occurs at V_c = 15 m/s. Figure 3.4.1 illustrates this point. For L'/ L = 0.01 the maximum value of the efficiency occurs at V_c = 15 m/s for throughput greater than 13.4 MTY. Similarly for L'/ L = 0.05 the maximum efficiency occurs at V_c = 15 m/s for throughputs greater than 19.5 MTY.

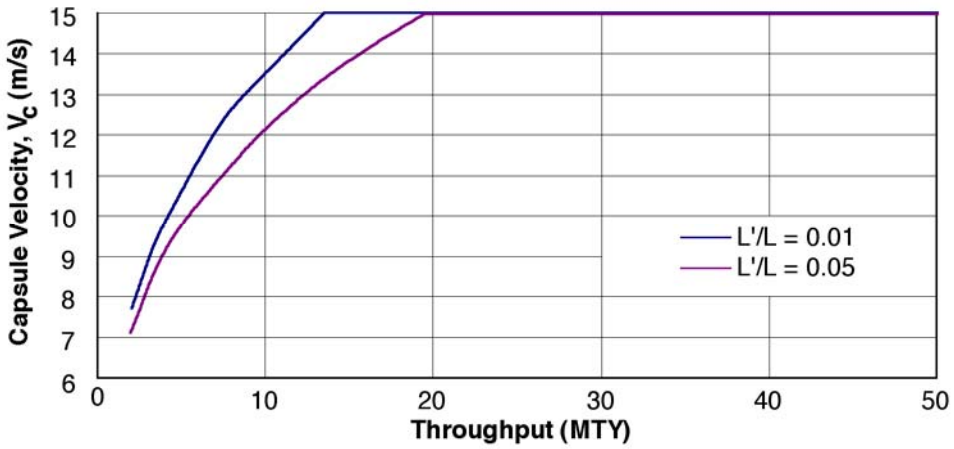

Figure 3.4.1- Capsule velocity V_c at maximum LIM efficiency for L =10,000 m (delivery line)

Figure 3.4.2 shows the maximum LIM-Pump efficiency under the restriction $V_c \leq 15$ m. It can be seen from the figure that L'/ L is an important parameter for the pump efficiency. Generally, the larger the values of L'/ L is, the more efficient the LIM pump becomes. A more

efficient LIM means saving of electrical power used by the system, and hence saving of operational cost. However, as L'/ L increases, the length of the LIM pump increases for a given length of the pipe or conduit, and hence the cost of the LIM (capital cost) will increases. In each case, one must compare the saving of operational cost with the increase in capital cost to determine what the best L'/ L is. The optimum L'/ L can be found through a life-cycle cost analysis of the system.

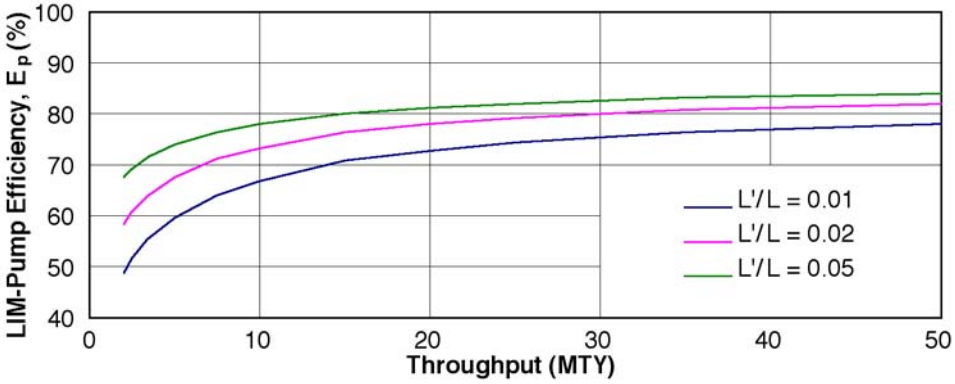

Figure 3.4.2 – Variation of maximum LIM-pump efficiency with throughput and L'/ L for L = 10,000 m (delivery line)

The design of the LIM motor units that make up the LIM section requires the velocity of the capsules in the LIM section, V_c', and the LIM force per capsule, F_e. Shown in Fig.3.4.3 are values of V_c' corresponding to maximum efficiency with the restriction $V_c \leq 15$ m/s. The abrupt change in slope of the curves shown in Fig.3.4.3 is due to the restriction $V_c \leq 15$ m. For point to the left of the abrupt change in slope, the capsule velocity V_c is less than 15 m/s. For points to the right of the change, V_c is equal to15 m/s. In Figure 3.4.3 all values of V_c' exceed V_c.

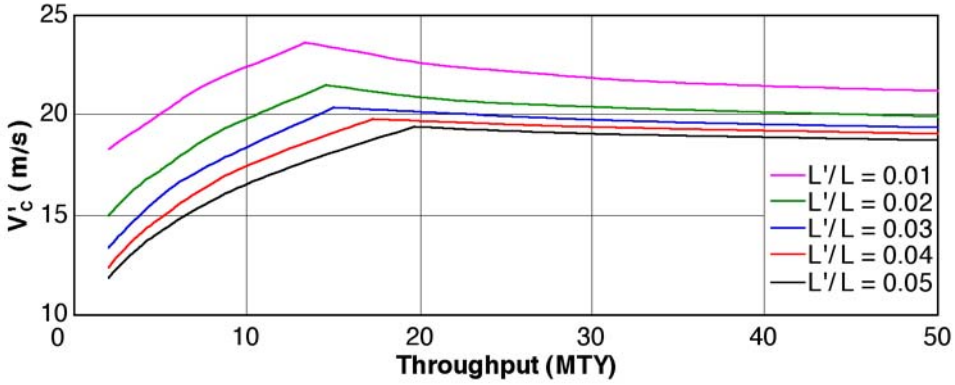

Figure 3.4.3 Variation of capsule velocity in LIM with throughput and L'/ L (delivery line)

Figure 3.4.4 shows the LIM force (thrust) on each side of a capsule, F_L. Since there is a LIM on either side of the capsule, the LIM force per capsule is $F_e = 2F_L$. The figure shows that for fixed L'/ L, F_L decreases with increasing throughput. This does not mean however, that the total LIM force on all capsules in the LIM decreases with increasing throughput. Indeed, the opposite is true. The total LIM force increases with increasing throughput, but not as rapidly as

the number of capsules in the LIM section. Hence, as the throughput increases, the LIM force on each side of any capsule in the pipe or conduit decreases.

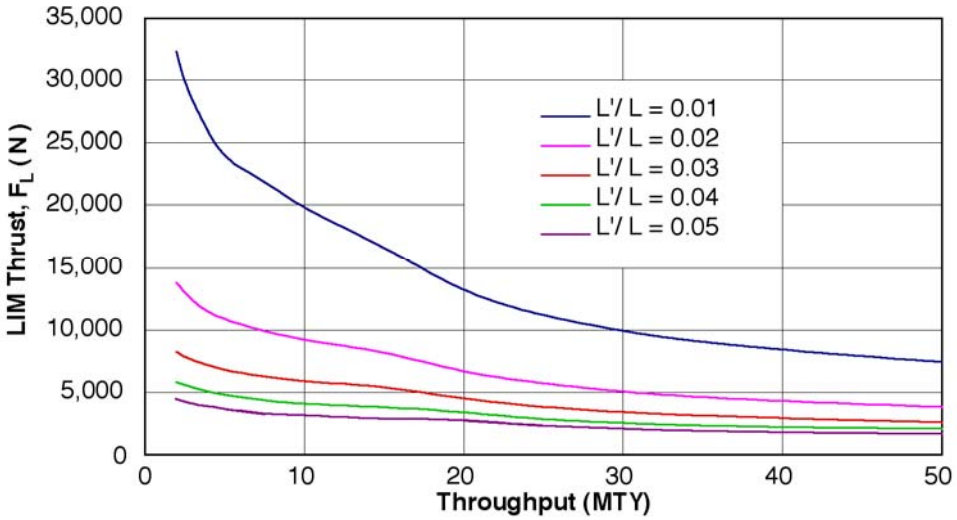

Figure 3.4.4 Variation of LIM force on each side of capsule as a function of throughput and L'/ L (delivery line)

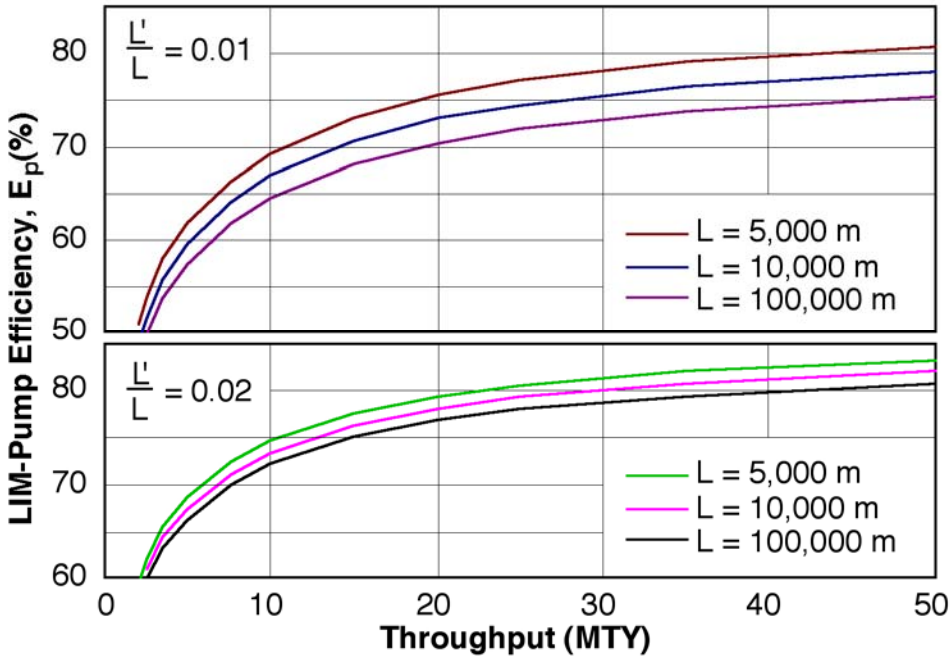

Figure 3.4.5 Variation of maximum LIM pump efficiency with throughput, L and L' /L (delivery line)

Figure 3.4.5 shows the maximum LIM-pump efficiency for three different pipe lengths and for L'/ L equal to 0.01 and 0.02. It can be seen that increasing the pipe length while holding L '/ L

constant decreases the maximum LIM pump efficiency. However, there is only about a 5% reduction in efficiency for a twenty fold increase in pipe length for L'/ L = 0.01 and only about a 3% reduction for L'/ L = 0.02. One can expect similar results for other values of L'/ L.

Note that Figs.3.4.2 and 3.4.5 give the LIM-pump efficiency, E_P, which is calculated from the fluid mechanics equations. On the other hand, to get the LIM-motor efficiency (simply called "LIM efficiency," E_L, one must use the electromagnetic equations given in Appendix III to design a LIM for each case, which is quite involved. However, this has been done based on an assumed slip of 5% for all cases, and the result of E_L as a function of throughput is given in Fig.3.4.6. As can be seen from Fig.3.4.6, the LIM motor efficiency E_L decreases as the ratio L'/ L increases. This is due to the fact that as the LIM length increases, the force or thrust needed from each unit of LIM decreases, causing a decrease in the capsule velocity in the LIM, which in turn causes a large slip (see Eq.III-2) and a small efficiency. Also, as the throughput decreases to below 15 MTY, the capsule velocity in LIM decreases with the decreasing throughput, which in turn increases slip and decreases LIM-motor efficiency. For most of the cases, the LIM efficiency is in the range of 85 to 90%, which is rather impressive. This is due to the good design of the various LIMs studied herein.

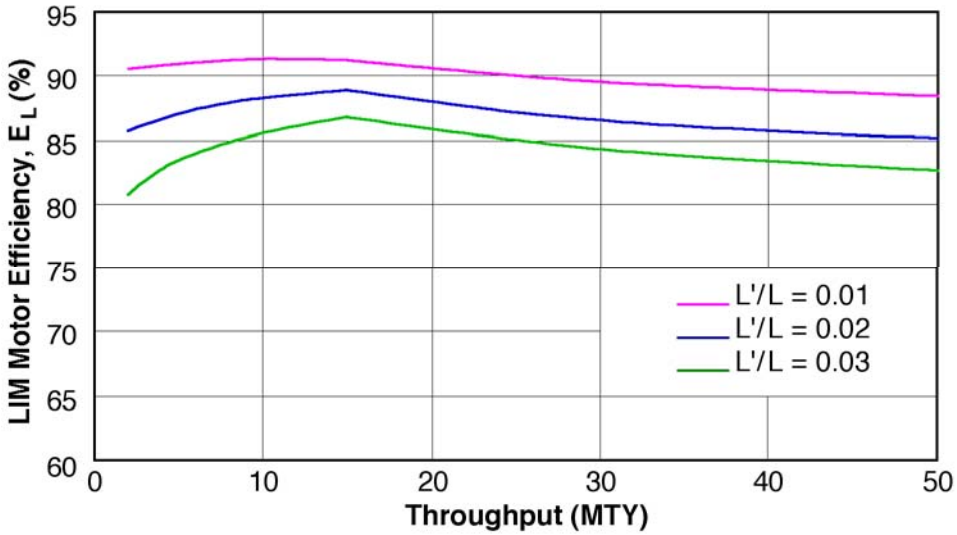

Figure 3.4.6 Variation of LIM motor efficiency with throughput of the PCP (delivery line)

As shown in Eq.3.3.34, the product of E_L and E_P yields the total system efficiency which is plotted in Fig.3.4.7. It can be seen that the system efficiency for the delivery line can be as high as 70% for large throughput, and it decreases rapidly with throughput decrease as the throughput is less than about 20 MTY. At throughput of 2 MTY, the system efficiency decreases to 50% when L'/ L is 0.02 or 0.03, and to 45% when L'/ L is 0.01.

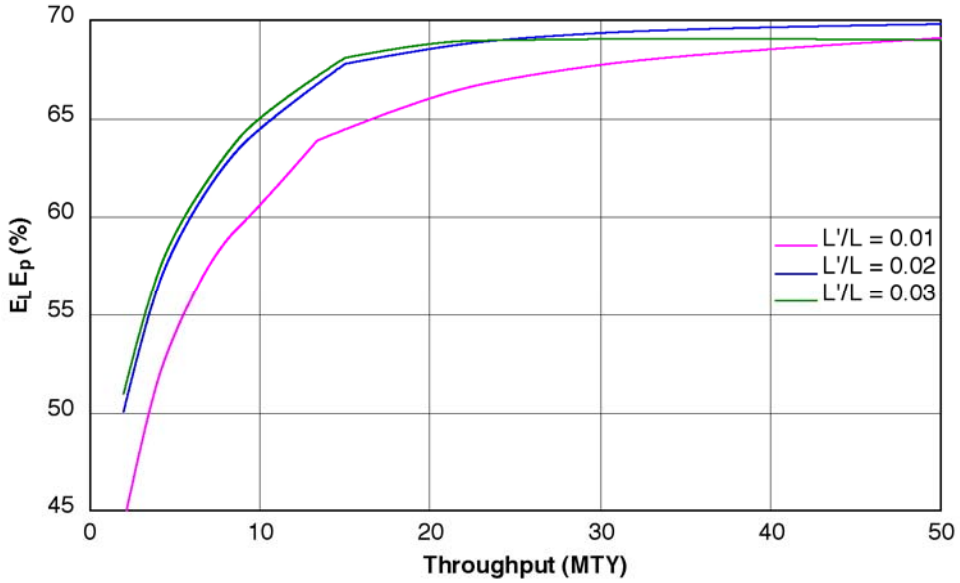

Figure 3.4.7 Variation of system efficiency ($E_P E_L$) with throughput of PCP for different L'/ L (delivery line)

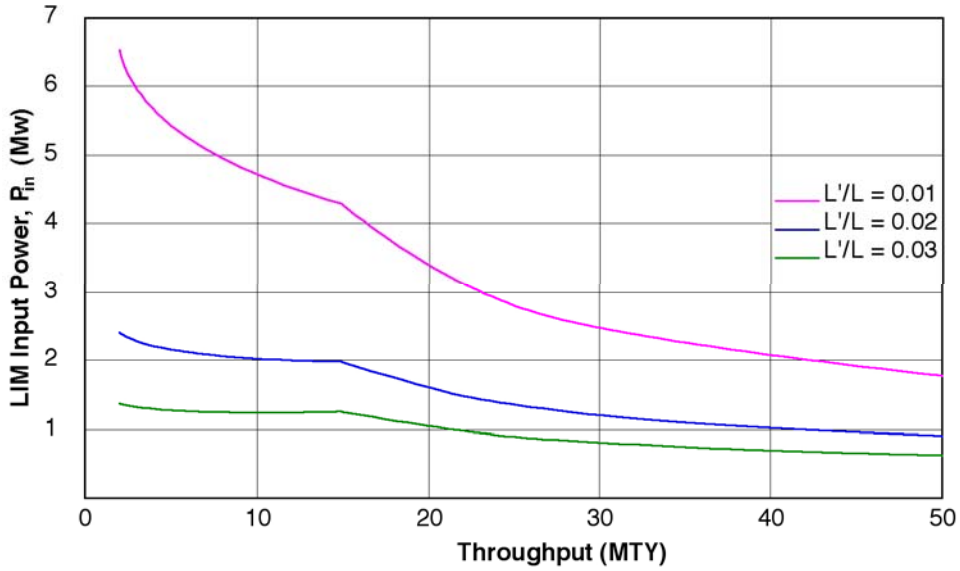

Figure 3.4.8 Power input of the LIM-driven PCP (delivery line)

The power input, P_{in}, to the delivery line of the LIM-driven PCP system is given in Fig.3.4.8. Note that this power is the average power to drive the PCP system during the time when capsules are present in the LIM. When there is no capsule in the LIM, the power electronic switching circuit cuts off the power to the LIM, resulting in zero power. Thus, the long-time average input power is $P_{in}\alpha$', where α' is the linefill rate in the LIM. From Fig.3.4.8, it can be seen that the longer the LIM is (i.e., the larger the ratio L'/ L is), the smaller is the input power of the LIM. This is caused by the fact that a longer LIM has more capsules in it over a longer time,

therefore requiring less power to do the same work. Also, Fig.3.4.8 shows that generally, the LIM input power increases with decreasing throughput. This is due to the decreased time that capsules are in the LIM for small throughputs. Larger power is required to drive the PCP system when the time for the LIM to push the capsules is short.

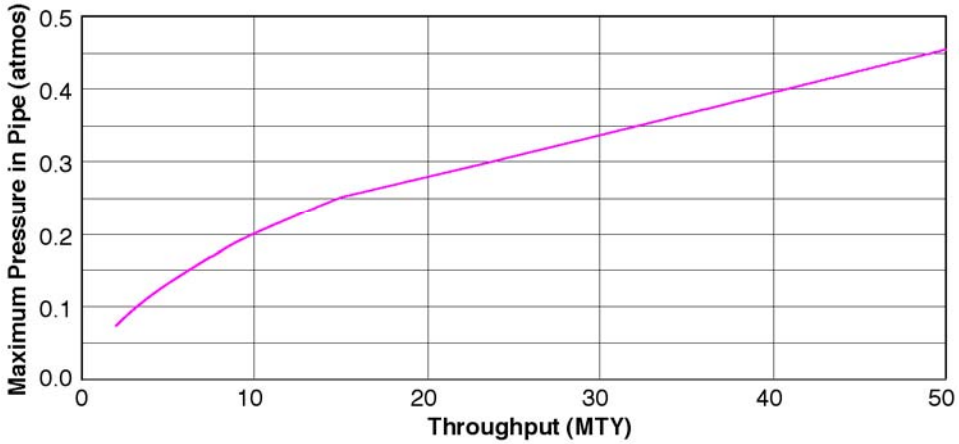

Figure 3.4.9 Maximum pressure in the PCP conduit and LIM (delivery line)

Finally, it is desirable to determine the total pressure drop, Δp, along the PCP conduit between the LIM outlet where the pressure is the highest (i.e., the pump pressure) and the outlet of the conduit where the pressure is the lowest (atmospheric). Since the gage pressure at the conduit outlet is zero (atmospheric), Δp also gives the highest gage pressure of the air in the conduit. It also sets the upper limit of the pressure in the LIM – near the outlet of the LIM. Figure 3.4.9 gives this highest gage pressure in terms of atmospheric pressure, which has an absolute pressure (above vacuum) of 14.7 psia. If the maximum pressure is one atmosphere, it means that the pressure is 14.7 psia above the atmospheric pressure and so forth. From Figure 3.4.9, it can be seen that the higher the throughput, the larger Δp becomes. For the maximum throughput of 50 MTY, this maximum pressure is only 0.45 atmosphere or 6.6 psi gage pressure. The relative smallness of this maximum pressure is a relief. It means that the conduit and the LIM can both be designed for a rather small internal pressure of 6.6 psig, which is manageable. Had the pressure been much larger, a very thick conduit wall would be needed, making the system costly.

(b) Return line with empty capsules

The dimensions of the LIM and the pipe (conduit) for the return line are the same as that for the delivery line, but the weights of the capsules in the two cases are quite different. Due to the lightness of the capsules in the return line, the LIM for the return line does not need to deliver as much thrust as that of the delivery line. The analysis of the behavior of the return line is similar to that for the delivery system. The LIM-pump efficiency is optimized with respect to V_c with the restriction $V_c \leq 15$ m/s.

Figure 3.4.10 gives the capsule velocity at maximum LIM-pump efficiency for various throughputs of the return line; it is a figure similar to Figure 3.4.1 for the delivery line. Note that

the throughput in Fig.3.4.10 is really the throughput of the delivery line instead of that of the return line. However, since the same number of capsules that pass through the delivery line in a year must pass through the return line in a year, the delivery line throughput is used to designate the throughput of the return line. As with the delivery line, the capsule speed in the return line is limited to15 m/s. The figure shows that for L'/L = 0.03, the optimum capsule velocity is less than 15 m/s over the entire throughput range up to 50 MTY, whereas for L'/L = 0.01 the optimum capsule velocity is less than 15 m/s only for throughputs up to 46.5 MTY. Comparison of Fig.3.4.10 with Fig.3.4.1 shows that for any given throughput, the train velocity is higher in the delivery line than in the return line.

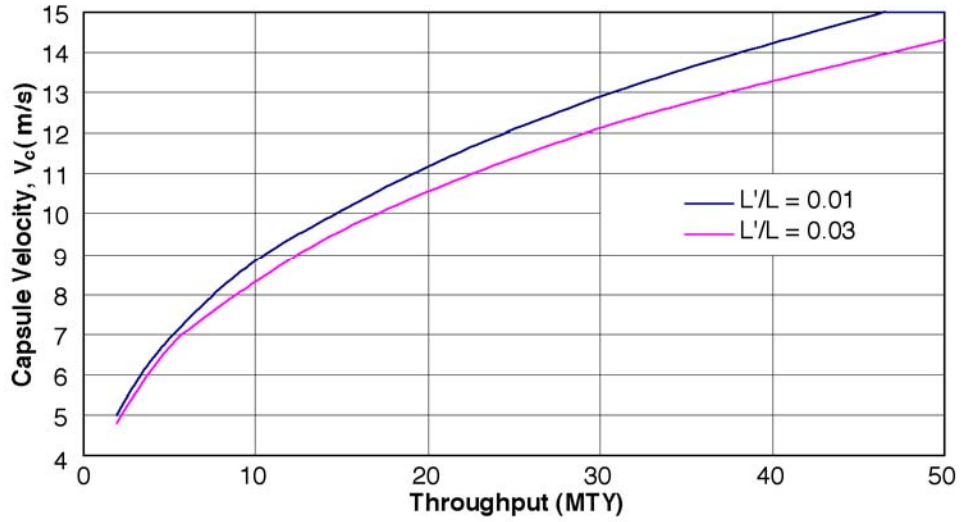

Figure 3.4.10 Capsule velocity V_c at maximum LIM efficiency for L =10,000 m (return line)

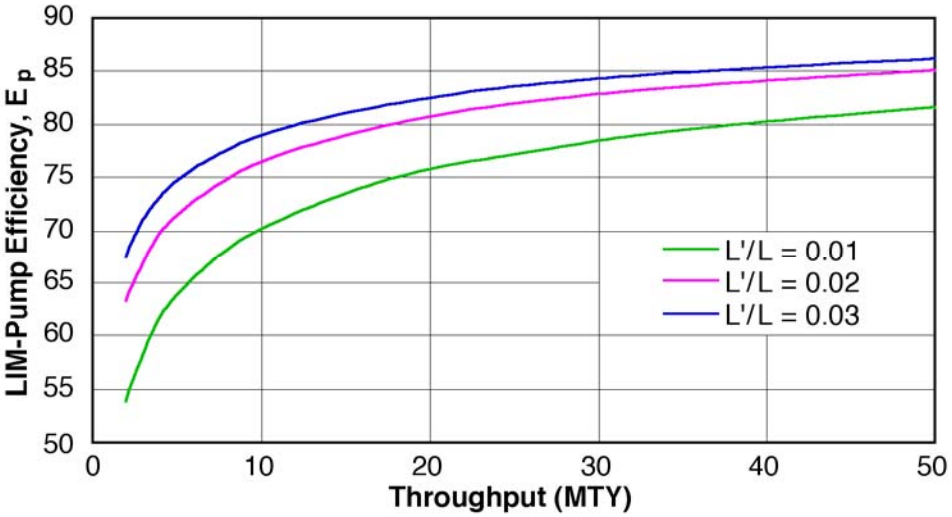

Figure 3.4.11 Maximum LIM-pump efficiency (return line)

Shown in Fig. 3.4.11 is the maximum LIM-pump efficiency with the restriction $V_c \leq 15$ m/s for the return line, the same restriction used for the delivery line. Comparing Fig.3.4.11 with Fig.3.4.2 shows that the maximum LIM-pump efficiency for the return line is somewhat better than for the delivery line at any given throughput. The reason for this increase in pump efficiency is probably due to the smaller velocity used in the return line than the delivery line. Smaller velocities generates less energy loss (head loss), therefore making the pumping action more efficient.

Figure 3.4.12 shows the capsule velocity in the LIM of the return line corresponding to maximum LIM pump efficiency. Comparing this figure with Fig.3.4.3 shows that the optimum capsule velocities in the LIM are lower for the return line than for the delivery line. While the restriction $V_c \leq 15$ m/s creates the abrupt change in slope for all of the three curves in Fig. 3.4.3, an abrupt change in slope occurs in Fig.3.4.12 only in the uppermost curve (for L'/L = 0.01).

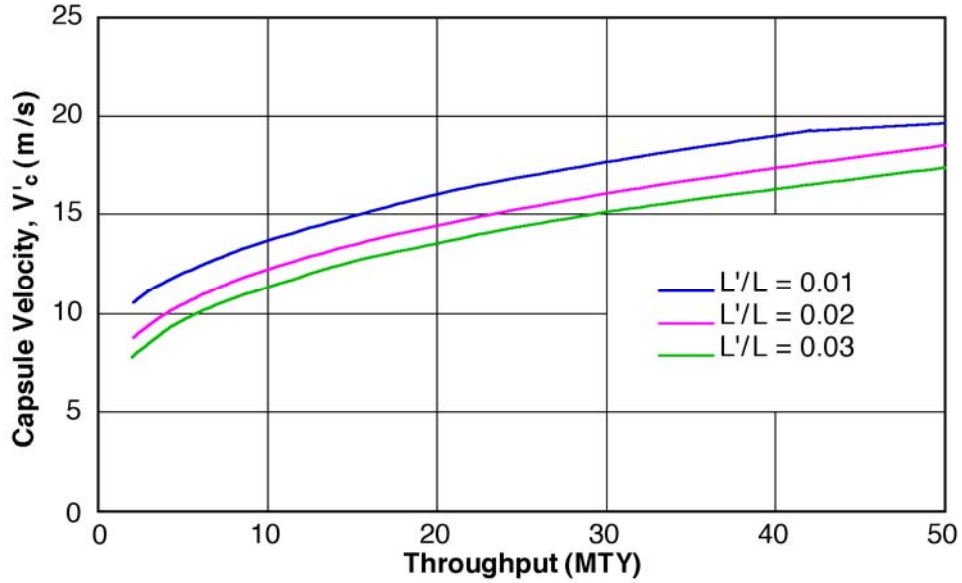

Figure 3.4.12 Variation of capsule velocity in LIM section with throughput and L'/L (return line)

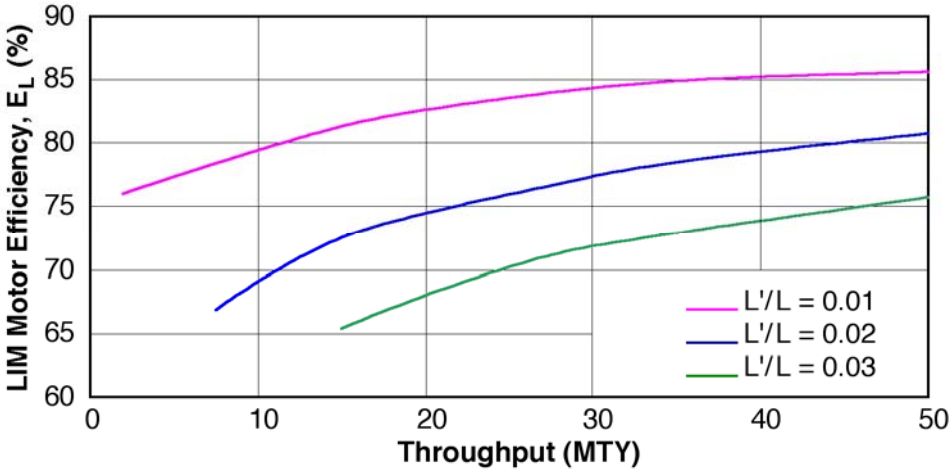

Figure 3.4.13 LIM-motor efficiency as a function of throughput and L'/L (return line)

Figure 3.4.13 gives the LIM-motor efficiency of the return line as a function of throughput and L'/L. From the figure, it can be seen that the motor efficiency decreases as L'/L increases. This is consistent with the LIM-motor efficiency of the delivery line given in Fig.3.4.6. Comparison of Fig.3.4.13 with Fig.3.4.6 shows that the motor efficiency of the return line is generally smaller than that of the delivery line for the same throughput and L'/L. The smaller efficiency is a result of the smaller capsule velocity used in return line than the delivery line—smaller capsule velocity always makes the LIM less efficient.

The PCP system efficiency for the return line, which is the product,$E_L E_P$, is given in Fig.3.4.14 as a function of the throughput and L'/L. For the same reason given to the delivery line, the system efficiency increases with the cargo throughput, and increases with decreased L'/L.

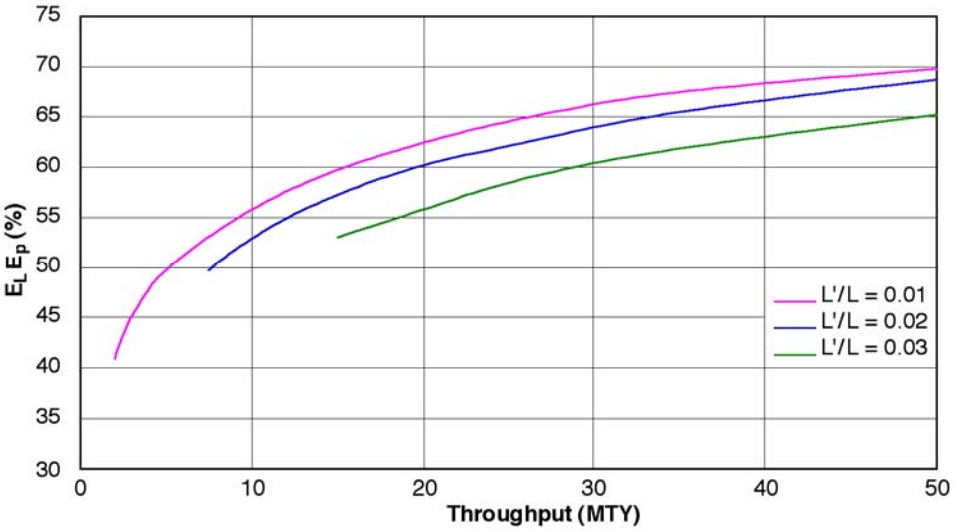

Figure 3.4.14 PCP system efficiency ($E_L E_P$) as a function of throughput and L'/L (return line)

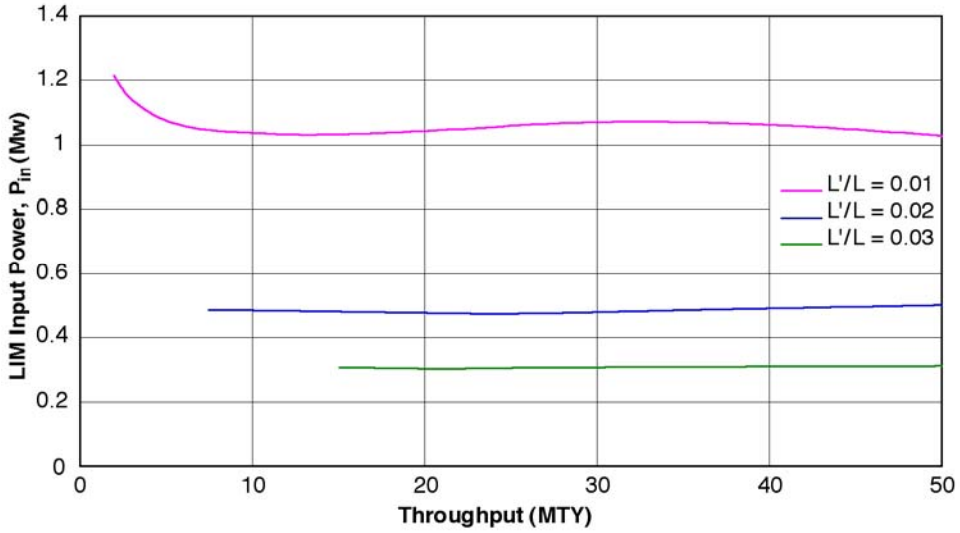

Figure 3.4.15 Power input of LIM-driven PCP while train is in LIM (return line)

The input power to the LIM-driven PCP system is plotted in Fig.3.4.15 as a function of throughput and L'/L. As can be seen from the figure, the power is approximately constant with the throughput, but it increases significantly with decreasing L'/L.

Finally, the total pressure drop in the PCP return line, Δp, which is also the maximum pressure in the PCP conduit and the LIM of the return line, is given in Fig.3.4.16. As expected, the maximum pressure in the return line is significantly lower than that in the delivery line. This is due to the fact that the capsules in the return line are empty and hence have a much smaller weight than the loaded capsules in the delivery line. Smaller weight generates smaller contact friction, which requires less pressure to overcome.

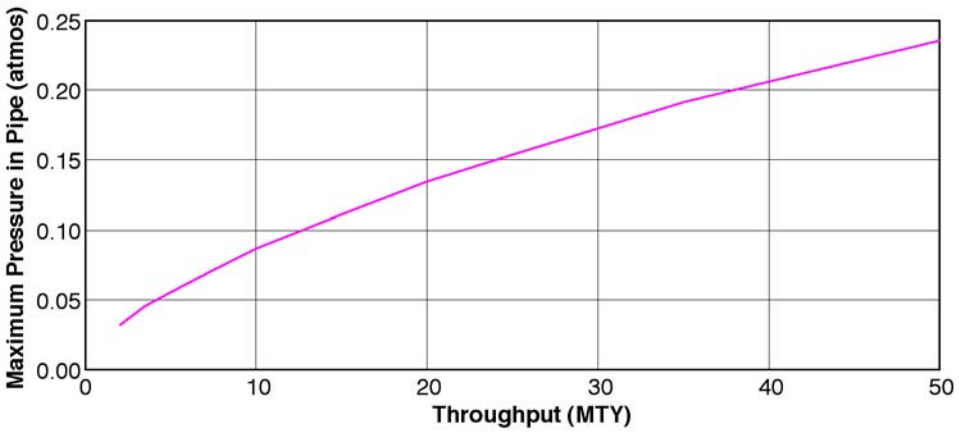

Figure 3.4.16 Maximum pressure in PCP conduit and LIM as a function of throughput for L'/L = 0.01 and L = 10,000 km (return line)

3.5 Prediction of Unsteady (Transient) Behavior of PCP Driven by LIM

(a) Derivation of equations

The steady-state theory of capsule trains considered in the previous section is for the case when the capsule flow has started for a long time, the pipeline or conduit is filled with capsules at a constant linefill, and the velocity of the air V and the capsule velocity V_c in the pipe are both constant (i.e., not a function of time). While analyzing the steady case is the most important for the design of the PCP system, there are also important unsteady flow problems that must be analyzed, such as what happens initially with the system during startup, how long will it take for the flow to reach the steady state, etc. To answer these questions will require unsteady or transient analysis of the capsule flow, which is to be considered in this section.

To simplify the unsteady flow analysis, it is assumed that the LIM and pipe (or conduit) are horizontal, and that the flow of air though the LIM and pipe is incompressible. Each train has an x-coordinate measured from the entrance of the LIM to the end disk of the lead car. Hence, for negative x the complete train will be located upstream of the LIM entrance. For x = 0, the end disk of the lead car will be at the LIM entrance. As in the foregoing description, L is the pipe (conduit) length, and L' is the capsule length. For x = L' the train will be in the LIM with lead car about to leave the LIM and enter the pipe. For x = L'+L the train will be in the pipe with the lead car about to exit the pipe.

For the purpose of computer coding, trains approach the entrance of the LIM at a constant speed V_o (no train acceleration), with spacing between trains consistent with V_o and the launching time interval T. Moreover, after a train has exited the pipe downstream, it will continue to move without acceleration. These simplifying approximations allows the total number of trains to remain fixed during program execution, thereby removing the need to code the creation of new trains to enter the LIM and destroying old trains that exit the pipe.

For trains entering the LIM, in the LIM, entering the pipe, in the pipe or exiting the pipe, the acceleration is calculated from the Newton's second law as follows:

$$\sum_{i=1}^{n} F_D + \sum_{i=1}^{n} F_L - n\, W_c\, \eta = 1.033\, n\, \frac{W_c}{g}\, \frac{dV_c}{dt} \qquad \ldots\ldots\ldots \quad (3.5.1)$$

In the above equation, F_D and F_L are the drag and LIM forces on individual cars of the train, and n is the number of cars in the train. Term W_c is the gross weight of each car, η is the coefficient of rolling resistance, and V_c is the train velocity. The coefficient 1.033 is a correction factor for the angular acceleration of the four wheels.

Equation 3.5.1 is used to calculate train acceleration whenever the train or any part of it is in the system consisting of the LIM and the pipe. If the train is totally outside the system, Eq.3.5.1 is not used, and the train acceleration is set to equal zero. The drag forces F_D in the equation may be either positive (in the x direction) or negative (in the minus x direction). The sign of these drag forces depend upon the train velocity V_c and the air velocity V' = Q/A' in the LIM, or the air velocity V = Q/A in the pipe. Term Q is the volumetric rate of the air flow. For a train in the LIM, the train velocity, V_c, is larger than the air velocity V ', and the drag forces will be negative. For a train in the pipe, the train velocity V_c is likely less that the air velocity V, and the drag forces will be positive.

The LIM force F_L in Eq.3.5.1 is either positive or zero, except in the unlikely event that V_c exceeds the synchronous speed of the LIM. Note that if x and V_c are known for a train and if the air discharge Q is known, then it is possible to calculate the train acceleration from Eq.3.5.1.

Equation 3.5.1 is used to calculate dV_c/dt for each train. A method is needed to calculate dQ/dt, where Q is the volume rate of the air flow through the system.

A control volume is shown in Fig.3.5.1 as a blue dashed line. This control volume is drawn inside the LIM and pipe sections next to the wall as show. External forces acting on this control volume are LIM and rolling resistance forces, and the force due to fluid shear, τ_p , between the moving air and the pipe walls. The left and right ends of the control volume are in contact with the atmosphere.

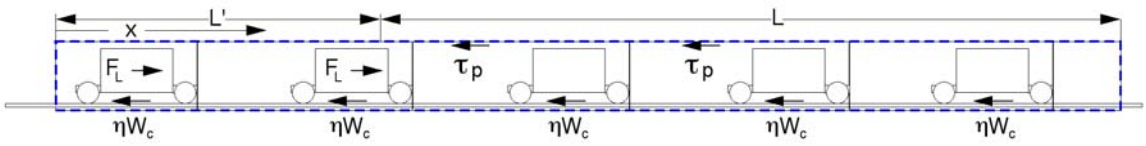

Figure 3.5.1 Control volume of LIM and pipe system

Applying the linear momentum equation to the control volume yields:

$$\sum_{i=1}^{N_L} F_L - (N_L + N_p) W_c \eta - \int_0^{L+L'} \pi d \tau_p \, dx = \int_{cs} \rho V_x \vec{V} \bullet \overrightarrow{dA} + \frac{d}{dt} \int_{cv} \rho V_x \, d\forall \qquad \ldots\ldots \quad (3.5.2)$$

In Eq.3.5.2, terms N_L and N_P are respectively the number of cars in the LIM and the number of cars in the pipe. These terms do not always take integer values because one car can be partly in the LIM and partly in the pipe at the same time. For example, N_L may be 5.25. This value would indicate that there are 5 capsules completely in the LIM and a sixth capsule is 25% in the LIM and 75% in the pipe. Should N_L and N_P have non-integer values, then they are rounded up for the purpose of evaluating the summation index i.

As a capsule enters the LIM, the term N_L will increase in value linearly according to how much of the car is in the LIM and how much is still outside. Similarly, as capsules leave the pipe, N_P decreases in value linearly according to how much of the capsule is in the pipe and how much is outside. For the moment however, we have assume there are no capsules entering or leaving the system.

The term d in the integral on the left side of Eq.3.5.2 is the equivalent diameter of the LIM or pipe, i.e., it takes the value D' for positions in the LIM and D for positions in the pipe. The last term on the right side of the equation is the rate of change of the total linear momentum in the control volume. This term works out to be

$$\frac{d}{dt} \int_{cv} V_x \rho \, d\forall = \rho (L' + L) \frac{dQ}{dt} + \left(\frac{W_c}{g} - \rho A_c L_c \right) \sum_{i=1}^{N_L + N_p} \frac{dV_{c,i}}{dt} \qquad \ldots\ldots. \quad (3.5.3)$$

The first term on the right side of Eq.3.5.2 works out to be

$$\int_{cs} V_x \rho \vec{V} \bullet \overrightarrow{dA} = \rho Q (V - V') \qquad \ldots\ldots\ldots\ldots.. \quad (3.5.4)$$

Combining the two above equations with Eq.3.5.2 gives

$$\sum_{i=1}^{N_L} F_L - (N_L + N_p) W_c \eta - \int_0^{L+L'} \pi d \tau_p \, dx = \rho Q (V - V') + \rho (L' + L) \frac{dQ}{dt} + \sum_{i=1}^{N_L + N_p} \left[\frac{W_c}{g} - \rho A_c L_c \right] \frac{dV_{c,i}}{dt} \qquad \ldots\ldots.(3.5.5)$$

Equation 3.5.5 can be used to evaluate dQ/dt when there are no capsules entering or leaving the system. We will now investigate the changes needed for the equation in to allow capsules to enter and leave the system.

Consider the case of a single capsule entering the LIM as shown in Figure 3.5.2.

Figure 3.5.2 Single capsule entering system

Evaluating the right side of Eq. 3.5.2 for a single capsule entering the LIM yields

$$\int_{cs} V_x \rho \vec{V} \bullet \vec{dA} + \frac{d}{dt}\int_{cv} V_x \rho \, d\forall = \frac{dV_c}{dt}\frac{z}{L_c}\left(\frac{W_c}{g} - A_c \rho L_c\right) + \rho \frac{dQ}{dt}(L + L') + \rho Q (V - V_1) + \rho V_c A_c (V_1 - V_c) \quad \ldots (3.5.6)$$

in which V_1 is the fluid velocity in the annular region between the car and the LIM wall given by

$$V_1 = \frac{Q - V_c A_c}{A' - A_c} \qquad \ldots\ldots\ldots\ldots\ldots \quad (3.5.7)$$

Comparing the right sides of Eqs.3.5.5 and 3.5.6, one can take $N_L = z / L_c$ and the two expressions would be in agreement if the term $\rho Q(V - V')$ is replaced by the term

$\rho Q (V - V_1) + \rho V_c A_c (V_1 - V_c)$.

Other cases of capsules entering and leaving the LIM and pipe have been investigated. To account for capsules entering and leaving the system, Eq.3.5.5 is modified as follows:

$$\sum_{i=1}^{N_L} F_L - (N_L + N_p) W_c \eta - \int_0^{L+L'} \pi d \, \tau_p \, dx = \rho (L' + L)\frac{dQ}{dt} + \sum_{i=1}^{N_L + N_p}\left[\frac{W_c}{g} - \rho A_c L_c\right]\frac{dV_{c,i}}{dt} + \text{term} \quad \ldots\ldots \quad .(3.5.8)$$

in which we have:

term = $\rho Q (V - V')$ when no capsule is entering or leaving;

term = $\rho Q (V - V_1) - \rho V_c A_c (V_c - V_1)$ for a capsule entering but no capsule leaving;

term = $\rho Q (V_2 - V') + \rho V_c A_c (V_c - V_2)$ for a capsule leaving but no capsule entering; and

term = $\rho Q (V_{2,2} - V_{1,1}) - \rho V_c A_{c,1} (V_{c,1} - V_{1,1}) + \rho V_c A_{c,2} (V_{c,2} - V_{2,2})$ for a capsule entering and a capsule leaving.

Note that terms $V_{c,1}$ and $V_{c,2}$ are respectively the velocity of the capsule entering and the capsule leaving the system. Terms V_1, V_2, $V_{1,1}$ and $V_{2,2}$ are given by

$$V_1 = \frac{Q - V_c A_c}{A' - A_c} \qquad V_{1,1} = \frac{Q - V_{c,1} A_c}{A' - A_c}$$

$$V_2 = \frac{Q - V_c A_c}{A - A_c} \qquad V_{2,2} = \frac{Q - V_{c,2} A_c}{A - A_c} \qquad \text{…….. (3.5.9)}$$

(b) Numerical procedure

To simulate the movement of N_t trains through the LIM and pipe system, the trains are numbered sequentially with the lead train being number 1. Each train has an x-coordinate x_i and a velocity $V_{c,i}$, where i = 1 … N_t . The discharge (volumetric flow rate) of air through the system is Q. Knowing the coordinates x_i , the velocities $V_{c,i}$ where i = 1 … N_t, and the discharge Q at any time t, it is possible to calculate the derivatives $dV_{c,i}/dt$ from Eq.3.5.1, and to calculate dQ/dt from Eq.3.5.8. The coordinate derivatives are equal to the train velocities (i.e., $dx_i/dt = V_{c,i}$). Thus, simulation requires the solution of $2N_t + 1$ simultaneous first-order differential equations. In matrix notation we have the following:

$$\frac{d\mathbf{Z}}{dt} = \mathbf{F}(t, \{ \mathbf{Z} \}) \qquad \text{where} \qquad \mathbf{Z} = \begin{bmatrix} V_{c,1} \\ V_{c,2} \\ \bullet\bullet\bullet \\ V_{c,Nt} \\ x_1 \\ x_2 \\ \bullet\bullet\bullet \\ x_{Nt} \\ Q \end{bmatrix} \qquad \text{…. (3.5.10)}$$

Term **Z** is a column matrix with the first N_t rows containing the train velocities, and the second N_t rows containing the train displacements. Row number $2N_t + 1$ contains the discharge.

Term { **Z** } indicates a list of the elements of **Z**. Term **F**(t, { **Z** }) is a column matrix whose elements are **functions** that calculate the derivative given time, t, and values for the elements of **Z**. These functions are based on Eq,3.5.11 for the first N_t rows, the kinematic relationship $V_c = dx/dt$ for the second N_t rows, and Eq.3.5.8 for the last row. The idea of the column matrix of functions, **F**(t, { **Z** }), is compatible with subprogram functions, which are available in almost all computer languages. The list { **Z** } is passed to the subprogram as a one-dimensional array which along with t and the row number returns the proper derivative. In other words, elements of the matrix **F**(t, { **Z** }) can be calculated by a single subprogram function.

A Runge Kutta 4th-Order method is used to solve the differential equation

$$\frac{d\mathbf{Z}}{dt} = \mathbf{F}(t, \{ \mathbf{Z} \}) \qquad \text{…….} \qquad (3.5.11)$$

This method provides a way to step form a known column matrix $\mathbf{Z}_n$ at time t_n to an unknown column matrix $\mathbf{Z}_{n+1}$ at time $t_{n+1} = t_n + \Delta t$, where Δt is a small time step. It takes the form

$$\mathbf{Z}_{n+1} = \mathbf{Z}_n + \frac{1}{6}\left(\mathbf{K}_1 + 2\,\mathbf{K}_2 + 2\,\mathbf{K}_3 + \mathbf{K}_4\right)$$

$$\mathbf{K}_1 = \Delta t\ \mathbf{F}\left(t_n, \{\mathbf{Z}_n\}\right)$$

$$\mathbf{K}_2 = \Delta t\ \mathbf{F}\left(t_n + \frac{1}{2}\Delta t, \{\mathbf{Z}_n + \frac{1}{2}\mathbf{K}_1\}\right) \qquad \ldots\ldots\ldots\ldots \quad (4.5.12)$$

$$\mathbf{K}_3 = \Delta t\ \mathbf{F}\left(t_n + \frac{1}{2}\Delta t, \{\mathbf{Z}_n + \frac{1}{2}\mathbf{K}_2\}\right)$$

$$\mathbf{K}_4 = \Delta t\ \mathbf{F}\left(t_n + \Delta t, \{\mathbf{Z}_n + \mathbf{K}_3\}\right)$$

The method begins with the initial condition $\mathbf{Z}_0$ at $t = 0$.

(c) Simulations

A number of simulations were run for system designs based on a payload throughput ranging between 2 and 50 MTY (million tonnes per year), a pipe length of 10,000 m, and 5 capsules per train. The dimensions of the capsule, the train, the LIM and the pipe were reported earlier in this report. The LIM for these systems was designed by selecting the LIM length, L', and the train velocity in the pipe, V_c, and calculating the train velocity in the LIM, V'_c, and the LIM force, F_L. These calculations were made using the steady-state theory. The LIM was designed using V_c' and F_L .

For the LIM units that make up the LIM, there is a choice of possible coil winding arrangements. For all simulations, a single-layer winding with a coil pitch of 1 was chosen. A double-layer configuration with a coil pitch of 2/3 was also considered. However, the characteristics of the single-layer and the double-layer machines were almost the same. Thus, only single-layer machines were used for the simulations.

The selection of V_c and L', for the LIM design was based on the efficiency described in the steady-state theory and some economic and mechanical considerations. For all simulations reported here the train launching velocity is V_c' .

Example 1

For the first example, the throughput is 20 MTY, L' = 200 m, L'/L = 0.02, and V_c = 15 m/s. For this throughput the launching interval, T, is 28.61 s.

The results of this simulation is shown in Fig.3.5.3, which gives the train displacements, x, versus time, t, for a number of trains. Each diagonal line in Fig.3.4.3 represents the trajectory of a train. The horizontal line at x = 200 m marks the end of the LIM section and the beginning of the pipe section. The top of the graph at x = 10,200 m marks the end of the pipe section. Hence, those trains that reach the top of the graph exit from the system. The trajectories are almost straight lines, which imply that the train velocity is almost constant.

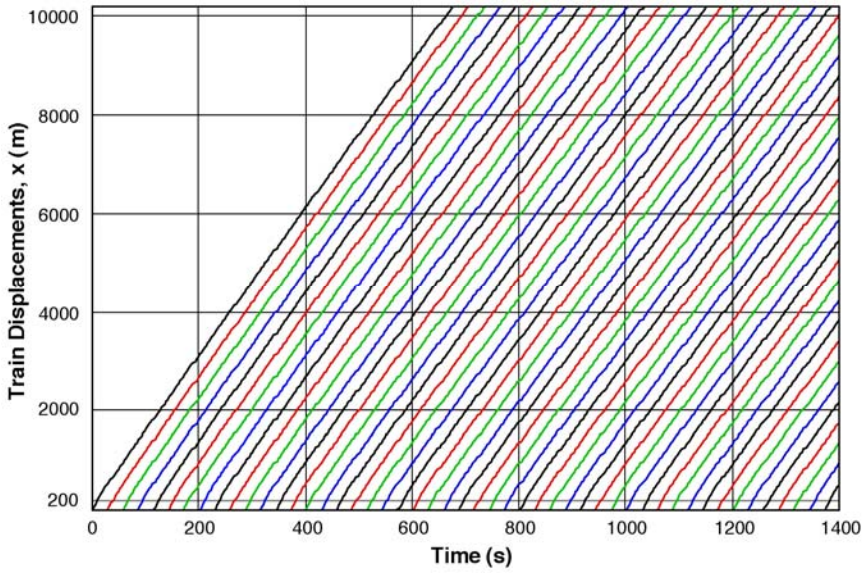

Figure 3.5.3 Capsule train displacement as a function of time

Shown in Fig.3.5.4 is a graph of the train velocities versus time. Only part of the trains is shown because a graph displaying all of the trains would be hopelessly confusing. In other words, all of the trains are included in the simulation but only part of the simulation results are displayed.

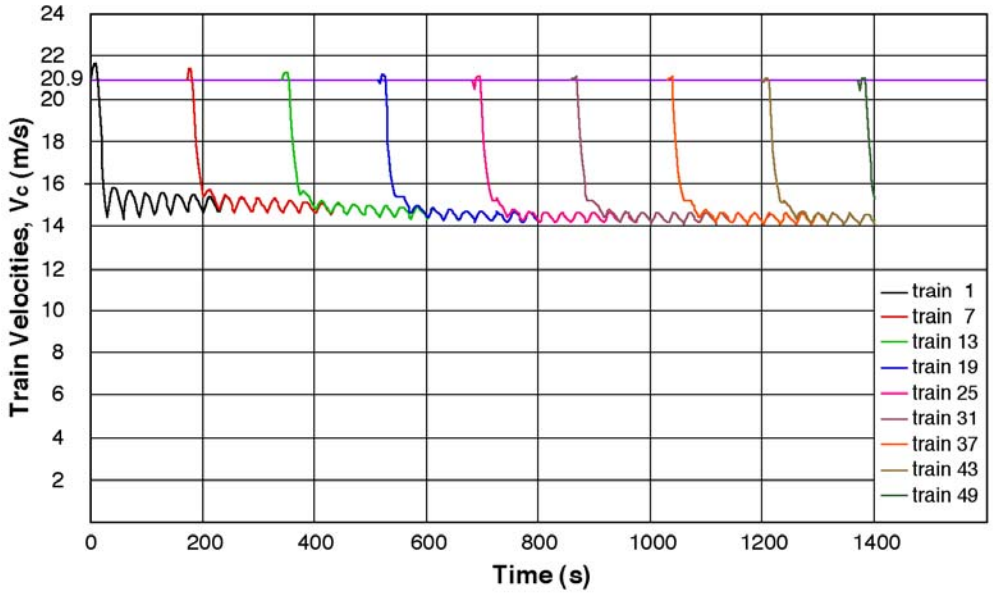

Figure 3.5.4 Selected capsule train velocities as a function of time

For this example the launching velocity is 20.9 m/s. Each train enters the LIM with this velocity but at a different time. In Fig.3.5.4 this entrance velocity is displayed as a horizontal

purple line. As each train enters the LIM, there is a brief period of acceleration (both positive and negative). After about 10 sec, each train enters the pipe (conduit) and slows down to a velocity that oscillates about a line near 14.5 m/s, which is comparable with the design value of 15 m/s. The oscillations decrease somewhat with time, but they do not disappear so long as new trains are being launched. Trains that are some distance downstream of the LIM move and oscillate as a group i.e., they are in locked steps with one another. The magnitude of train oscillations in the conduit is not large for large throughput such as our current example (20 MTY). However, for smaller throughput the oscillations become more important as we shall see later in the next example.

Shown in Fig.3.5.5 is the electrical energy input to the LIM for each train as it passes through the LIM. It can be seen from the figure that the energy input for the first train is a little under 13,000 kws (kilowatt seconds) which is equivalent to 3.61 kwh (kilowatt hours), and that for train 2 the energy input drops to a value under 9,000 kws (2.5 kilowatt hours). Thereafter the energy input increases with each train until trains start to leave the pipe downstream. After the trains start leaving the system, the energy input for each train entering the system plateaus out at about 14,554 kws (4.04 kwh). There are two main effects at work here. For the first train, air in the system is at rest and extra energy input is needed to accelerate the air. Hence, the energy input for the first train is high. The second train and subsequent trains encounters air that is already in motion; hence the drop in energy input for the second train and so on. The second effect has to do with the pressure required at the junction between the LIM and the pipe. This pressure must increase with time to overcome increasing rolling resistance and fluid shear as more and more trains accumulate in the pipe. This required increase in pressure explains the linear increase in input energy per train for trains numbered 2 through 28. Beyond train 28, trains leave the pipe at approximately the same rate as they enter the LIM, and more or less constant energy per train is observed.

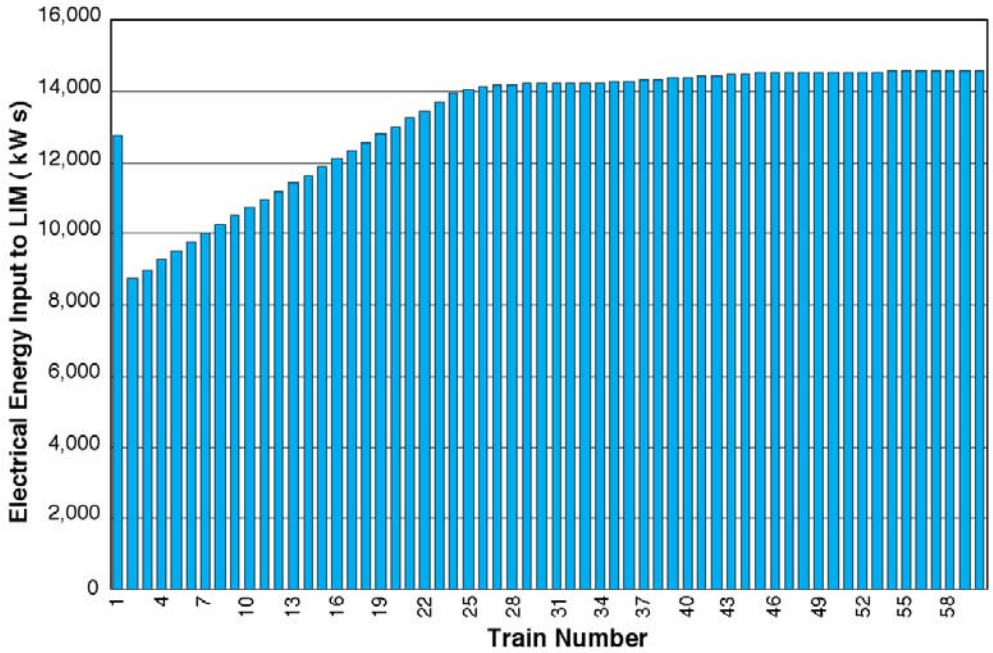

Figure 3.5.5 Electrical energy input to LIM per capsule train during startup

Example 2

For the second example, the throughput is only 2 MTY (million tonnes per year), the LIM length is L' = 300 m, L'/L = 0.03, and the design value of V_c is 7.4 m/s. The launching interval is 286.10 s or ten times as large as in the last example which had ten times larger throughput.

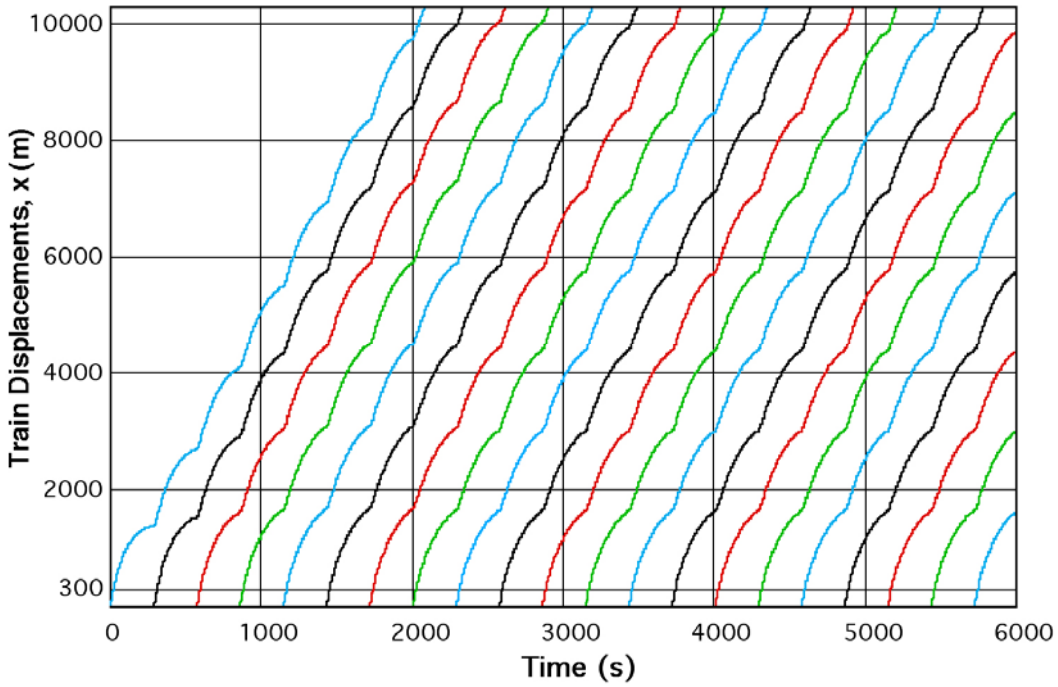

Figure 3.5.6 Capsule train displacements versus time during startup

Figure 3.5.6 shows the train displacement, x, versus time for this second example during startup. The horizontal line at x = 300 m marks the end of the LIM section and the beginning of the pipe section. The top of the graph at x = 10,300 m marks the end of the pipe section. Those trains that reach the top of the graph exit from the system. The train trajectories show a slope that oscillates in time with the launching interval. Moreover, beyond the first few trains the trajectories appear to be identical except for a time shift T, suggesting that the trains move in synchrony.

Figure 3.5.7 shows selected train velocities versus time. The trains are launched with a velocity of 13.4 m/s. This velocity is marked by a horizontal purple line in the figure.

From Fig.3.5.7, it can be seen that after a train is launched and passes through the LIM, its velocity oscillates between about 1.8 m/s and about 8 m/s with an average velocity of about 4.9 m/s. The design value for this example was V_c = 7.4 m/s. Apparently, for this case the steady-state theory failed to predict a large enough LIM force F_L.

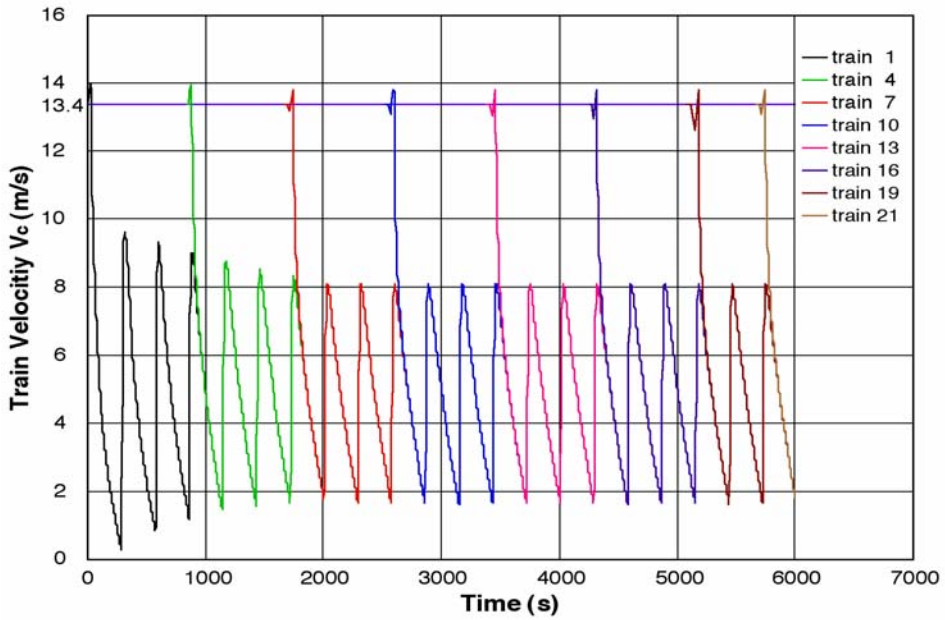

Figure 3.5.7 Variation of velocity of selected capsule trains during startup

Shown in Fig. 3.5.8 is the energy input to the LIM for each train. It can be seen that the energy input increases linearly until the conduit is populated with trains and stabilizes to reach about 25,000 kws (6.94 kwh) thereafter. Comparing Fig.3.5.8 with Fig.3.5.5 from the previous example, one does not see a high energy input for the first train. For this example, the air is at rest when the first train enters the LIM, just as it was for the previous example. Additional energy is dissipated to accelerate the air. What is different from the previous example is that the second and third trains encounter only slow moving air and each train must accelerate the air.

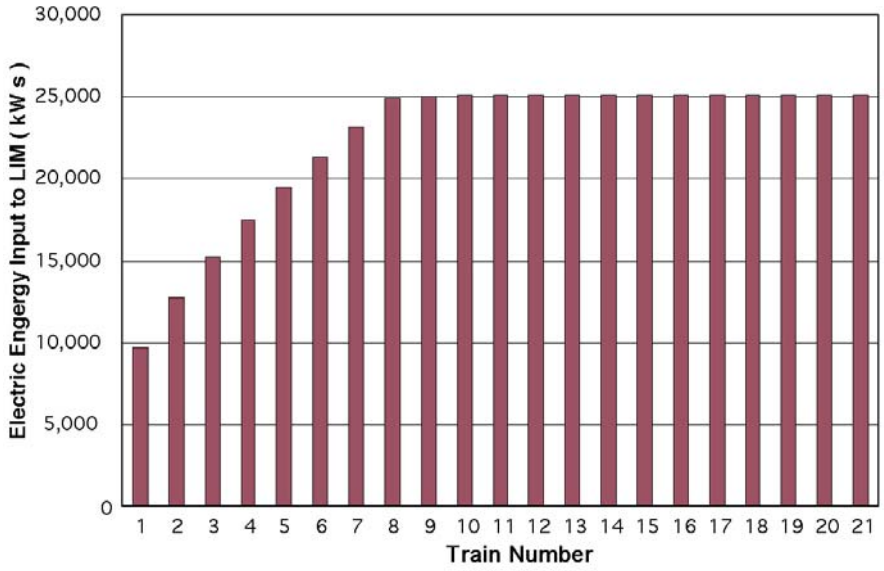

Figure 3.5.8 – Electric energy input to LIM per capsule train during startup

Figure 3.5.9 shows that the air velocity in the LIM is below 1 m/s as the second train enters the LIM, and is about 1 m/s for the third train and so on. Hence, no single train requires significantly more energy to accelerate air than the one following it.

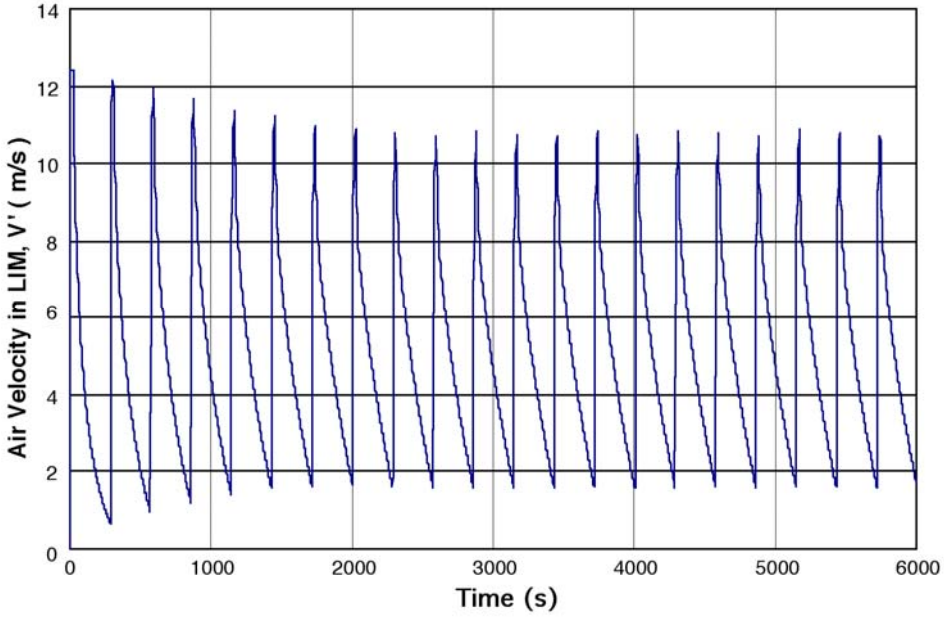

Figure 3.5.9 Air velocity in LIM versus time during startup

The LIM output energy per train can be calculated from the steady-state theory as the total LIM force on the train times the length of the LIM section, L' . This yields 24,789 kws (6.89 kwh).

According to the simulation results for this example, the LIM average efficiency for each train is about 0.789. Hence using this efficiency and the steady-state output energy, we can calculate the LIM input energy per train, yielding 31,418 kws (8.73 kwh). From Figure 3.5.8, one can see that the simulation does not predict a high energy input for any train. Thus, the simulation results indicates less energy input to the LIM and lower velocity in the conduit of the system than predicted from the steady-state theory. Moreover, there are large oscillations in train and air velocities in the conduit. These oscillations dissipate more energy than a more orderly motion with the same average values.

In spite of the difficulties with this second example, the simulation suggests that the design using the steady-state theory would actually work and the power requirements would be below the design values. The average train speed in the conduit would be about 34% lower than the steady state, but the throughput would be maintained. Due to the oscillations in velocities, the trains exit the conduit at a velocity between 2 and 8 m/s.

(d) Summary of simulation results

Delivery line:

Shown in Table 3.5.1 are the pertinent results of seven simulations including the two simulations in the two foregoing examples –all for the delivery line. As discussed before, the throughput, the LIM length L', and the capsule velocity in the conduit V_c are selected on the

basis of system efficiency as presented in the steady-state theory. From this steady-state theory, V_c' and F_L are calculated. The launching interval T is calculated from the throughput, the number of capsules in each train, and the payload for each capsule. The LIM force F_L is used to design the LIM units that make up the LIM section. In Table 3.5.1, F_L in expressed in N (Newton) per car side which is convenient for the design of the LIM units.

Table 3.5.1 – Summary of simulation results (delivery line)

Throughput (MTY)	T (sec)	L'/L	V_c (m/s)	V_c' (m/s)	F_L (N)	Ave. V_c (m/s)	Ave. V_c' (m/s)	Ave. LIM Eff., E_L(%)	LIM Energy per Train (kW s)	LIM EI (BTU/TM)	KE EI (BTU/TM)	Total EI (BTU/TM)
50	11.44	0.01	15.00	21.18	7,404	15.64	21.20	89.0	8,034	31.7	22.0	54
50	11.44	0.02	15.00	19.93	3,822	15.67	19.91	86.0	8,959	35.0	19.3	54
35	16.35	0.02	15.00	20.23	4,592	15.06	20.19	86.9	10,763	42.0	19.9	62
20	28.61	0.02	15.00	20.93	6,608	14.49	20.94	88.4	14,554	56.8	21.3	78
10	57.22	0.02	13.35	19.99	9,360	12.31	20.08	88.7	18,786	73.4	19.4	93
5	114.44	0.02	10.50	17.38	10,921	9.06	17.54	86.7	19,906	77.8	14.7	92
2	286.10	0.03	7.40	13.40	8,263	4.90	13.50	78.9	25,105	97.1	8.6	106

Table 3.5.1 includes V_c and V'_c from the steady-state theory and values of train velocity in the LIM and in the conduit from the simulations. These latter values are identified in the table as average V_c and V'_c. These average velocities are calculated from the amount of time it is in the conduit.

From Table 3.5.1, one can see that for all simulations the average velocity in the LIM is in good agreement with the value obtained from the steady-state theory. This agreement is probably due to the characteristics of the LIM, which tries to move everything at a speed slightly below synchronous speed, and will develop a very large force if the velocity fall much below the synchronous speed. Comparing the average velocity in the conduit with the steady state V_c, one can see variations between the simulations and the steady-state theory. However, the two differ by no more than 1.44 m/s for throughputs greater than 5 MTY.

Shown in column 10 of Table 3.5.1 is the electrical input energy per train to the LIM. This energy input is important because it is needed for calculating the power cost and in addition, the energy intensiveness, EI, discussed in the steady-state theory. The values in the table are determined from the last train to pass through the LIM before simulation ended.

Knowing the payload per train, the LIM length, the conduit length, and the electrical input energy per train, it is possible to calculate the energy intensiveness, EI, which is tabulated in column 11. Energy is also needed to bring the trains up to speed before they enter the LIM. A second energy intensiveness can be calculated using for energy input the kinetic energy of a train divided by an assumed efficiency. In Table 3.5.1, this assumed efficiency is 80%. The total EI is also tabulated in the last column of the table.

The simulations do include train acceleration effect and do consider the train length when calculating the LIM force on a train. The steady-state theory does not consider train acceleration or train length. Hence, one cannot expect the simulations to be always in agreement with the steady-state theory. However, for throughput greater than 5 MTY one can expect V'_c and F_L obtained from the steady-state theory to be accurate enough to design the LIM. For throughput

less than 5 MTY, one can get an initial LIM design based on steady-state theory and then modify the LIM design by using the simulation results based on unsteady theory.

Return line:

The unloaded capsules in the return line, being empty, weigh only about 27% of the loaded capsules in the delivery line. Hence, much less energy is needed to return the empty trains to the loading site (inlet station) than to run the loaded trains to the unloading site (outlet station).

Table 3.5.2 gives a summary of the unsteady flow simulations for the return line. As in the case of the delivery line, V_c was selected to optimize the LIM pump efficiency as defined in the steady-state theory. Because trains are lighter for the return line, V_c , V'_c and F_L are all smaller for the return line than for the delivery line for the same throughput and L'/L. Table 3.5.2 shows that values of V'_c obtained from steady-state equations is in good agreement with the average values V'_c obtained from unsteady flow simulation.

Table 3.5.2 – Summary of simulation results (return line)

Throughput (MTY)	T (sec)	L'/L	V_c (m/s)	V_c' (m/s)	F_L (N)	Ave. V_c (m/s)	Ave. V_c' (m/s)	Ave. LIM Eff., E_L(%)	LIM Energy per Train (kW s)	LIM EI (BTU/TM)	KE EI (BTU/TM)	Total EI (BTU/TM)
50	11.44	0.01	15.00	19.68	4,467	14.89	19.63	85.5	5,276	20.8	6.4	27
50	11.44	0.02	14.90	18.53	2,177	15.07	18.48	82.1	5,455	21.3	5.6	27
35	16.35	0.01	13.60	18.39	4,928	13.26	18.36	85.1	5,747	22.7	5.6	28
35	16.35	0.02	13.20	16.82	2,276	13.15	16.77	80.0	5,898	23.0	4.6	28
20	28.61	0.01	11.20	16.05	5,365	10.65	16.05	82.5	6,142	24.2	4.3	29
20	28.61	0.02	10.90	14.51	2,446	10.61	14.48	74.6	6,593	25.8	3.4	29
10	57.22	0.01	8.80	13.58	6,041	7.90	13.61	78.3	6,804	26.8	3.1	30
10	57.22	0.02	8.60	12.22	2,707	8.60	12.24	72.9	7,015	27.4	2.5	30
5	114.44	0.01	6.90	12.05	6,938	5.74	12.14	76.3	7,645	30.2	2.4	33
5	114.44	0.02	6.70	10.36	2,983	5.80	10.41	66.5	7,978	31.2	1.8	33
2	286.10	0.01	5.00	10.57	8,745	2.81	10.66	72.2	9,489	37.4	1.9	39

According to the steady-state theory the LIM-pump efficiency should increase as L'/L increases provided that the throughput is held constant. However, the total LIM energy per train in column 10 of Table 5.3.2 is consistently higher for $L'/L = 0.02$ than it is for $L'/L = 0.01$. The total LIM energy/train also depends on the average LIM efficiency shown in column 9, which is consistently lower for $L'/L = 0.02$. Hence, as the LIM-pump efficiency increases the average LIM efficiency decreases.

As discussed in the section on the steady-state theory, the EI for the return line is defined using the payload of the delivery line. Hence to find the total IE for both the delivery and return line operation, one can simply add the total EI from Table 5.3.1 and Table 5.3.2, for the same throughput and L'/L . For small throughput, the total EI shown in Table 5.3.1 and Table 5.3.2 are actually smaller than those found from the steady-state theory. This is surprising because the EI values found in the section on design analysis by steady-state theory are based on LIM output energy. However, one should note that V_c and average V_c are very different for these cases.

4. ENERGY EFFICIENCY OF THE SYSTEM

4.1 Introduction

According to Hirst [20], the energy efficiency of any freight transportation system can best be determined from a quantity called the "***energy intensiveness***" or "***EI***", which is defined as the energy needed to transport one unit weight of cargo over a unit distance. The units of EI used by Hirst and later by Liu and others [21, 22] is Btu/TM, which stands for the BTU of energy used for transporting one ton (American ton, which is 2,000 lbs) of cargo over one mile of transportation distance. Hirst found that the average values of EI for oil pipelines, waterway (barge), railroads, trucks and airplanes are respectively 450, 550, 680, 2300 and 37000 Btu/TM. It is of interest to calculate the EI of the LIM-driven PCP system studied in this report, and then compare the results with the above figures given by Hirst for the other five modes to see how energy efficient is the LIM-driven PCP as compared to these other transportation modes.

4.2 Energy Intensiveness (EI) Computation and Results

Based on the definition of the energy intensiveness (EI) described above, the EI of a LIM-driven PCP can be calculated from the following equation:

$$EI = \frac{P_{sys}}{T_h L} \qquad \text{……} \qquad (4.2.1)$$

where P_{sys} is the power input to the PCP system in ***Btu/year***, T_h is the cargo throughput in ***million tons (American tons) per year***, L is distance in ***miles***, and EI is in ***Btu/TM***.

Note that the power input to the PCP system, P_{sys} , includes not only the electrical power input to the LIM, $(P_i)_L$, but also the power P_v needed to accelerate capsules from zero velocity to the capsule velocity at the LIM entrance, which is approximately 20 m/s. Therefore,

$$P_{sys} = (P_i)_L + P_v \qquad \text{……} \qquad (4.2.2)$$

While the input power of the LIM, $(P_i)_L$, is obtained from the graphs in Sec.3.4, the power P_v is obtained from the kinetic energy of each capsule at the LIM entrance, $M_c(V_c')^2/2$, multiplied by the number of capsules entering the PCP in each second, n, given by Eq.3.3.2, or divided by the capsule injection time interval, T, in seconds, namely,

$$P_v = \frac{nM_c(V_c')^2}{2} = \frac{M_c(V_c')^2}{2T} \qquad \text{……} \qquad (4.2.3)$$

Because in this report power is usually given in ***watts***, throughput is given in ***million tonnes (metric tons) per year,*** and distance is given in ***m*** (***meters***), to be able to use readily the results of this report for calculating the EI in Eq.4.2.1, we must make the following conversions of units: 1 kw (kilowatt) = 1000 watts = 0.947 Btu/s = 29.9 x 10^6 Btu/yr, 1 tonne (metric ton) = 1.1 American tons, 1 km = 1000 m = 0.621 mile. Upon such conversion, Eq.4.2.1 can be used to calculate the EI values for each case of LIM-driven PCP system.

Using the foregoing approach, the EI values of the LIM-driven PCP system for various cases were calculated, and the results for the delivery line of the PCP are plotted in Fig.4.2.1.

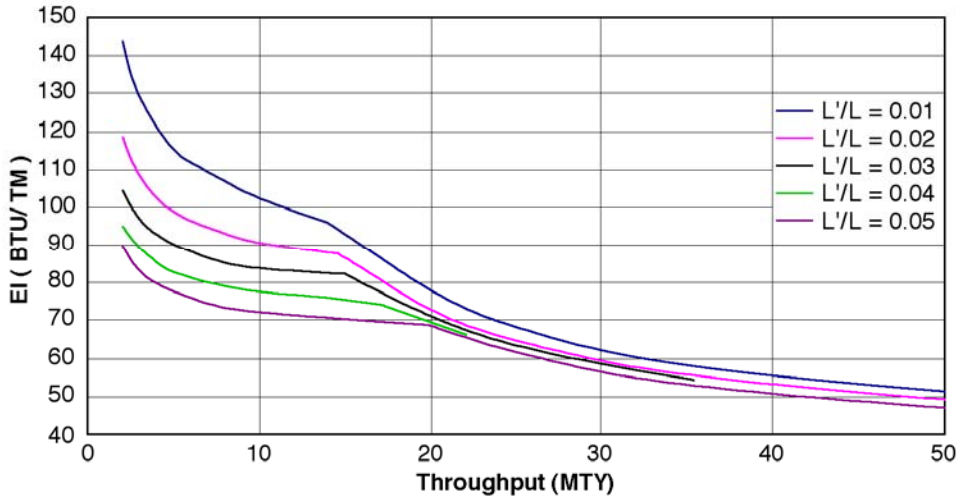

Figure 4.2.1 Variation of energy intensiveness (EI) of LIM-driven PCP system with throughput and L'/L (**delivery line)**

For generality, the EI given in Fig.4.2.1 assumed that the efficiency of the LIM were100%. Since in reality the LIM efficiency is much less than 100%, for each case the value obtained from Fig.4.2.1 must be divided by the LIM efficiency obtained from Fig.3.4.5 for the delivery line). Likewise, the EI for the return line based on 100% efficiency is given in Fig.4.2.2.

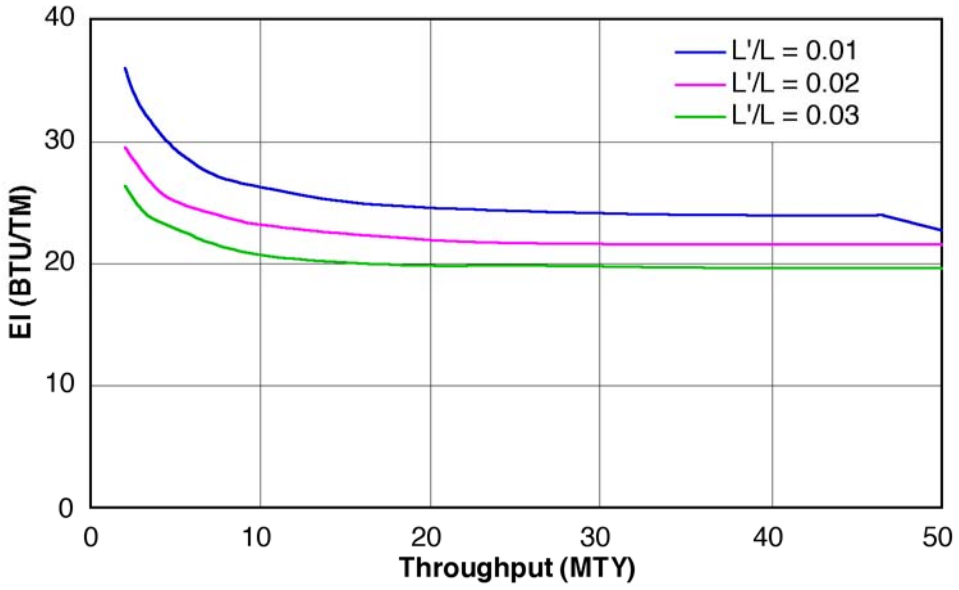

Figure 4.2.2 Variation of energy intensiveness (EI) of LIM-driven PCP with throughput and L'/L (**return line**)

Figure 4.2.1 shows that the EI decreases with increasing throughput, and decreases with increasing L'/L. This means both larger throughput and longer LIM make the system more

energy efficient. However, even for the smallest throughput (2 MTY) and the shortest LIM (L'/L = 0.01) analyzed, the value of EI is 144 Btu/TM. If we divide this value by the corresponding LIM motor efficiency of 90 % obtained from Fig.3.4.6, the EI for the delivery line is still only 160 Btu/TM. For the return line at 2 MTY and L'/L = 0.01, Fig.4.2.2 yields an EI value of 36 Btu/TM, and Fig.3.4.13 yields an efficiency of 76 %. This means the **actual EI for the return line is 47 Btu/TM**. Adding the two EI values (one for the delivery line and the other for the return line) yields the **total EI of the system, which is 207 Btu/TM.** Comparing this value with the value of 680 Btu/TM for ordinary railroad and 2300 Btu/TM for truck given by Hirst [20], it can be seen that the LIM-driven PCP technology for this small throughput of 2 MTY uses approximately 30 % of the energy used by railroad train and uses approximately 9 % of the energy used by truck to transport the same cargo over the same distance.

If we increase the throughput to 50 MTY, the value of using PCP is even more impressive. For the delivery line, Fig.4.2.1 yields an EI value of 52 Btu/TM, and Fig.3.4.6 yields a motor efficiency of 89 %. This means the **actual EI value for the delivery line is 58 Btu/TM.** For the return line at 50 MTY and L'/L = 0.01, Fig.4.2.2 yields an EI of 24 Btu/TM, and Fig.3.4.13 yields an efficiency of 85 %. Thus, the **actual EI for the return line is 28 Btu/TM**. Adding the EI of the delivery line to the EI of the return line yields the **total EI of the system, which is 86 Btu/TM**. This value is only 13% of the energy used by ordinary railroad and 4% of the energy used by truck, for transporting the same cargo over the same distance. **This shows the great value that the LIM-driven PCP can have in conserving energy**, especially for systems that require large throughputs, and when the PCP is used in lieu of truck instead of train (railroad). Even when using this PCP in lieu of railroad, much energy can be saved if the throughput is high. **Another advantage of using PCP instead of truck or train for freight transport is that it uses electricity instead of oil. This means cleaner air and less reliance on imported oil for transportation**, which is consistent with the nation's goal of reducing the consumption of imported oil, and having cleaner air.

4.3 Energy Consumption of LIM

Operation of the LIM requires an automatic switching circuit which turns each unit of the LIM on when there is capsules present in the unit, and turns the unit off when there is no capsule passing through the unit. Therefore, the operation of the LIM is intermittent, drawing power when LIM is on, and using no power when the LIM is off. Based on such an operational mode, the total amount of electrical energy used by the LIM during any period T is

$$E_N = P\Delta T \qquad \text{……..} \qquad (4.3.1)$$

in which E_N is the energy consumed by the LIM during the period T; P is the power drawn by the LIM when it is on; and ΔT is the period during T when the LIM is on. Because $\Delta T/T$ is equal to α', the linefill rate in the LIM, Eq.4.3.1 can be rewritten as:

$$E_N = PT\alpha' \qquad \text{……..……..} \qquad (4.3.2)$$

Using Eq.4.3.2, the energy used by the LIM in a year is calculated for various throughputs and L'/L. The result is plotted in Fig. 4.3.1 for the delivery line, and in Fig.4.3.2 for the return line.

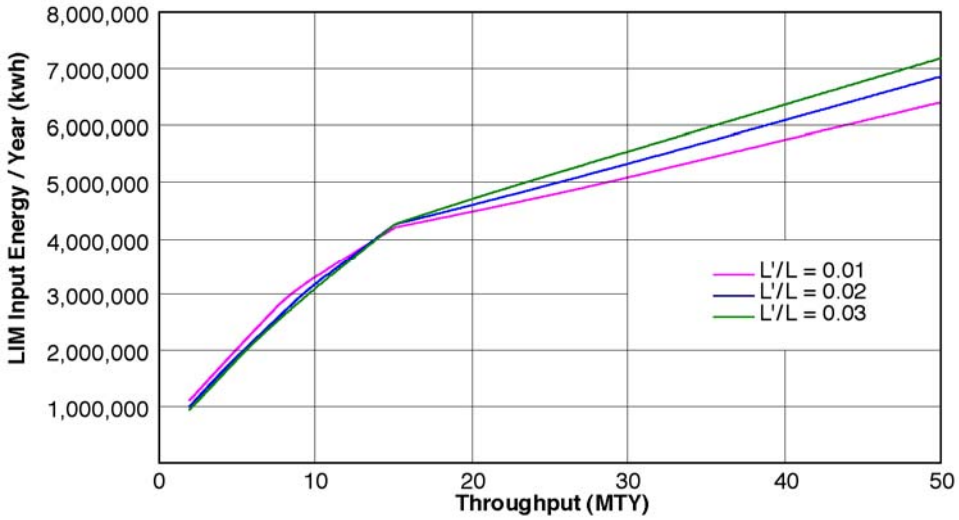

Figure 4.3.1 Annual LIM input energy (delivery line)

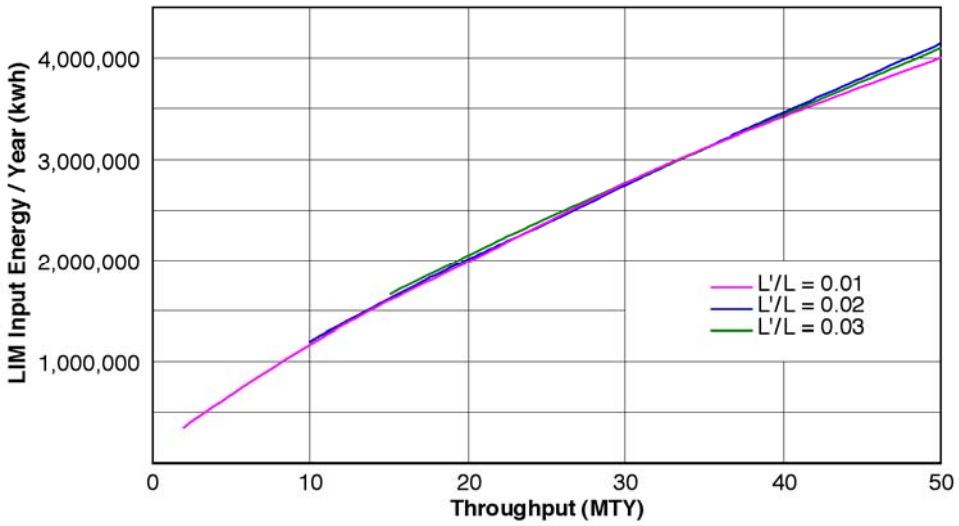

Figure 4.3.2 Annual LIM input energy (return line)

As expected, the LIM input energy increases with increasing throughput both for the delivery line and the return line. Comparing the results of the two above figures shows that the delivery line uses almost twice as much as the energy used by the return line. Note that these two figures will be used in Sec.5 to determine the annual cost of energy for operating the PCP system.

5. COST ANALYSIS

5.1. Introduction

While it is highly desirable to perform a cost analysis of any new technology such as the one studied herein, it should be mentioned at the outset that any general (generic) cost analysis such as the one to be performed in this section must be viewed with caution due to the following:

- A large part of the total capital cost is the construction cost of the tubes (conduits) in the advanced PCP system, which is strongly site-specific. For instance, in dry open country or flat plains such as the Powder River Basin in Wyoming, the land value is low and construction is easy, so the construction cost is expected to be much below that for the same system to be built in mountainous areas. For the generic study conducted here, the construction cost figures are assumed to be significantly (20 to 50%) higher than that will be encountered at the Powder River Basin, but significantly less than those could be in mountainous areas. Also, labor cost is also site specific – high in the United States using union workers which is the assumed condition, and much lower in most other nations, especially developing nations.
- The system designed here has not been optimized. Optimization of the system in the future will certainly lead to lower costs.
- The analysis used here assumes that the company owning the system pays a 37% of corporate income tax. In actual situations, depending on project location the tax may be much lower.
- The cost analysis includes an above-inflation-rate of ROI (Return-on-Investment) of 15%, and a project life of 20 years. Should these assumptions be changed significantly, quite different results will be obtained.

Due to these as well as other uncertainties, the cost figures to be found in this analysis must be viewed and interpreted with caution. The main value of this cost analysis is that the results will show general trends, such as how the unit cost (i.e., the cost for transporting each tonne of cargo through the system) varies with the transportation distance and throughput. Once we understand such trends, we can then seek opportunities to use this new technology in situations where it may be most cost-effective, and avoid wasting time on planning its use in situations where it is expected to be not cost-effective. When comparing the unit cost or the unit-distance cost (i.e., the cost for transporting each tonne of cargo over each kilometer distance) obtained from this generic study with those by alternative transportation modes such as truck for any given case, one must keep the assumptions used here in mind, and recognize the uncertainties mentioned above in drawing conclusions. For accurate comparison, one must perform a site-specific cost analysis using this or a similar method, instead of relying on the values obtained from this generic study for comparison and drawing serious conclusions. Therefore, this generic cost analysis also serves as a means or model for future use in evaluating real cases of mineral or mine waste transports.

5.2. Methodology The cost analysis of this study is based on the cost model, equations, procedures and assumptions discussed in detail in Appendix IV. A recapitulation of the essential steps is given as follows:

(1) The current value of the total capital cost, C_c, and the current value of the total annual operation-maintenance cost, C_o, are determined respectively from Eqs.IV-22 & IV19.

(2) Determine the economic life to be used for the cost analysis, N. To be conservative, for a system for mining N should not be more than 20 years. Also, determine the depreciation period, N_d, in number of years. Note that N_d should not be greater than N for each case.
(3) Use the N_d value assumed to calculate the depreciation for each year, d_n, using Eq.IV-4 (i.e., Eq.4 of Appendix IV).
(4) Using an assumed after-tax return-on-investment (ROI) such as 15%, and an assumed inflation rate I such as 3%, determine the discount rate δ using Eq.IV-7.
(5) Knowing C_o and an assumed annual cost escalation rate e_c, the annual operation-maintenance cost for any subsequent year n, C_n, is calculated from Eq.IV-18.
(6) Knowing the foregoing values of C_c, C_n, d_n, δ, and N, and knowing the values of the freight throughput Q in tons per year, the corporate income tax rate t, and the revenue escalation rate e_r, Eq.IV-14 can be used to calculate the unit price U_o, which is the present cost that customers must pay to have each ton of minerals or mine waste transported through the LIM-driven PCP system. This unit price can then be compared with the price that the customer must pay for using alternative modes to transport the same ton of cargo over the same distance.

5.3. Case Studies (Scenarios)

Using the foregoing approach, various cases (scenarios) of the advanced PCP system driven by LIM for transporting minerals or mine wastes can be analyzed as illustrated as follows:

(a) Case 1 : Basic Case

This is the case where the system has two tubes (twin conduits), with one as the delivery line to transport loaded capsules, and the other as the return line to return empty capsules. Moreover, the system is operated continuously around the clock (24 hours a day non-stop) and year-round (365 days a year). Using the methodology explained in Appendix IV, the cost of the system is analyzed by using the Excel software over the distance range of 10 to 1,000 km, and over the throughput range of 1 to 50 MTY (million tonnes per year). Analyzing over such a wide range makes it possible to determine the cost-effectiveness of the system over a wide range of distance and throughput. The result of this analysis is presented next.

The current value of the total capital cost of the system, C_c, is given in Table 5.1 as a function of distance L and throughput T_h. It can be seen from the table that the capital cost is affected more by the transportation distance L than by the throughput T_h. For instance, at the throughput of 10 MTY, the capital cost of the system is M$100.6 (million dollars) for a 10 km system, while it becomes M$465.8 for a 100 km system. Thus, a tenfold increase in the distance increases the capital cost by 4.63 times. On the other hand, when the distance is fixed (say at 10 km), the system cost is M$52.8 for the throughput of 1 MTY and M$100.62 for the throughput of 10 MTY. This means a tenfold increase in throughput only increased the capital cost by 1.91 times. The stronger effect of distance than throughput on the capital cost is due to the reason that the tube cost is a major part of the capital cost, and having a ten times increase in distance (length of the tube) will increase the tube cost by ten times.

Table 5.1 Variation of Capital Cost in with Distance and Throughput (million dollars)

Transport Distance L (km)	Cargo (Mineral or Mine Waste) Throughput, T_h (MTY)					
	1	2	5	10	20	50
10	52.8	58.0	74.2	100.6	153.9	313.6
20	92.9	97.9	114.3	141.2	195.4	358.1
50	213.0	217.9	234.7	262.9	319.7	491.9
100	413.3	417.7	435.5	465.8	526.9	714.7
200	813.7	817.4	836.9	871.6	941.3	1160.4
500	2015.0	2016.5	2041.2	2088.8	2184.5	2497.6
1000	4017.3	4014.9	4048.3	4117.6	4256.6	4726.2

The current value of the annual operation/maintenance (O/M) cost of the system, $C_{o,}$ has also been calculated by summing up the various components in Eq.IV-19. The result, as a function of L and T_h, is given in Table 5.2.

Table 5.2. Variation of Annual Operation/Maintenance Cost with Distance and Throughput (million dollars per year)

Transport Distance L (km)	Cargo (Mineral or Mine Waste) Throughput, T_h (MTY)					
	1	2	5	10	20	50
10	6.60	7.10	8.63	11.07	15.87	30.02
20	9.68	10.23	11.90	14.55	19.63	34.45
50	18.90	19.61	21.73	24.98	30.92	47.76
100	34.26	35.25	38.10	42.38	49.74	69.93
200	65.00	66.53	70.85	77.16	87.37	114.28
500	157.20	160.36	169.09	181.50	200.26	247.33
1000	310.86	316.74	332.82	355.41	388.42	469.08

As it is the case with the capital cost, the annual operation/maintenance (O/M) cost increases more rapidly with an increase in the transportation distance than with the increase of throughput. For instance, by increasing the distance by tenfold from 10 to 100 km while holding the throughput constant at 1 MTY, the O/M cost is increased from M$6.60 to M$34.26, which is a 5.19 times. In contrast, by increasing the throughput by tenfold from 1 to 10 MTY while holding the distance constant at 10 km, the O/M cost is increased from M$6.6 to M$11.07, which is an increase of 1.68 times only. The reason that distance has a stronger effect than throughput on the O/M cost is due to the fact that energy cost is a major part of the O/M cost, and the energy cost increases by approximately ten times when transportation distance increases by ten times.

Using the values of the capital cost and the O/M cost given in Tables 5.1 and 5.2, and using additional assumptions described before and in Appendix IV, the unit cost of transporting minerals (or mine wastes) by using the advanced PCP system, U, in $/T (dollars per tonnes), is given in the following table and figure.

Table 5.3 Variation of Unit Cost, U, with Distance and Throughput ($/Tonne)

Transport Distance L (km)	Cargo (Mineral or Mine Waste) Throughput, T_h (MTY)					
	1	2	5	10	20	50
10	21.30	11.62	5.85	3.91	2.93	2.34
20	35.51	18.74	8.74	5.38	3.70	2.68
50	78.15	40.11	17.40	9.81	5.99	3.69
100	149.21	75.72	31.85	17.19	9.81	5.37
200	291.33	146.95	60.73	31.96	17.46	8.74
500	717.69	360.63	147.37	76.25	40.40	18.84
1000	1428.30	716.76	291.78	150.07	78.62	35.67

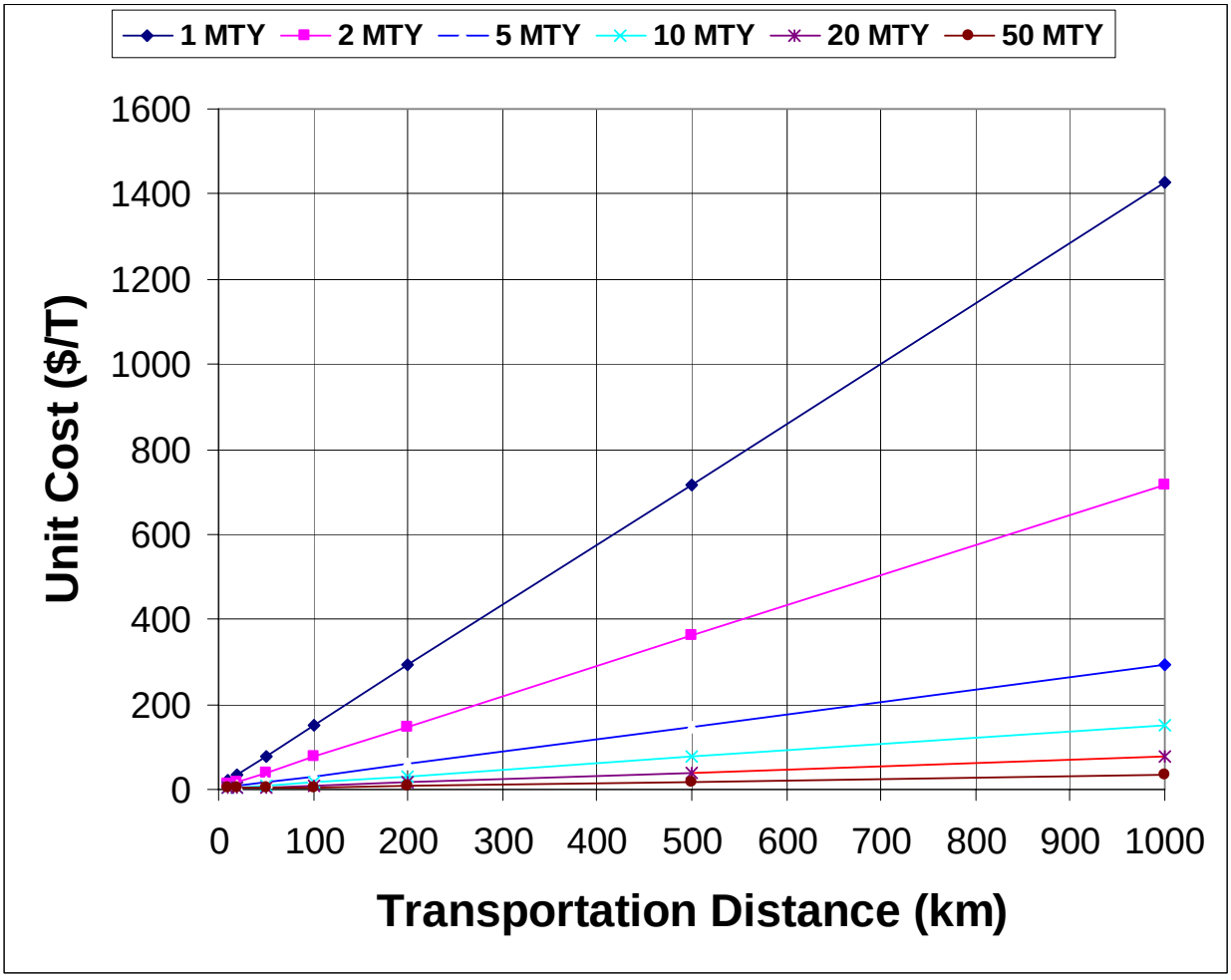

Figure 5.1 Variation of unit cost with transportation throughput and distance

From Figure 5.1, the unit cost for transporting minerals or mine waste by using the system is almost linearly proportional to the transportation distance, and it decreases with the increase of throughput. The higher the throughput becomes, the lower the cost is for transporting each tonne of materials (minerals or wastes) through the system. For instance, while transporting a tonne of

materials for 10 km through a system having a throughput of only 1 MTY will cost approximately $21.30, to transport a tonne of the same materials for the same distance (10 km) in a system of 50 MTY throughput will be only about $2.34. This means the advanced PCP system designed and studied in this report is cost-effective only for systems that have high throughput – over approximately 5 MTY. The higher the throughput is, the more cost-effective the system becomes.

This cost advantage of high throughput can be seen even more clearly in Table 5.4 and Figure 5.2, which give the variation of the unit-distance cost for transporting materials through the PCP system. By definition, the ***unit-distance cost*** is the cost for transporting a unit weight of cargo over a unit distance, given in the unit of $/T/km (dollars per tonne per kilometers).

Table 5.4 Variation of unit-distance cost with transportation distance and throughput ($/T/km)

Transport Distance L (km)	Cargo (Mineral or Mine Waste) Throughput, T_h (MTY)					
	1	2	5	10	20	50
10	2.13020887	1.1615426	0.585178	0.390603	0.293436	0.234482
20	1.7757078	0.9369046	0.436996	0.269124	0.184943	0.134074
50	1.56300706	0.8021216	0.348087	0.196237	0.119848	0.073829
100	1.49210675	0.7571941	0.31845	0.171941	0.09815	0.053748
200	1.45665669	0.7347303	0.303632	0.159793	0.0873	0.043707
500	1.43538665	0.7212522	0.294741	0.152504	0.080791	0.037682
1000	1.42829655	0.7167591	0.291778	0.150075	0.078621	0.035674

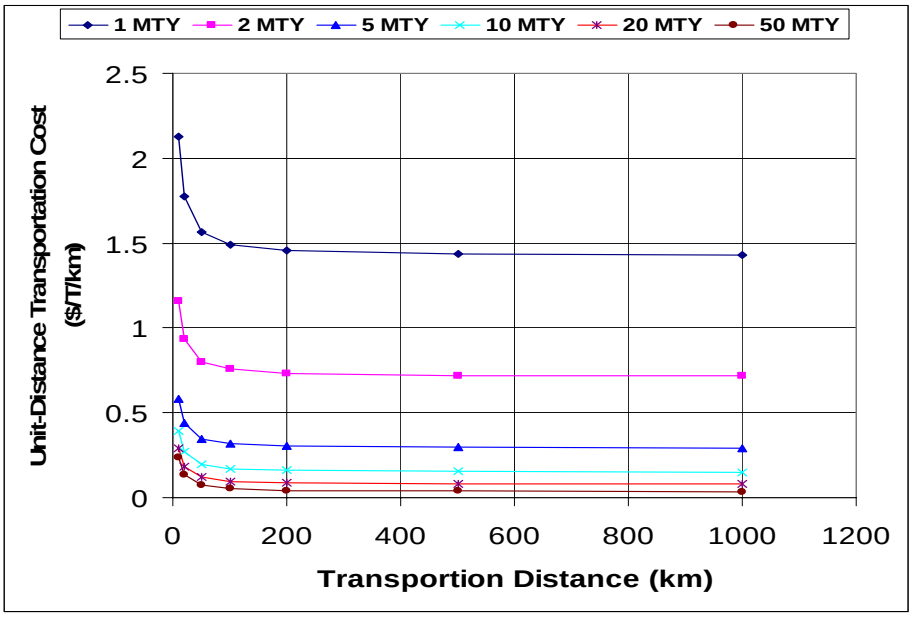

Figure 5.2 Variation of unit-distance transportation cost with distance and throughput

From Figure 5.2, it is clear that the greatest change of the unit-distance cost occurs within approximately 100 km. Within this distance, increasing the distance drastically decreases the

unit-distance cost. On the other hand, for distances longer than 100 km, increasing distance can reduce the unit-distance cost only slightly. This trend can also be seen from Table 5.4.

Note that this PCP system is intended for use in mining in mountainous areas where transportation by ordinary modes such as truck, is expensive. When comparing with trucking cost in mining, one may find that the PCP system has a cost advantage in many situations when the throughput is large.

(b) Case 2: Single-Tube Operation

This is the case where only a single tube is used -- alternatively as the delivery line for delivery of minerals (or mine wastes), and as the return line for retuning empty capsules. To be able to use the same tube for both delivery and return, a LIM is needed at each end of the tube. The one near the inlet station is used only during the operation of the delivery line, whereas the one near the outlet station is used only during the operation of the return line. **Using a common tube for both delivery and return saves money when the system throughput is small**, as will be demonstrated here.

Consider the system with a conduit length (transportation distance) of 50 km, and a throughput of 5 MTY. Due to the use of a single tube instead of twin tubes, the cost of the tube (including the rail and track inside the tube) is only one half that of the twin-tube system. Namely, the tube cost will be $80.35 million if concrete conduits are used. The single tube system will need two LIMs, one on each end of the tube. Because the single tube operates 50% of time as delivery line and 50% of time as return line, the throughput at any given time must be 10MTY, or twice that of each of the twin lines. With this throughput and a LIM on each end, the capital cost of the LIM will be $9.92 million. The capsule cost will be the same as that for the twin system, which is $2.83 million. The inlet and outlet station costs will be the same as those for the twin-line system for 10 MTY. They are respectively $34.52 million and $17.82 million. Thus, the total capital cost of the single-tube system is $145.4 million as compared to the $234.7 million for the twin-tube system. This is a saving of $89.3 million in capital cost, which is a quite significant cost saving.

As to the O/M cost of the single-tube system, the energy cost, fuel cost, natural gas cost, salaries, tax/insurance, and maintenance cost are, respectively (in million dollars), 1.13, 0.02, 0.04, 1.48, 3.64, and 7.27. The total is $13.58 million, as compared to $21.73 million for the twin-tube system. This means that using the single tube system also saves an annual O/M cost of $8.15 million, which is a rather significant saving.

Due to the significant savings in both the capital cost and O/M cost, the single-tube system has a unit cost of only $15.2 /T as compared to $17.4/T for the twin-line system. Also, the unit distance cost is now $0.304/T/km as compared to $ 0.348 /T/km for the twin-line system. This shows that considerable savings can be accomplished by using single-tube PCP systems when the throughput is small. This is an important strategy for reducing costs by using the advanced PCP system studied herein.

When throughput is relatively low, further savings can be accomplished by using other strategies, such as operating the single-tube system periodically – e.g., running the system at the high throughput of 30 MTY only 8 hours a day (4 hours in each direction), and having the system idling during the remaining 16 hours of the day. This will enable the system to transport an average of 5 MTY, the same as the system analyzed before, except that it will cost less – due to the idling hours which cost less to operate.

5.4. Conclusion on Cost Analysis

Through the foregoing analysis, it can be seen that both long distance and large throughput reduce unit-distance cost, and hence make the advanced PCP system driven by LIM more cost effective and competitive with truck and other transportation modes. By using large throughput, the PCP system is quite cost competitive with trucks, especially in mountain areas where transportation by truck is difficult and costly, and takes a much longer path (due to tortuous roads) than PCP which can follow a relatively straight path with large slope. Note that while the slope of roads for trucks must be limited to 10 degrees, with tight seals LIM-driven PCPs can have slopes up to about 40 degrees without operational problem. When the throughput is relatively small (say less than 20 MTY), using a single-tube system will result in considerable cost saving from that of using a dual-tube system. Further cost saving can be accomplished by running the system only for a few hours a day, while letting the system idle during the rest of the day. The methodology used here for making cost analysis can serve as a model for analyzing future advanced PCP systems driven by LIM.

6. Conclusion and Recommendation

This project, sponsored by the Mining Program of the National Energy Research Laboratory, U.S. Department of Energy, completed the design and analysis, including cost analysis, of an advance PCP (pneumatic capsule pipeline) system driven by LIM (linear induction motor), to be used for transporting minerals and/or mine wastes. The capsules of the system possessing steel wheels travels on small rails imbedded inside the tube or conduit of the PCP. The specific system chosen for design and analysis has a square cross-section of 1m x 1m. A LIM is placed at the pipeline inlet and at every 10 km intervals along the tube as "booster pumps." The detailed design and analyses performed led to the following conclusions and recommendation:

6.1. Conclusions

- **The system is highly energy efficient**, having an EI (energy intensiveness) between 50 Btu/TM (for the largest throughput of 50 MTY) and 140 Btu/TM (for the smallest throughput of 1 MTY). Note that EI is the most suitable quantity for comparing the energy efficiency of different transportation system. Physically, it is the energy consumed (in **Btu**) for transporting each ton of cargo over unit distance (one **mile**). It is known that the average EI values for truck and train are respectively 2,300 Btu/TM, and 680 Btu/TM. This means that even at the lowest throughput of 1 MTY, the advanced PCP system studied here uses less than one-tenth of the energy used by an average truck and less than one-fourth of the energy used by an average train, for transporting the same amount of cargo over the same distance. The system is very energy efficient even though we must understand that the EI for PCP is based on electric power whereas the EI values for truck and train are based on the thermal energy contained from burning diesel fuel. So, we are comparing here electrical energy with the thermal energy of diesel fuel. Even with this difference taken into account, it can be concluded that **the LIM-driven PCP system is a super-efficient system which uses much less energy than truck and even train for transportation**. **Therefore, use of this new transportation system in mining will benefit the U.S. in terms of energy conservation, reduction of the nation's reliance on imported oil, and less air pollution and greenhouse gas generated by diesel driven trucks used for transporting mining products or mine wastes.**
- **The system is environmentally friendly**. By using such underground PCPs instead of aboveground trucks and trains for transporting minerals or mine wastes, traffic jam, accidents and noise causes by trucks on roads and by trains at rail crossings are eliminated. Since the PCP system is powered electrically, air pollution (emission of diesel fume) generated by trucks and trains are also eliminated.
- Because the PCP system is enclosed and the capsules cannot run outside the fixed route of the conduit, the capsules cannot be hijacked by terrorists and used as truck bombs or train bombs to attack another target**.** Also, being underground, it is far more difficult to sabotage a PCP than to sabotage a truck or train. Therefore, one can conclude that **using the PCP instead of truck or train to transport minerals and mine wastes enhances the security of mining operations, and enhances transportation security.**
- **The system has a huge throughput range** between 2 MTY and 50 MTY (million tones per year). Within this range the system can run smoothly not only continuously but also intermittently including startup, shutdown, and restart. For any throughput less than 2 MTY, the system is not only uneconomical but also may have problem running smoothly.

It is possible to run the system for throughput higher than 50 MTY but the logistic for feeding capsules into the tube and for loading capsules with minerals or wastes becomes very challenging.

- It is possible to design highly efficient LIM pumps for this system with motor efficiency approaching 90% at least for the case analyzed here where the capsules speed in the conduit is at 15 m/s approximately. The overall efficiency of the system (i.e., the motor efficiency times the pump efficiency) can be above 70%.
- Generally, higher capsule speeds generate higher motor efficiency but lower pump efficiency. The highest overall efficiency for this system happens when the capsule speed is in the neighborhood of 15 m/s.
- For very large throughput, such as above 10 MTY, the special PCP system studied here can be cost-effective as compared to using trucks by using twin tubes (double conduits) – one for the delivery line to transport loaded capsules and one for the return line to return empty cargoes. However, for throughputs less than about 10 MTY, to make the system cost-effective will require the use of a single tube or conduit, used alternatively for delivery of loaded capsules and for the return of empty capsules. For such relatively small throughputs, to reduce cost further consideration should be given to operating the system periodically, such as running the single-tube system at high capacity during day time and stopping the system at night, and so forth.
- This special PCP system provides a new means or tool for mining engineers to use in mining – for transporting minerals and mine wastes for projects that require large throughputs. In such cases, use of this system not only can reduce transportation cost but also will conserve energy, increase mining safety, and reduce environmental impacts. It can greatly benefit the mining industry and the public.
- For relatively small throughputs, such as less than 10 MTY, it is possible to save money by using smaller than 1m x 1m conduits. However, care must be exercise when using systems with small conduits. Not only must one make sure that the cost of loading each tonne of material into capsule will not go up dramatically when using smaller capsules, one must also device a practical means to remove capsule trains from the conduit following an accident. Based on Japan's 30-year experience in using blower-driven PCP systems, even though accidents in PCP are rare, there is always the possibility of accidents caused by capsules losing a wheel while moving through the pipe or conduit or by some other causes. Whenever happens, there must be a means to either fix the problem on site or remove the damaged capsules from the system, so that the system can restart and continue to operate soon. For the 1m x 1m system, this is not a problem. A person can be sent into (crawl through) the conduit from either end, to tie a rope on the first capsule train on each end, and to pull the train out by the rope using a rotating machine located outside the conduit. By doing so, trains near the two ends of the conduit can be easily pulled out. For trains away from the two ends, a small battery-operated car similar to a railroad handcar can be sent into the conduit with a driver to perform the task of pulling out trains. By doing so, train-by-train can be pulled out from the two ends of the conduit rather easily, until the damaged train is located, and is fixed on-site (such as changing a wheel while the capsule is in the conduit). Then, the system can be restarted. This clearly sets a limit as to how much smaller than 1m x 1m the PCP conduit can be. Also, for smaller system one must make sure that the LIM design is still efficient, and automatic loading is cost-effective.

- For throughput smaller than 10 MTY, it is worthwhile to consider a special PCP system using circular steel pipe of 1 m (40-inch) or smaller diameter, without using rails in the pipe. The system may use either blowers or LIM of circular cross-section (i.e., tubular LIM). Due to the use of circular pipes without rails, in order to keep capsules stable in the pipe each capsule must have the kind of wheel assemblies at the two ends of the capsule as shown in Fig.1(a). Instead of using rubber wheels for the wheel assemblies as used in Japan, steel wheels are recommended for mining use since it will significantly reduce contact friction which saves energy, and enable the use of higher capsule speeds than can be tolerated by using rubber wheels. Note that experience in Japan showed that capsules with rubber tires running in round pipes causes the tire temperature to rise. The capsule speeds of the Japanese PCP systems are limited to about 10 m/s in order to prevent excessive temperature rise of the tire, and resultant premature tire wear and damage. For throughputs smaller than 10 MTY, a LIM-driven PCP system using regular steel pipe smaller than 1 m in diameter is expected to be more cost-effective than using the 1m x 1m system studied in this project. However, the circular-pipe system is beyond the scope of this project, and hence not analyzed herein. It can be studied in a similar project if funding exists for such a study.

6.2. Recommendation

It is recommended that DOE sponsor a project to demonstrate this special PCP technology for mining use. To be most meaningful, the demo project should have participation and cost share from mining entities which wish to use this technology for their benefit. For demonstration purpose, it would be adequate to build, operate, and test such a 1m x 1m system for a length of 1 km, approximately, at the location of a given active or abandoned mine. This will enable the demonstration project to be completed in three years within a budget limit of 20 million dollars. Then the system will be ready for commercial use. The demo project will not only prove the technical feasibility of this new technology, but will enable checking the correctness and accuracy of the equations used in the design and analysis of this new technology. It will also generate the engineering and cost data needed for improving the design of the future commercial systems. It appears to be a worthwhile project for DOE and certain forward-looking mining companies to undertake.

7. REFERENCES

[1] Zandi, I. (1976), Transport of Solid Commodities via Freight Pipeline, Vol.2, Freight Pipeline Technology, U.S. Department of Transportation, Report No. DOT-TST-76T-36, Washington, D.C.

[2] ASCE (1998), "Freight pipelines: Current status and anticipated future use," report of the Task Committee on Freight Pipelines, ASCE, *J. of Transportation Engineering*, 124(4), 300-310.

[3] Cohen, R. A. (1999), "The Pneumatic Mail Tubes: New York's Hidden Highway and Its Development," Proceedings of the 1st International Symposium on Underground Freight Transport by Capsule Pipelines and Other Tube/Tunnel Systems, Columbia, Missouri, 1999, pp.189-202.

[4] Kosugi, S. (1992), "A Capsule Pipeline System for Limestone Transportation," Proc., 7th Int. Sym. on Freight Pipelines, Wollongong, Australia, Institution of Engineers, pp.13-17.

[5] Kosugi, S. (1999), "Pneumatic Capsule Pipelines in Japan and Future Developments," Proc., 1st Int. Sym. on Underground Freight Transport, Columbia, Missouri, pp.61-73.

[6] Civil Engineering News (2002), "Pneumatic Capsule Pipeline Removes Soil Vertically," Civil Engineering, Vol. 72, No.3, American Society of Civil Engineers, page 22.

[7] Liu, H. (2003), Pipeline Engineering (Chapter 7 Capsule Pipelines), CRC Press (Lewis Publishers), Boca Raton, Florida, pp.175-204.

[8] Esveld, C. (2001), Modern Railway Track, 2nd Edition, MRT-Production, the Netherlands.

[9]Central Rail Supply Website (2005), www.centralrailsupply.com/teerail2.htm.

[10] Hanson Pipe & Products, Inc. (2004), www.hansonconcreteproducts.com.

[11] Laithwaite, E.R. (1971), Linear Electric Motors, Mill & Boon Ltd., London, England.

[12] Yamamura, S. (1979), Theory of Linear Induction Motors, 2nd Edition, John Willey & Sons, Inc., New York.

[13] Gieras, J.F. (1994), Linear Induction Drives (Sec. 8.7, Finite Element Approach), Oxford Science Publications, England.

[14] Assadollabaik, M. (1984), Linear Induction Motors for Pumping Capsules in Pipes, Ph. D dissertation, Department of Civil Engineering, University of Missouri-Columbia, 182 pages. (Advisor: Henry Liu).

[15] Assadollabaik, M., Liu, H. and Hoft, R.G. (1986), "Experiments on an Electromagnetic Capsule Pump," Journal of Energy Resources Technology, American Society of Mechanical Engineers, Vol. 108, pp.262-268.

[16] Assadollabaik, M.; Liu, H. (1986), "Optimal design of electromagnetic capsule pump for capsule pipeline", Journal of Pipelines, Vol.5, 157-169.

[17] Plodpradista, W. (2002), Tubular Linear Induction Motor for Pneumatic Capsule Pipeline System, Ph. D dissertation, Department of Electrical Engineering, University of Missouri-Columbia, 202 pages. (Advisor: Robert M. O'Connell).

[18] O'Connell, R. M. (2003), " Linear Induction Motors for Pneumatic Capsule Pipeline Propulsion," Proceedings of the International Conference on Pipeline Engineering and Construction, American Society of Civil Engineers, Baltimore, Maryland, pp.1635-1646.

[19] Bhamidi, S.P. (2004), Design of a Single Sided Linear Induction Motor (SLIM) Using a User Ineractive Computer Program, M.S. Thesis, Department of Electrical Engineering, University of Missouri-Columbia, 90 pages.

[20] Hirst, E. (1973), "Energy Intensiveness of Transportation," Transportation Engineering Journal, American Society of Civil Engineers (ASCE), Vol. 99, No.1, pp.111-122.

[21] Liu, H. (2003), Pipeline Engineering (Chapter 1 Introduction), CRC Press (Lewis Publishers), Boca Raton, Florida, pp.3-16.

[22] Liu, H. and Assadollahbaik, M. (1979), Energy Conservation Value of Hydraulic Container Pipeline (HCP), Report prepared for the U.S. Department of Energy under Contract No. EM-78-02-4935, (DOE Report No. COO-4935-1), 38 pages.

[23] Liu, H., Noble, J., Zuniga, R. and Wu, J. P., Economic Analysis of Coal Log Pipeline Transportation of Coal, Capsule Pipeline Research Center, University of Missouri-Columbia, CPRC Report No. 95-1, July 1995.

[24] Liu, H. Noble, J., Wu, J. P. and Zuniga, R., "Economics of Coal Log Pipeline for Transporting Coal," Transportation Research-A, Vol. 32, No. 5, 1999, pp. 377-391.

[25] Liu, H. and Yadong Li [2000], Economic Analysis of Compacting and Transporting Biomass Logs for Co-Firing with Coal in Power Plants, report submitted to the U.S. Department of Energy under Contract DE-RA-98FT40155.

8. APPENDICES

Appendix I: Calculation of Capsule Velocity and Drag for a Steady Flow of Capsules in a Pneumatic Capsule Pipeline

I-1. Plain Capsule in Pipe (Conduit)

For plain capsules (i.e., capsules without end disk or end plate) of both circular cross-section and rectangular cross-section moving through a pneumatic capsule pipeline (PCP) of respectively circular and rectangular cross-sections, the capsule velocity and the drag on the capsule can be predicted in the same manner as for hydraulic capsule pipeline (HCP) as shown in (Gao 1999). In regime 2 where the fluid velocity V is greater than the capsule velocity V_c, use of the one-dimensional continuity, momentum and energy equations of fluid mechanics yields:

$$C_{21}(V-V_c)^2 + C_{22}(V-k^2V_c)^2 = C_{23} \quad \text{..... (I-1)}$$

where

$$C_{21} = C_p + b^2 - 1 + ab^3 f_c + C_L\eta \quad \text{..... (I-2)}$$

$$C_{22} = akb^3 f_p \quad \text{..... (I-3)}$$

$$C_{23} = 2gL_c(S-1)(\sin\theta + \eta\cos\theta) \quad \text{..... (I-4)}$$

$$k = \frac{D_c}{D} = \sqrt{\frac{A_c}{A}} \quad \text{..... (I-5)}$$

$$b = \frac{A}{A-A_c} = \frac{1}{1-k^2} \quad \text{..... (I-6)}$$

$$a = \frac{L_c}{D_c} = \frac{L_c}{\sqrt{4A_c/\pi}} \quad \text{..... (I-7)}$$

In the above equations, C_p is the pressure coefficient facing the flow and is equal to 0.8 approximately; C_L is the lift coefficient which is much smaller than 1.0 and hence is negligible; η is the contact friction coefficient between the capsule and the pipe; g is the gravitational acceleration which is equals to 9.81 m/s^2 (32.2 ft/s^2 in English units); S is the density ratio, which is the capsule density ρ_c divided by the fluid density ρ; and θ is the incline angle of the sloped pipe – θ is positive when the pipe is rising and so forth. Note that for rectangular capsules in a rectangular pipe, the quantities k, b and a in Eqs. I-5, I-6 and I-7 should be calculated from the cross-sectional areas A_c and A instead of the diameters D_c and D, or the diameter ratio k. The quantities f_c and f_p are friction factors for the capsule and the pipe, respectively. Their values can be found from the Moody diagram in fluid mechanics using the following Reynolds numbers:

For f_c :

$$R_c = \frac{D(V-V_c)}{\nu(1+k)} = \frac{\sqrt{(4A/\pi)}(V-V_c)}{\nu(1+k)} \quad \text{..... (I-8)}$$

For f_p:
$$R_p = \frac{D(V - k^2 V_c)}{\nu(1+k)} = \frac{\sqrt{(4A/\pi)}(V - k^2 V_c)}{\nu(1+k)} \quad \text{..... (I-9)}$$

For turbulent flow, the values of f_c and f_p depend on not only the Reynolds numbers R_c and R_p, respectively, but also the relative roughness ε_c and ε_p, respectively. The last two quantities are calculated from:

$$\varepsilon_c = \frac{e_c}{D - D_c} = \frac{e_c}{\sqrt{4/\pi}(\sqrt{A} - \sqrt{A_c})} \quad \text{..... (I-10)}$$

and
$$\varepsilon_p = \frac{e_p}{D - D_c} = \frac{e_p}{\sqrt{4/\pi}(\sqrt{A} - \sqrt{A_c})} \quad \text{..... (I-11)}$$

More accurate values of f_c and f_p can be obtained by using computer and the Colebrook formula, instead of the Moody diagram, as follows:

$$\frac{1}{\sqrt{f}} = 1.14 - 2.0LOG\left[\varepsilon + \frac{9.35}{R\sqrt{f}}\right] \quad \text{..... (I-12)}$$

where f is the friction factor, LOG is the common logarithm based on 10, ε is the relative roughness, and R is the Reynolds number. The above equation can be used for both f_c and f_p, using values of ε_c and ε_p given by Eqs. I-10 and I-11, and values of R_c and R_p given by Eqs. I-8 and I-9, respectively. Since Eq.I-12 is implicit (having f on both sides of the equation), it must be solved by iteration which is simple with computer.

The foregoing equations can be used to predict the value of capsule velocity, V_c, from any known velocity of the fluid, V. Once both V and V_c are known, the drag force on the capsule can be calculated from

$$F_D = (C_p + b^2 - 1)\frac{\rho(V - V_c)^2}{2}A_c + A_c\frac{ab^3\rho}{2}[f_c(V - V_c)^2 + kf_p(V - k^2V_c)^2]$$
..... (I-13)

Then, the drag coefficient on the capsule, C_D, can be calculated from

$$C_D = \frac{2F_D}{A_c\rho(V - V_c)^2} \quad \text{..... (I-14)}$$

I.2 Plain Capsule in LIM

For a plain capsule (i.e., capsule without end disk or end plate) in a LIM under steady-state condition, the capsule velocity V_c' is higher than the air velocity V'. The situation is similar to region 3 of HCP, which yields (Kao 1999):

$$\frac{2F_e}{\rho A_c} + C_{31}(V_c' - V')^2 + C_{32}(V' - k'^2 V_c')\left|V' - k'^2 V_c'\right| = C_{33} \quad \text{..……..} \quad \text{(I-15)}$$

where $C_{31} = C_L\eta' - (C_p + b'^2 - 1 + a'b'^3 f_c')$ …… (I-16)

$C_{32} = a'k'b'^3 f_L'$ …… (I-17)

$C_{33} = 2gL_c(S-1)(\sin\theta + \eta'\cos\theta)$ ……. (I-18)

$k' = \frac{D_c}{D'} = \sqrt{\frac{A_c}{A'}}$ ……..…….. (I-19)

$b' = \frac{A'}{A' - A_c} = \frac{1}{1 - k'^2}$ …….. (I-20)

$a' = a = \frac{L_c}{D_c} = \frac{L_c}{\sqrt{4A_c/\pi}}$ ……... (I-21)

In the above equations, C_p is the pressure coefficient facing the flow and is equal to 0.8 approximately; C_L is the lift coefficient which is much smaller than 1.0 and hence is negligible; η' is the contact friction coefficient between the capsule and the LIM; g is the gravitational acceleration which is equals to 9.81 m/s^2 (32.2 ft/s^2 in English units); S is the density ratio, which is the capsule density ρ_c divided by the fluid density ρ; and θ is the incline angle of the sloped pipe – θ is positive when the pipe is rising and so forth. Note that for rectangular capsules in a rectangular LIM, the quantities k', b' and a in Eqs. I-5, I-6 and I-7 should be calculated from the cross-sectional areas A_c and A' instead of the diameters D_c and D', or the diameter ratio k'. The quantities f_c' and f_L' are friction factors for the capsule and the LIM, respectively. Their values can be found from the Moody diagram in fluid mechanics using the following Reynolds numbers:

For f_c' : $R_c' = \frac{D'(V_c' - V')}{\nu(1+k')} = \frac{\sqrt{(4A'/\pi)}(V_c' - V')}{\nu(1+k')}$ …….. (I-22)

For f_L' : $R_L' = \frac{D'\left|V' - k'^2 V_c'\right|}{\nu(1+k')} = \frac{\sqrt{(4A'/\pi)}\left|V' - k'^2 V_c'\right|}{\nu(1+k')}$ …….. (I-23)

For turbulent flow, the values of f_c' and f_L' depend on not only the Reynolds numbers R_c' and R_L', respectively, but also the relative roughness ε'_c and ε'_L, respectively. The last two quantities are calculated from:

$$\varepsilon_c' = \varepsilon_c = \frac{e_c}{D' - D_c} = \frac{e_c}{\sqrt{4/\pi}(\sqrt{A'} - \sqrt{A_c})} \quad \text{……..} \quad \text{(I-24)}$$

and $$\varepsilon_L = \frac{e_L}{D' - D_c} = \frac{e_L}{\sqrt{4/\pi}(\sqrt{A'} - \sqrt{A_c})} \quad \text{..... (I-25)}$$

More accurate values of f_c and f_L can be obtained by using computer and the Colebrook formula, instead of the Moody diagram, as given in Eq.I-12.

The foregoing equations can be used to predict the value of capsule velocity, V'_c, from any known velocity of the fluid, V', and known electromagnetic force F_e. Alternatively, the equations can be used to calculate the electromagnetic force F_e if both V' and V'_c are known. Once both V' and V'_c are known, the drag force on the capsule can be calculated from

$$F'_D = -(ab'^3 f'_c + C_p + b'^2 - 1)\frac{\rho(V'_c - V')^2}{2} A_c + A_c \frac{ab'^3 k' f'_L \rho}{2}(V' - k'^2 V'_c)\left|V' - k'^2 V'_c\right| \quad \text{..... (I-26)}$$

Note that the above equation is expected to yield a negative value of F'_D which means that the drag force on the capsule in the LIM is in the opposite direction of the mean flow, which in turn means a transfer of energy from the capsule to the flow instead of the other way around when the capsule is in the pipe (outside the LIM) under steady state.

Using the value of F'_D determined from Eq.I-26, the drag coefficient on the capsule, C_D, can be calculated from

$$C'_D = \frac{2\left|F'_D\right|}{A_c \rho (V'_c - V')^2} \quad \text{..... (I-27)}$$

I-3. Capsule train with a single end disk or plate on each capsule

As described in Sec.3, the capsules to be used for transporting minerals and mine wastes will be linked together in trains with each train containing five capsules. In such an operation, the lead capsule of each train encounters a greater drag force than the trailing capsules. To determine the total drag of a train, the drag must be separately calculated for the leading capsule and the trailing capsules. Then, they are combined (summed up) to yield the total drag for the train. Therefore, it is necessary to derive the equations for predicting the drag for the lead capsule separately from that for the trailing capsules.

(a) Drag for the lead capsule

An accurate account of the drag on capsules with end disks or plates must include both the form drag due to pressure difference and the skin drag due to shear on the capsule wall. This is especially true when the capsule diameter is relatively large – say, when D_c/D is greater than 0.95, or when $(D-D_c)$ is less than 0.05D. Pertinent equations for this case, including both form drag and skin drag, are derived as follows:

Figure I-1 shows a capsule with diameter D_c and with an end disk of diameter D_d. The length of the capsule is L_c. The diameter of the pipe surrounding the capsule is D. Term V is the fluid velocity in the pipe away from the capsule, V_c is the velocity of the capsule, and V_a is the fluid velocity in the annular region. All velocities are positive when they are in the x

direction. **The fluid velocity V is assumed to be greater than the capsule velocity V_c.** From the continuity equation of incompressible flow, we have

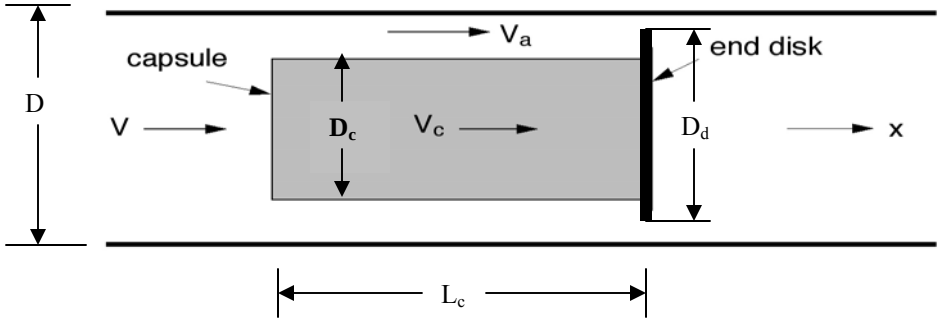

Figure I-1. Analysis of a capsule with an end Disk

$$V_a = \frac{1 - k^2 V_c}{1 - k^2} \qquad \text{(I-28)}$$

in which $k = D_c / D$. One can expect that the drag force F_D on the capsule and the end disk is positive (i.e., in the x direction) when $V > V_c$ and negative when $V < V_c$.

Figure I-2 shows the flow pattern around the capsule and end disk as viewed from the moving capsule, when $V > V_c$. The approach velocity is now $V - V_c$ and the capsule appears to be stationary. The fluid velocity in the annular region is $V_a - V_c$. There is a stagnation point on the left end of the capsule, a separation region around the left edge of the capsule and a second separation region behind the end disk forming a large wake region. The drag force F_D is shown in the figure along with the fluid shear stresses τ_c and τ_p, where τ_c is the shear on the capsule, and τ_p is the shear on the pipe.

As shown in Figure I-2, the cross section (1) is upstream of the capsule, and cross section (2) cuts the separation region at it maximum diameter. Cross section (3) is located a small distance upstream of the end disk, and section (4) is located s small distance downstream of the end disk at the maximum diameter of the wake.

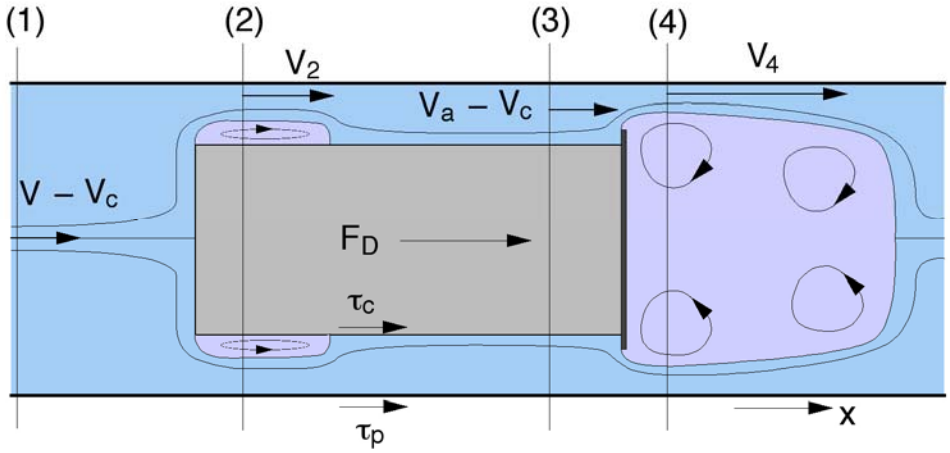

Figure I.2 Flow relative to a moving capsule when $V > V_c$

The Bernoulli's equation can now be written along a streamline between cross sections (1) and (2) to yield

$$\rho \frac{(V - V_c)^2}{2} + p_1 - \rho \frac{V_2^2}{2} - p_2 = 0 \qquad \ldots\ldots \qquad \text{(I-29)}$$

The above equation can be used to calculate the pressure difference $p_1 - p_2$ provided that V_2 can be expressed in terms of V and V_c. This can be done by introducing a contraction coefficient

$$C1_c = \frac{A_2}{A_{annular}} \qquad \text{(I-30)}$$

in which A_2 is that part of the flow area between the pipe wall and the separation region. Term $A_{annular}$ is the cross-sectional area of the annular region. Equation I-30 can be written

$$C1_c = \frac{A_2}{A(1 - k^2)} \qquad \text{(I-31)}$$

in which A is the cross-sectional area of the pipe. From continuity we have

$$V_2 = \frac{(V - V_c)}{C1_c(1 - k^2)} \qquad \ldots\ldots\ldots\ldots \text{(I-32)}$$

We will discuss later how $C1_c$ is evaluated.

Similarly an equation for the difference in the pressure on sections (3) and (4) is

$$\rho \frac{(V_a - V_c)^2}{2} + p_3 - \rho \frac{V_4^2}{2} - p_4 = 0 \qquad \ldots. \qquad \text{(I-33)}$$

To calculate V_4, a second contraction coefficient, C_c, is introduced and

$$V_4 = \frac{(V - V_c)}{C_c(1 - k_d^2)} \qquad \text{(I-34)}$$

in which $k_d = D_d / D$. Evaluation of C_c is discussed later.

The difference in pressure between (2) and (3) can be calculated by application of the momentum equation to the control volume shown in blue in Figure I-3.

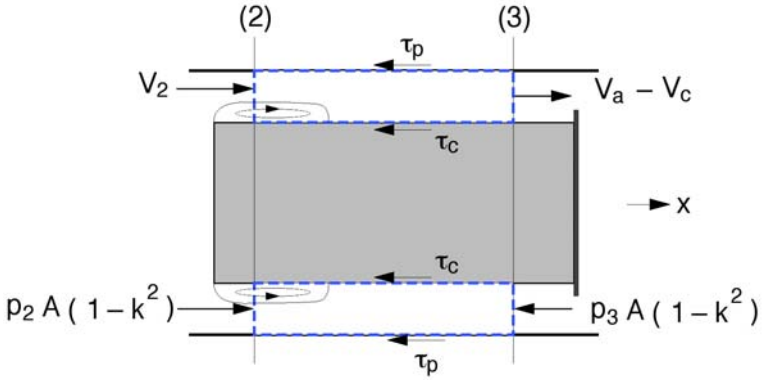

Figure I-3 Control volume between (2) and (3)

The resulting equation is

$$p_2 - p_3 - 4 L_c \frac{\tau_p + k\,\tau_c}{D\,(1 - k^2)} - \rho\,(V_a - V_c)\,(V_a - V_c - V_2) = 0 \qquad \ldots\ldots \quad \text{(I-35)}$$

Figure I-4 shows a control volume, taken between (1) and (4), that contains the capsule and end plate. For this control volume, F_D is reversed from Figure I-2 because it is the external force required to hold the capsule stationary. The momentum equation gives

$$(p_1 - p_4)A - F_D - \tau_p \pi D L_c - \rho A (V - V_c)(V_4 - V + V_c) = 0 \qquad \ldots\ldots\ldots \text{(I-36)}$$

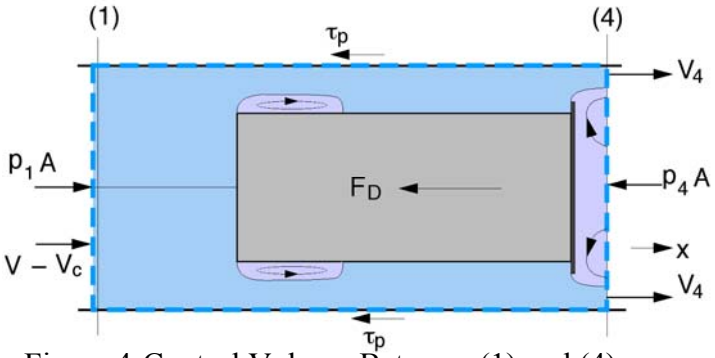

Figure 4-Control Volume Between (1) and (4)

By combining Eqs. I-28 through I-36, one can obtain

$$\frac{2 F_D}{\rho A (V - V_c)^2} = b^2 \left(\frac{1}{C1_c} - 1\right)^2 + \left(\frac{b_d}{C_c} - 1\right)^2 + 8\, b\, \frac{L_c}{D} \frac{(k\,\tau_c + k^2\,\tau_p)}{\rho\,(V - V_c)^2} \qquad \ldots \text{(I-37)}$$

where $b_d = 1/(1-k_d^2)$.

The shear stress terms can be expressed as

$$\tau_c = \rho \frac{f_c}{8} \frac{(V - V_c)\,|V - V_c|}{(1 - k^2)^2} \qquad \ldots\ldots\ldots\ldots \text{(I-38)}$$

$$\tau_p = \rho \frac{f_p}{8} \frac{(V - k^2 V_c)\,|V - k^2 V_c|}{(1 - k^2)^2} \qquad \ldots\ldots\ldots \text{(I-39)}$$

in which f_c and f_p are resistant coefficients obtained from the Colebrook formula or a Moody diagram. The Reynolds numbers are calculated from Equations I-8 and I-9. The relative roughnesses are calculated from Equations I-10 and I-11. Combining Equations I-37, I-38 and I-39 yields

$$F_{form} = \frac{1}{2} \rho A C_{form} (V - V_c)^2 \qquad \text{……..(I-40)}$$

$$C_{form} = b^2 (\frac{1}{C1_c} - 1)^2 + (\frac{b_d}{C_c} - 1)^2 \qquad \text{…….(I-41)}$$

where $F_D = F_{form} + F_{shear}$ and

$$F_{shear} = \frac{1}{2} \rho A b^3 f_c k \frac{L_c}{D} (V - V_c) | V - V_c | + \frac{1}{2} \rho A b^3 f_p k^2 \frac{L_c}{D} (V - k^2 V_c) | V - k^2 V_c | \qquad \text{…….(I-42)}$$

Note that while Eq.I-41 is valid only for $V > V_c$, Eq.I-42 is valid for all combinations of V and V_c .

Equation I-13 is the drag force on a capsule without any end disk or end plate. One can see that the shear drag given by Eq.I-42 is the same as the second group of terms in Eq. I-13. Recall that $A_c = k^2 A$. For a capsule without end disk the form-drag coefficient given by Eq. I-41 reduces to

$$C_{form} = b^2 (\frac{1}{C1_c} - 1)^2 + (b - 1)^2 \qquad \text{…….……(I-43)}$$

Combining Equations I-40 and I-43 and equating the F_{form} to the first term in Eq. I-13 yields

$$b^2 (\frac{1}{C1_c} - 1)^2 + (b - 1)^2 = (C_p + b^2 - 1) k^2 \qquad \text{… (I-44)}$$

Solving for $C1_c$ yields

$$C1_c = \frac{1}{1 + \frac{k}{b} \sqrt{b + C_p - 1}} \qquad \text{……..(I-45)}$$

Kosugi's equation with one end disk is

$$C_D = 2 k_d^4 b_d^2 \qquad \text{…….(I-46)}$$

This equation discussed earlier is for stationary capsules. Judging from the absence of capsule dimensions, Eq. I-46 best describes a capsule that has a diameter much smaller than the end-disk diameter. Setting k = 0 in Eq. I-41 yields

$$C_{form} = (\frac{b_d}{C_c} - 1)^2 \qquad \text{…… (I-47)}$$

Equating the above equation to Eq. I-46 yields

$$\left(\frac{b_d}{C_c} - 1\right)^2 = 2\, k_d^6\, b_d^2 \qquad \text{……. (I-48)}$$

Solving for C_c yields Eq.I-45.

Note that the form drag on the lead capsule given by Eqs.I-41 is correct only when the air velocity V is larger than the capsule velocity V_c. In places where this is not the case, as in the LIM when the capsule velocity is greater than the air velocity, a similar derivation to that given above can be conducted, which yields **the following result for the case of $V_c > V$:**

$$C_{form} = (1 - b)^2 + \left(b - \frac{b_d}{C_c}\right)^2 \text{ for } V < V_c \qquad \text{……. (I-49)}$$

As mentioned before, while the form drag is different for the case $V<V_c$ from the case $V>V_c$, the skin drag of the two cases are identical, given by Eq.I-42.

(b) Drag for the trailing capsules

The form drag coefficient on any trailing capsule is

$$C_{form} = \left(\frac{b_d}{C_c} - b\right)^2 \qquad \text{……. (I-50)}$$

The above equation holds for both $V>V_c$ and $V<V_c$.

The skin drag for the trailing capsule can be calculated from

$$F_{shear} = \frac{1}{2}\rho A b^3 f_c k \frac{L_c}{D}(V - V_c)|V - V_c| + \frac{1}{2}\rho A f_p \left(b^3 k^2 \frac{L_c}{D} - b^2 \frac{L_s}{D}\right)(V - k^2 V_c)\,|V - k^2 V_c| \qquad \text{……(I-51)}$$

for the case $V>V_c$, and can be calculated from

$$F_{shear} = \frac{1}{2}\rho A b^3 f_c k \frac{L_c}{D}(V - V_c)|V - V_c| + \frac{1}{2}\rho A b^3 f_p k^2 \frac{L_c + L_s}{D}(V - k^2 V_c)\,|V - k^2 V_c| \qquad \text{… (I-52)}$$

for the case $V<V_c$.

(c) Combined drag on capsule train

Once the air velocity V and the capsule velocity V_c are known or assumed, the combined (total) drag on each capsule train can be calculated from a summation of the form drag and the skin drag on individual capsules in the train, namely,

$$F_D = F_{form} + F_{shear} \qquad \text{…….. (I-53)}$$

The drag force acting on the leading capsule in the train is computed from Eqs.I-40, I-41 and I-42 when V is greater than V_c, and from Eqs.I-40, I-49 and I-42 when V is smaller than V_c.

For each of the trailing capsules, the drag is computed from Eqs.I-50 and I-51 when V is greater than V_c, and from Eqs.I-50 and I-52 when V is smaller than V_c.

The total drag on the train is then the sum of the drags on the individual capsules in the train, including both the lead capsule, and the trailing capsules.

Appendix II: Amendment of Steady-State Equation for Pressure Drop Across LIM

In the steady-state fluid mechanics analysis of the pressure drop along PCP, the following equation was used:

$$\Delta p' = \Delta p \qquad \ldots\ldots\ldots\ldots\ldots\ldots\ldots\ldots \qquad (3.3.23)$$

where Δp is the pressure drop across the pipeline or conduit, from the outlet of the LIM mounted upstream, to the exit of the pipe or conduit, and $\Delta p'$ is the pressure rise across the LIM from inlet to outlet. Equation 3.3.23 is actually incorrect if one considers the fact that the capsules entering the LIM at a speed of approximately 20 m/s, and leaves the LIM at approximately the same speed, but the speed quickly reduces to the pipe velocity of 15 m/s within a short distance downstream of the LIM. This drop in capsule speed causes a transfer of momentum to the fluid (air) in the pipe, thereby increases the pressure in the pipe. This pressure rise is not accounted for by Eq.3.2.23, and can significantly underestimate the pressure drop Δp along the pipe. To fix this problem, Eq.3.3.23 must be modified as follows:

$$\Delta p' + \Delta p^{*} = \Delta p \qquad \ldots\ldots\ldots\ldots\ldots\ldots\ldots\ldots \qquad (II\text{-}1)$$

where the quantity Δp^{*} represents the correction term needed to take care of the momentum change mentioned above. The correction term is obtained as follows:

Figure II-1 shows a capsule entering the LIM from the left at a velocity V_c'. The LIM length is L' whereas the pipe length is L. Note that for clarity, the vertical scale of the drawing has been exaggerated while the horizontal scale has been reduced. Also note that the LIM diameter D' is slightly smaller than the pipe diameter D. In the LIM, capsule velocity is V_c' and the capsule spacing is TV_c'; in the pipe the capsule velocity and spacing are respectively V_c and TV_c. A control volume is drawn in the center of Fig.II-1, represented by the blue dashed line.

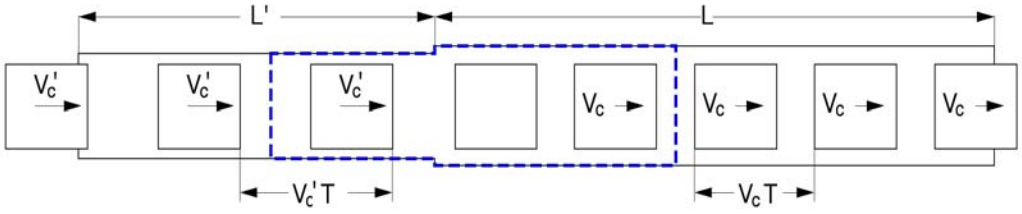

Figure II-1- Sketch to analyze the effect of pressure rise at the LIM

Because capsules enter the control volume at velocity V_c' but leave the control volume at velocity V_c, where V_c' is greater than V_c, the momentum of capsules entering the control volume is greater than the momentum of those leaving the control volume. This change in momentum gives rise to a pressure increase, designated as Δp^*. The magnitude of this pressure increase can be obtained by using a quasi-steady approach, i.e., treating the flow as steady by viewing it at a fixed time.

Suppose at time t = 0 the capsules are at the location shown in Figure II-1. For a constant launching interval, T, the placement of capsules at t = T, 2T, … would be exactly the same provided all of the capsule are identical. The capsule spacing and position in the LIM would remain the same from one time interval to the next, and the capsule spacing and position in the pipe would also be the same at different time intervals. From this prospective, the momentum inside the control volume would be constant. During the time between intervals, one capsule would leave and one would enter the control volume. Hence momentum enters into the control volume at the rate of $M_C\ V'_C / T$ and leaves the control volume at the rate of $M_C\ V_C / T$, where M_C is the mass of each capsule. Consequently, the change in momentum is

$$\frac{M_c}{T} (V_c - V'_c)$$

The cross-sectional areas of the LIM and the pipe are almost the same. Thus, the pressure rise across the control volume is

$$\Delta p^* = \frac{M_c}{T\ A} (\ V'_c - V_c\ ) \qquad \text{……..} \qquad \text{(II-2)}$$

in which A is the cross-sectional area of the LIM, the pipe or some average of the two.

Substituting Eq.II-2 into Eq.II-1 yields

$$\Delta p = \Delta p' + (V'_c - V_c)\frac{M_c}{TA} \qquad \text{……..} \qquad \text{(II-3)}$$

A way is needed to evaluate the pumping action efficiency of the LIM and capsules. For a normal motor-pump arrangement, the efficiency of the pump would be defined as the ratio of output power V A Δp developed by the pump to the output power of the motor. For our case, the LIM-pump efficiency is defined as

$$\eta = \frac{V'\ A'\ \Delta p'}{F_{em}\ V'_c} \qquad \text{…….} \qquad \text{(II-4)}$$

in which V ', A ' and Δp' are respectively the air velocity in the LIM, the cross-sectional area of the LIM, and the pressure rise across the LIM. The rise in pressure across the LIM, Δp ', does not include Δp*. Term F_{em} is the LIM force on all of the capsules in the LIM and V_c' is the capsule velocity in the LIM.

Appendix III: Equations and Procedures for the Design of LIM for Use in Pneumatic Capsule Pipeline (PCP)

III-1. Basic Concept

Note that PCPs based on round (circular) pipes require different types of LIMs governed by somewhat different equations than PCPs based on rectangular conduit. The PCP using a round pipe can best be powered by LIMs of round cross-section – the tubular LIM, acronymed "TLIM". On the other hand, the PCP that uses a rectangular conduit with capsule running on guided rails as in this DOE project can best be powered by two parallel single-sided flat LIMs, acronymed "SLIMs", mounted on opposite walls as shown in Figures III-1 and III-2.

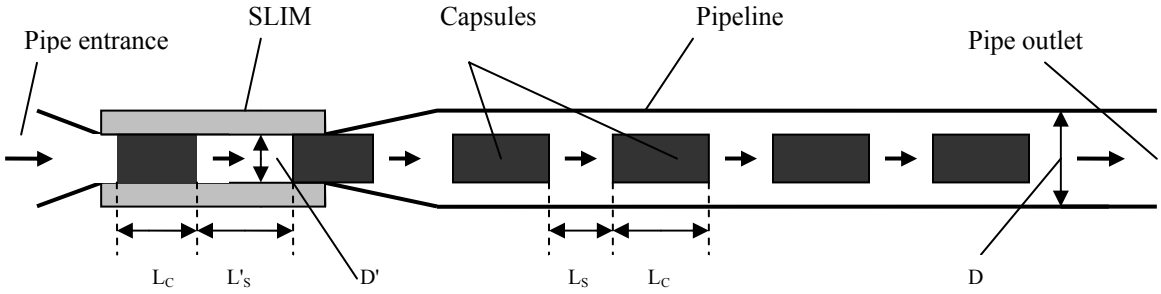

Figure III-1 Top View of a PCP of Rectangular Cross Section Driven by a Parallel-Stator Single-Sided LIM

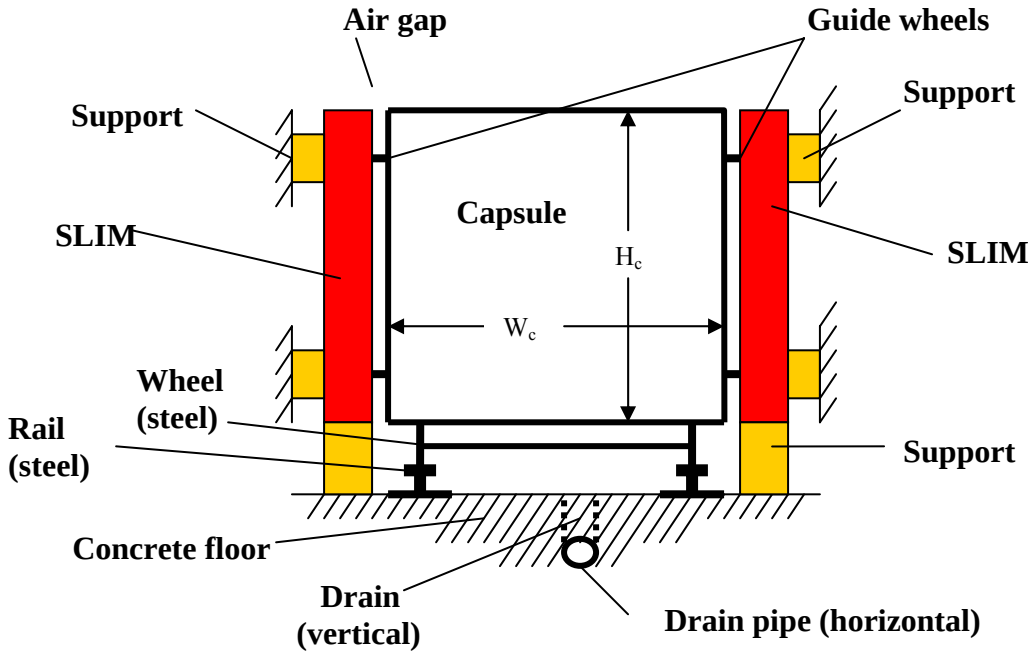

Figure III-2 Cross-sectional view of a SLIM pump needed for driving a PCP of rectangular cross section

Conceptually, each single-sided LIM (namely each SLIM) is formed by cutting the stator (primary) of a rotary motor of the induction type along its radius, and then unfolding (unrolling) it into a plane or flat plate – see Figure III-3(a) & (b). By rolling the SLIM into a round tube along the main (longitudinal) axis of the SLIM, a tubular linear induction motor (TLIM) is formed – see Figure III-3(b). The LIM pump to be designed and analyzed herein is made of two SLIMs placed on the opposite sides of a rectangular cross section of the PCP as shown in Figures III-1 and III-2. By making the two halves identical and connecting them to the same 3-phase ac power source that drives the LIM pump, each half can be analyzed by using the same equations for a SLIM. Thus, the electromagnetic force F_e generated by the LIM pump on each capsule calculated from fluid mechanics equations must be provided by the two SLIMs, or each SLIM providing $0.5F_e$ to each capsule.

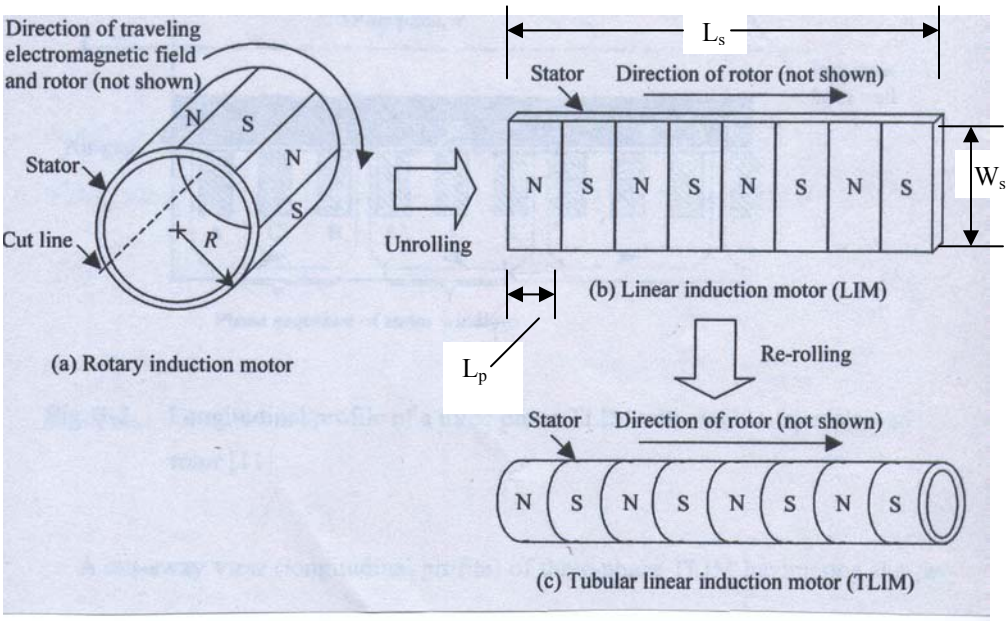

Figure III-3 Transformation from rotary induction motor to SLIM and then to TLIM

Most of the theories and equations for conventional rotary induction motor are applicable to the SLIM and TLIM. A fact common to all types of induction motors is that the "*stator*" (i.e., the "*primary*" or the stationary part), when energized electrically, generates a changing magnetic field in the "*rotor*" (i.e., the "*secondary*" or the moving part), which in turn produces an eddy current in the rotor. This eddy current, when interacting with the changing magnetic field, produces a force F_r on the rotor which is the driving force of the motor. For the rotary type of induction motors, this driving force is in the circumferential direction, causing the rotor and its shaft to turn. In contrast, for SLIM and TLIM, the force is linear (longitudinal), causing the rotor such as a capsule to move longitudinally in a pipe. A force in the transverse (lateral) direction is also generated, which either pushes the rotor away from the stator (repulsion), or pulls the rotor towards the stator (attraction), depending on the operational condition of the motor. With the use of two identical SLIMs as show in Figures III-1 and III-2, the transverse force generated on the capsule by each of the two SLIMs is of equal magnitude but opposite directions, thereby canceling out. The same holds for TLIMs; no net force in the transverse (radial) direction is generated.

III-2. Equations

(a) Basic Equations

The following equations for the design of LIMs for PCP are derived from various previous studies, including [11-19].

All types of induction motors operate at a rotor velocity (speed) V_r that is a few percent smaller than the synchronous velocity or speed V_s, which is the speed of the moving magnetic field. A dimensionless quantity, S, called the "***slip***", is defined as

$$S = \frac{V_s - V_r}{V_s} \quad \text{……} \quad \text{(III-1)}$$

For efficient operation of induction motors, S is usually less than 5%, or 0.05. For any type of LIMs used in pneumatic capsule pipeline (PCP), the rotor is the capsule, and so the rotor velocity V_r becomes the capsule velocity in the LIM, V'_c. Therefore, Eq.III-1 becomes

$$S = \frac{V_s - V'_c}{V_s} \quad \text{……..} \quad \text{(III-2)}$$

Equation III-2 can be rearranged to yield

$$V_s = \frac{V'_c}{1 - S} \quad \text{……} \quad \text{(III-3)}$$

As in the case of rotary induction motors, each SLIM or TLIM consists of several pairs of poles (north poles and south poles) as shown in Figure III-3 (b) and (c). The number of poles of each LIM, an even number, is designated as N_p. N_p equals 2, 4, 6, etc., respectively for LIMs of 2 poles, 4 poles, 6 poles, etc. The LIM in Figure III-3(b) has eight poles. The linear distance between neighboring poles, from N to S, is called the "***pole pitch***"; it is designated as L_p as indicated in Figure III-3 (b). The total length of each unit of the LIM is L_1. Generally,

$$L' = n\, L_1 \quad \text{…….....} \quad \text{(III-4)}$$

and

$$L_1 = N_p L_p \quad \text{……} \quad \text{(III-5)}$$

where n is the number of units of SLIMs to form a LIM pump of length L'.

The synchronous speed V_s is related to the pole pitch L_p as follows:

$$V_s = 2\, f\, L_p \quad \text{……} \quad \text{(III-6)}$$

or

$$L_p = \frac{V_s}{2f} \quad \text{……} \quad \text{(III-7)}$$

where f is the frequency of the power supply, which is 60 hertz in the United States and 50 hertz in Europe.

(b) Power Rating and Rated Input Phase Current

The time-averaged value of the input electric power to each unit of SLIM, P_i, called the "***active power***" in electrical engineering, can be found from the following formula:

$$P_i = m(V_1)_{rms}(I_1)_{rms}\cos\Phi \quad \ldots\ldots\ldots\ldots\ldots\ldots \quad \text{(III-8)}$$

where m is the number of electrical phases, $(V_1)_{rms}$ and $(I_1)_{rms}$ are the root-mean-square (RMS) values of the input phase voltage V_1 and current I_1, respectively, and Φ is the phase angle between the voltage V_1 and I_1. The quantity $\cos\Phi$ is generally referred to as the "***power factor***."

The output power of each SLIM is

$$P_o = F_1 V_c' \quad \ldots\ldots\ldots\ldots\ldots\ldots \quad \text{(III-9)}$$

where F_1 is the force (thrust) exerted by one unit of SLIM on the capsule, and V_c' is the capsule velocity in the SLIM. The quantity F_1 is related to the total force F_e exerted by different units of the SLIM on the entire capsule in the following manner:

$$F_1 = \frac{L_1}{L_c} F_e \quad \ldots\ldots\ldots\ldots\ldots\ldots \quad \text{(III-10)}$$

Note that the single-unit SLIM length L_1 is usually smaller than the capsule length L_c. Thus, from Eq.III-10, F_1 is smaller than F_e. The value of F_e is known from fluid mechanics calculations.

From Eqs. III-8 and III-9, the efficiency of the SLIM is

$$E_m = \frac{P_o}{P_i} = \frac{F_1 V_c'}{m(V_1)_{rms}(I_1)_{rms}\cos\phi} \quad \ldots\ldots\ldots\ldots \quad \text{(III-11)}$$

From Eq.III-11, if a typical value of $E_m\cos\Phi$ is assumed, the RMS value of the input phase current I_1 can be calculated from

$$(I_1)_{rms} = \frac{F_1 V_c'}{m(V_1)_{rms} E_m \cos\phi} \quad \ldots\ldots\ldots\ldots \quad \text{(III-12)}$$

(c) Magnetic Flux and Induced Voltage

With a sinusoidal electric current going through a one-turn coil, the magnetic flux Φ generated is:

$$\Phi = \Phi_p \sin 2\pi ft \quad \ldots\ldots\ldots\ldots\ldots\ldots\ldots\ldots \quad \text{(III-13)}$$

where Φ_p is the amplitude of the flux per pole. The corresponding induced voltage is

$$e_1 = \frac{d\Phi}{dt} = 2\pi f \Phi_p \cos(2\pi ft) \quad \ldots\ldots\ldots\ldots\ldots\ldots \quad \text{(III-14)}$$

The RMS value of e_1 is

$$e_{1rms} = \frac{2\pi}{\sqrt{2}} f\Phi_p = \sqrt{2}\pi f \Phi_p \quad \ldots\ldots\ldots\ldots\ldots\ldots \quad \text{(III-15)}$$

For a SLIM of N_1 turns per phase, the induced voltage is e, and the RMS of the induced voltage generated is

$$e_{rms} = \sqrt{2}\pi f \Phi_p k_w N_1 \quad \ldots\ldots\ldots\ldots\ldots\ldots\ldots \quad \text{(III-16)}$$

where the quantity k_w is the winding factor determined from

$$k_w = \frac{\sin(\frac{\pi}{2m})}{q_1 \sin(\frac{\pi}{2mq_1})} \sin(\frac{Y\pi}{2}) \qquad \text{……..} \qquad \text{(III-17)}$$

where Y=1 for single-layer winding and Y=2/3 for double-layer winding. Note that when Y is 1 and when the number of slots per pole per phase q_1 is 1, Eq. III-17 yields $k_w = 1$.

The SLIM flux per pole Φ_p in Eq.III-16 is determined from

$$\Phi_p = (B_g)_{av} \frac{L_1 W_s}{N_p} \qquad \text{……} \qquad \text{(III-18)}$$

where $(B_g)_{av}$ is the average air-gap flux density, and W_s is the width of the SLIM (namely, the stator width). Note that for sinusoidal ac waves,

$$(B_g)_{av} = \frac{2}{\pi}(B_g)_{\max} \qquad \text{……..} \qquad \text{(III-18a)}$$

(d) Effective Air Gap, Slot Dimensions and Stator Yoke Dimension

As shown in Fig.III-4, a single-sided LIM pump consists of two main parts: the **stator** which is the stationary part and the **rotor** which is the moving part. The stator includes a set of coils of copper wire (shown here as yellow squares) wound between the teeth and the yokes, which are both made of laminated iron (shown in red layers). It also has a thin surface layer facing the rotor, made of Epoxy or stainless steel (shown in green). The rotor, on the other hand, is the capsule wall made of an inner steel layer (shown in red) and an outer aluminum layer (in blue). A thin layer of air (shown in white), called the “air gap”, exists between the rotor and the stator.

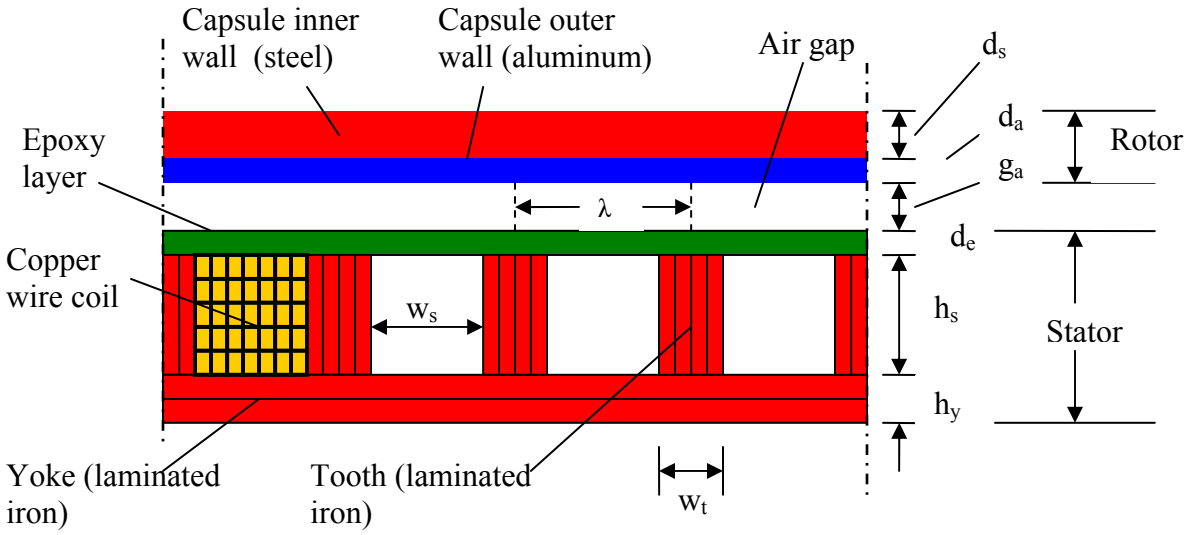

Figure III-4 Longitudinal profile of a single-sided LIM pump for PCP

From Fig.III-4, the distance or spacing between the ferromagnetic materials of the stator and the rotor, called the "***magnetic gap***" can be calculated from

$$g_m = d_a + g_a + d_e \quad \ldots\ldots\ldots\ldots\ldots\ldots\ldots\ldots\ldots\ldots \quad \text{(III-19)}$$

where g_m is the magnetic gap, d_a is the thickness of the aluminum layer, g_a is the physical or true air gap, and d_e is the thickness of the Epoxy or stainless steel layer used to prevent direct contact between the rotor and the stator when the air gap becomes zero.

According to Gieras [13],

$$g_e = K_c g_m \quad \ldots\ldots\ldots\ldots\ldots\ldots\ldots\ldots\ldots\ldots\ldots\ldots \quad \text{(III-20)}$$

where g_e is the effective air gap, and K_c is the Carter factor determined from

$$K_c = \frac{\lambda}{\lambda - g_m \gamma} \quad \ldots\ldots\ldots\ldots\ldots\ldots\ldots\ldots\ldots\ldots\ldots\ldots \quad \text{(III-21)}$$

where λ is the slot width (i.e., the center-to-center distance between teeth marked in Fig.III.4), which can be calculated from

$$\lambda = \frac{L_p}{m q_1} \quad \ldots\ldots\ldots\ldots\ldots\ldots\ldots\ldots\ldots\ldots\ldots\ldots \quad \text{(III-22)}$$

The quantity γ in Eq.III-21 is given as follows:

$$\gamma = \frac{4}{\pi}\left[\frac{w_s}{2g_m}\arctan\left(\frac{w_s}{2g_m}\right) - \ln\sqrt{1+\left(\frac{w_s}{2g_m}\right)^2}\right] \quad \ldots\ldots\ldots\ldots\ldots\ldots \quad \text{(III-23)}$$

where w_s is the slot width – see Fig.III-4.

Since the sum of the slot width and the tooth width is the slot pitch, we have

$$w_s = \lambda - w_t \qquad \text{(III-24)}$$

In order to avoid magnetic saturation in the tooth, the minimum tooth width depends on the maximum allowable magnetic flux density in the tooth, B_{tmax}, in the following manner [17]:

$$w_{t\min} = \frac{\pi}{2}\frac{(B_g)_{av}}{(B_t)_{\max}}\lambda \qquad \text{(III-25)}$$

where $(B_g)_{av}$ is given in Eq.III-18.

The slot depth, h_s, marked in Fig.III-4, multiplied by the slot width, w_s, yields the cross-sectional area of the slot A_s. Therefore, the slot depth can be found from

$$h_s = \frac{A_s}{w_s} \qquad \text{(III-26)}$$

On the other hand, the slot area A_s is proportional to the cross-sectional areas of the wire used in the slot, A_w, and the number of turns of the wire in each slot, N_w, as follows:

$$A_s = N_L(\varepsilon N_w A_w) \qquad \text{(III-27)}$$

where N_L is the number of layers of winding – 1 for single-layer and 2 for double-layer; ε is the fraction of the cross-sectional area of the slot occupied by the copper wire instead of the insulation and air space around the wire. Approximately, ε is equal to 1.4.

The number of turns of the wire in each slot, N_w, is related to the number of turns of the wire per phase in one unit of the stator, N_1, as follows:

$$N_1 = 2N_L N_w q_1 \qquad \text{(III-28)}$$

As with Eq.III-27, N_L is 1 for single-layer winding and 2 for double-layer winding.

The wire cross-sectional area, A_w, can be found from

$$A_w = \frac{(I_1)_{rms}}{J_1} \qquad \text{(III-29)}$$

where $(I_1)_{rms}$ is the RMS value of the input current determined from Eq.III-12, and J_1 is the allowed current density in the wire.

Note that for continuous operation of electric motors using forced air circulation to cool the motor, the maximum J_1 allowed is approximately 4 A/mm^2 or 4×10^6 A/m^2. In contrast, for continuous operation of water cooled motors, the maximum allowed J_1 is equal to or greater than 15 A/mm^2, or 15×10^6 A/m^2. If a motor is operated intermittently as in the case of the LIM used

in PCP, the allowable current density for any given type of motor cooling system used is increased by a factor of 1/α', where α' is the capsule linefill rate in the LIM. Therefore, for any continuously air-cooled LIM pump of PCP with each unit of the LIM operating intermittently only while there is a capsule passing through the unit, the maximum allowed current density is

$$(J_1)_{\max} = \frac{4}{\alpha'} \times 10^6 \ \text{A/m}^2 \qquad \text{(III-30)}$$

From Eq.III-30, if α' in the LIM is 0.1 (i.e., 10% linefill), the maximum current density allowed will be 40×10^6 A/m^2, or ten times that is allowed for continuously operated motors with air cooling. For this reason, and for conserving energy, all the LIM units used for PCP should be operated intermittently, being turned on only when there is a capsule passing through the unit.

Finally, the yolk height h_y in Fig.III-4 can be determined from [17]

$$h_y = \frac{\Phi_p}{2(B_y)_{\max} W_s} \qquad \text{(III-31)}$$

where $(B_y)_{max}$ is the maximum magnetic flux density in the yoke, W_s is the stator width, and Φ_p is the magnetic flux per pole, given by Eq.III-18. The minimum value of h_y will be given later in Eq. .

(e) Magnetomotive Force

According to Prodpradista [17], the motor magnetomotive force, M, generated by the stator winding is

$$M = \frac{g_e (B_g)_{\max}}{\mu_o} \qquad \text{(III-32)}$$

and

$$M = \frac{\sqrt{2} m k_w N_1 I_m}{N_p \pi} \qquad \text{(III-33)}$$

where I_m is the magnetizing current.

Equating the right-hand side of Eq.III-32 to that of Eq.III-33 yields

$$I_m = \frac{N_p g_e (B_g)_{\max} \pi}{\sqrt{2} m k_w N_1 \mu_o} \qquad \text{(III-34)}$$

(f) Equivalent Circuit Model Parameters

The performance of a SLIM can be modeled by using the equivalent circuits shown in Fig.III-5. The per-phase equivalent circuit (a) is for the case of a SLIM without the rotor or capsule present, and the per-phase equivalent circuit (b) is for the case with the rotor or capsule present. The various parameters of these two equivalent circuits are given as follows:

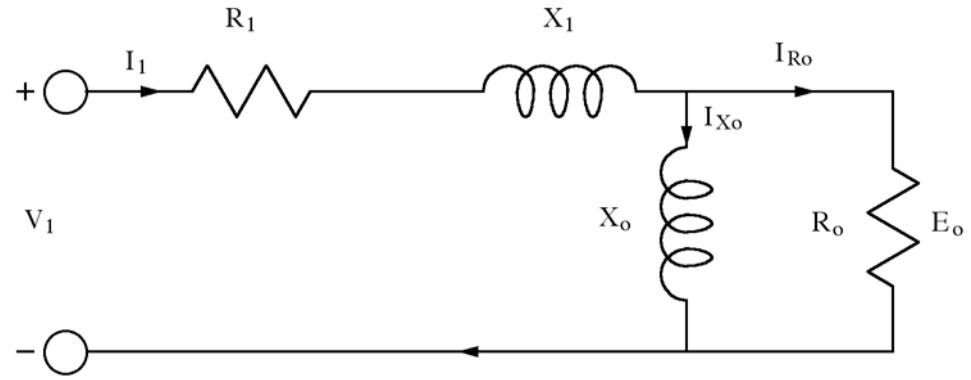

(a) **Without** capsule passing through LIM

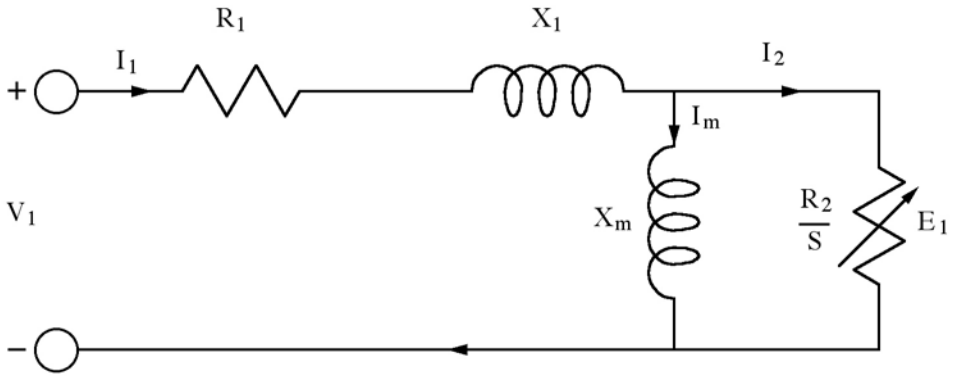

(b) **With** capsule passing through LIM

Figure III-5 Per-phase equivalent circuits of a unit SLIM for PCP

R_1 is the resistance of the per-phase winding of each unit of SLIM which can be determined from

$$R_1 = \rho_w \frac{L_w}{A_w} \qquad \text{……} \qquad \text{(III-35)}$$

where ρ_w is the volume resistivity of the copper wire used in the winding, I_w is the length of the wire per phase per unit, and A_w is the cross-sectional area of the wire given by Eq.III-29.

The length of the wire per phase, L_w, can be determined from:

$$L_w = (4a + 2L_{ce})N_1 \qquad \text{……..} \qquad \text{(III-36)}$$

where 2a is the stack width (i.e., the stator width W_s), and L_{ce} is the coil end connection length to be calculated from

$$L_{ce} = h\sqrt{2}\,\lambda \quad \ldots\ldots\ldots\ldots\ldots\ldots\ldots \quad \text{(III-37)}$$

where h = 3 for single-layer winding, and h= 2 for double-layer winding.

Substituting Eq.III-36 into Eq.III-35 yields [19]:

$$R_1 = \rho_w (4a + 2L_{ce}) \frac{N_1}{A_w} \quad \ldots\ldots\ldots\ldots\ldots \quad \text{(III-38)}$$

The reactance X_1 is caused by the leakage of magnetic flux caused by the open rectangular slots of the stator. For a SLIM, Bhamidi [19] gives the following:

$$X_1 = \frac{8\pi\mu_o f}{N_p}\left[[\lambda_s(1+\frac{3}{N_p})+\lambda_d]\frac{2a}{q_1}+\lambda_e L_{ce}\right]N_1^2 \quad \ldots\ldots\ldots \quad \text{(III-39)}$$

where the parameters λ_s, λ_d and λ_c are given respectively by the following formulas:

$$\lambda_s = \frac{1}{12}\frac{h_s}{w_s}(1+3\beta_1) \quad \ldots\ldots\ldots\ldots\ldots\ldots\ldots\ldots \quad \text{(III-40)}$$

$$\lambda_d = \frac{5(g_e / w_s)}{5+4(g_m / w_s)} \quad \ldots\ldots\ldots\ldots\ldots\ldots\ldots\ldots \quad \text{(III-41)}$$

$$\lambda_e = 0.3(3\beta_1 - 1) \quad \ldots\ldots\ldots\ldots\ldots\ldots\ldots\ldots\ldots \quad \text{(III-42)}$$

In the above equations, the quantity β_1 is the pitch factor which is a number smaller than 1.0. Bhamidi used the value of 0.5 for β_1.

The per-phase magnetizing reactance X_m is

$$X_m = \frac{48\pi\mu_o f a_e k_w N_1^2 L_p}{\pi^2 N_p g_e} \quad \ldots\ldots\ldots\ldots\ldots\ldots\ldots \quad \text{(III-43)}$$

where $$a_e = a + \frac{g_o}{2} \quad \ldots\ldots\ldots\ldots\ldots\ldots\ldots \quad \text{(III-44)}$$

The per-phase rotor resistance R_2 is

$$R_2 = \frac{X_m}{G} \quad \ldots\ldots\ldots\ldots\ldots\ldots\ldots\ldots\ldots \quad \text{(III-45)}$$

where G is the goodness factor defined as

$$G = \frac{2\mu_o f L_p^2 d_a}{\pi \rho_r g_e} \qquad \text{……} \qquad \text{(III-46)}$$

Referring to Fig.III-5(b), the total impedance of the equivalent circuit of the LIM with capsule passage is

$$Z = \frac{V_1}{I_1} = R_1 + jX_1 + \frac{j(\frac{R_2}{S} X_m)}{\frac{R_2}{S} + jX_m} \qquad \text{……} \qquad \text{(III-47)}$$

where Z is written in complex variable, V_1 is the complex input voltage, I_1 is the complex current through the equivalent circuit, and j is the imaginary number $\sqrt{-1}$.

Separating the right side of Eq.III-47 into a real part and an imaginary part yields

$$Z = \Re + j\Im \qquad \text{……} \qquad \text{(III-48)}$$

where

$$\Re = \frac{R_1 R_2^2 + S X_m^2 (R_1 S + R_2)}{R_2^2 + S^2 X_m^2} = R_1 + \frac{S X_m^2 R_2}{R_2^2 + S^2 X_m^2} \qquad \text{..…} \qquad \text{(III-49)}$$

$$\Im = \frac{X_1 R_2^2 + X_1 S^2 X_m^2 + R_2^2 X_m}{R_2^2 + S^2 X_m^2} = X_1 + \frac{X_m R_2^2}{R_2^2 + S^2 X_m^2} \qquad \text{…...} \qquad \text{(III-50)}$$

The amplitude of Z is

$$|Z| = \sqrt{\Re^2 + \Im^2} \qquad \text{……..} \qquad \text{(III-51)}$$

The phase shift between the sinusoidal input voltage and the sinusoidal current, Φ, is the phase angle of Z. Therefore, we have

$$\cos\phi = \frac{\Re}{\sqrt{(\Re^2 + \Im^2)}} \qquad \text{……..} \qquad \text{(III-52)}$$

The RMS value of the current I_1 is

$$(I_1)_{rms} = \frac{(V_1)_{rms}}{|Z|} \qquad \text{…….……} \qquad \text{(III-53)}$$

The complex current I_2 in the equivalent circuit of Fig.III-5(b) is

$$I_2 = \frac{I_1 X_m}{\frac{R_2}{S} + jX_m} \qquad \text{……..} \qquad \text{(III-54)}$$

Thus, the amplitude of I_2 is

$$|I_2| = \sqrt{\left[\frac{(X_m R_2 / S)}{(R_2/S)^2 + X_m^2}\right]^2 + \left[\frac{X_m^2}{(R_2/S)^2 + X_m^2}\right]^2} = \frac{|I_1| X_m}{\sqrt{(\frac{R_2^2}{S})^2 + X_m^2}} \quad \text{…..} \quad \text{(III-55)}$$

The RMS value of I_2 is

$$(I_2)_{rms} = \frac{|I_2|}{\sqrt{2}} \qquad \text{……} \qquad \text{(III-56)}$$

The amplitude and RMS value of the magnetizing current I_m are, respectively,

$$|I_m| = \frac{1}{X_m}|I_2|\frac{R_2}{S} \qquad \text{……..} \qquad \text{(III-57)}$$

and

$$(I_m)_{rms} = \frac{|I_m|}{\sqrt{2}} \qquad \text{……...} \qquad \text{(III-58)}$$

Finally, combination of Eqs.III-18, 18a, 31, 34 and 58 yilds

$$(h_y)_{\min} = \frac{2(I_m)_{rms} k_w L_1 m N_1 \mu_o}{\pi^2 N_p^2 g_e (B_y)_{\max}} \qquad \text{……} \qquad \text{(III-59)}$$

And, Eqs.18a, 25, and 34 can be combined to yield

$$(w_t)_{\min} = \frac{2(I_m)_{rms} k_w m N_1 \lambda \mu_o}{\pi (B_t)_{\max} g_e N_p} \qquad \text{……..} \qquad \text{(III-60)}$$

(g) Thrust, Power and Efficiency

The magnetic thrust developed by each unit of LIM on a capsule is

$$F_1 = \frac{m I_{1rms}^2 R_2}{\left[\frac{1}{(SG)^2} + 1\right] V_s S} \qquad \text{……..} \qquad \text{(III-61)}$$

The power output of each unit of the SLIM is

$$(P_o)_{LIM} = F_1 V_c \quad \ldots\ldots\ldots\ldots\ldots\ldots\ldots \quad \text{(III-62)}$$

The power input of each unit of the SLIM is the sum of the output power and the energy losses in the stator and rotor, due to their resistances, namely

$$(P_i)_{LIM} = (P_o)_{LIM} + mI_{1rms}^2 R_1 + mI_{2rms}^2 R_2 \quad \ldots\ldots\ldots\ldots\ldots\ldots \quad \text{(III-63)}$$

Thus, the efficiency of the SLIM is

$$E_L = \frac{(P_o)_{LIM}}{(P_i)_{LIM}} \quad \ldots\ldots\ldots\ldots\ldots\ldots \quad \text{(III-64)}$$

Note that the power $(P_o)_{LIM}$ is the power that each LIM stator has transmitted to its rotor (capsule), and the power $(P_i)_{LIM}$ is the input electrical power consumed by the unit LIM. The former should be considered as the motor output power (brake power), and the latter should be considered as the motor input power. The efficiency E_L is the LIM motor efficiency. This efficiency must be multiplied by the pump efficiency, E_p, found from fluid mechanics consideration, in order to determine the total efficiency of the LIM pump, namely,

$$E \text{ (total efficiency of the LIM Pump)} = E_L \times E_p \quad \ldots\ldots\ldots\ldots \quad \text{(III-65)}$$

III-3. Design Procedures

The design procedures of the SLIM for a PCP is as follows:

(a) Assign values to the following electromagnetic parameters (constants):
- μ_o (permeability of free space) = $4\pi\times10^{-7}$ H/m;
- ρ_w (volume resistivity of copper wire) = 19.3×10^{-9} Ω-m;
- ρ_r (volume resistivity of rotor conductor – alumimum) = 28.9×10^{-9} Ω-m;
- B_{tmax} (maximum allowable flux density in **tooth**) = 1.6 Wb/m^2; and
- B_{ymax} (maximum allowable flux density in **yoke**) = 1.3 Wb/m^2.

(b) Specify design values of the following electromagnetic variables:
- m (number of phases of the input power) = 3;
- V_L (line-to-line voltage) = 480 volts;
- f (line frequency) = 60 Hz;
- N_p (number of poles) = 4;
- q_1 (number of slots per pole per phase) = 1;
- S (slip) = 5% = 0.05 (also analyze and compare with S=1, 2, 3 and 4%);
- W_s (stator width) = same as capsule wall height H_c—see Figure III-2;
- J_1 (stator current density) = 6×10^6 A/m^2 (maximum allowed for continuous operation of LIM), and $6\times10^6/\alpha$' A/m^2 (maximum allowed for intermittent operation with linefill α' in LIM).

(c) Specify capsule dimensions: same as for fluid mechanics calculations. The capsule dimensions are such that the physical air gap g_p between the capsule walls and the LIM walls is maintained to be 10 mm.

(d) Specify length of the SLIM pump:
- L' (total length of the SLIM pump) – same as that used in analyzing fluid mechanics.

(e) Specify capsule velocity V_c' in SLIM: same as that obtained from fluid mechanics.

(f) Calculate the synchronous speed V_s from Eq. 3. (If S is 0.05, then Eq.3 yields $V_s = V_c'/0.95 = 1.053V_c'$.)
(g) Calculate the pole pitch L_p from Eq.III-7.
(h) Calculate the length of each SLIM unit, L_l by using Eq.III-5.
(i) Calculate the slot pitch, λ, from Eq.III-22.
(j) Calculate the target thrust from each unit of the SLIM, F_1, by using Eq.III-10.
(k) As the first step of iteration, set the number of turns of the winding in each slot, N_w, equal to 1 (one).
(l) Use Eq.III-28 to calculate the number of turns of the winding for each phase, N_1.
(m) Assume that the value of $E_s\cos\Phi$ is less than 1 (one) but greater than 0 (zero), such as 0.5.
(n) Use Eq.III-12 to calculate the RMS value of the stator current I_1.
(o) Use Eq.III-29 to calculate the cross-sectional area of the wire, A_w, and use Eq.III-27 to calculate the slot area, A_s.
(p) Assume that the slot width, w_s, is equal to twice the tooth width, w_t. From Eq.III-24 calculate w_s. Then find $w_t = 0.5\ w_s$. Then, calculate the slot depth h_s from Eq.III-26.
(q) Calculate the magnetic gap g_m, the Carter factor K_c, the effective gap g_e, and the goodness factor G, respectively from Eqs.III-19, 21, 20 and 46.
(r) Determine the equivalent circuit components, R_1, X_1, X_m and R_2, respectively from Eqs.III-38, 39-42, 43-44, and 45.
(s) Calculate $\Re$, $\Im$ and $|Z|$ from Eqs.III-49, 50 and 51, respectively.
(t) Calculate $\cos\phi$ from Eq.III-52.
(u) Calculate I_{2rms} from Eqs.III-56 and 55.
(v) Use Eq.III-62 to calculate $(P_o)_{LIM}$, and use Eq.III-63 to calculate $(P_i)_{LIM}$. Then, use Eq.III-64 to calculate the LIM motor efficiency E_L.
(w) Use the new value of $E_L\cos\Phi$ in Eq.III-12 to calculate the RMS value of I_1. This represents an iteration of step n through v. Iteration should continue until the calculated value of $E_L\cos\Phi$ is close to the value obtained in the previous iteration.
(x) Calculate F_1 from Eq.III-61 and compare the result with the value of F_1 obtained from Eq.10, using the value of F_e obtained from fluid mechanics. If the two values differ significantly, increase the number of turns of the wire in each slot by one-- i.e., assume N_w is equal to 1 (one) plus the last assumed value of N_w , and iterate steps l (lower case of L) through w.

III-4. Example

To illustrate the use of the foregoing procedure to design SLIM for PCP, lets assume the following: S (slip) = 0.05, B_{ymax} (maximum allowed yoke flux density) = 1.1 tesla, B_{tmax} (maximum allowed tooth flux density) = 1.9 tesla, W_s (stator width) = 0.5 m, V_c (capsule velocity) = 21.87 m/s, N_p (number of poles) = 4, F_1 (thrust of each unit of SLIM) = 3,987 N, use 3-phase a.c. at 480 volts, copper wire for stator winding, aluminum of 2 mm thick for capsule surface. Design the SLIM and determine its properties such as power and efficiency.
[Solution]

Three LIM units of different tooth-width-to-tooth-spacing ratio, w_t/λ, were investigated. They have w_t/λ equal to 0.25, 0.50 and 0.75. The LIM unit efficiency, force F_1 and input power was investigated for V'_c between 0 and 23 m/s. The synchronous speed for the three cases was 23.02 m/s. The foregoing design procedure was followed to prepare a software for calculating

some key properties of the LIM as a function of capsule velocity. Using this software, the following results were found:

Shown in Figure III-6 is the LIM unit force versus capsule velocity in the LIM, V_c', for the case $w_t/\lambda = 0.50$. The other cases $w_t/\lambda = 0.25$ and 0.75 are not shown because they produced nearly identical results which are difficult to distinguish from one another when plotted.

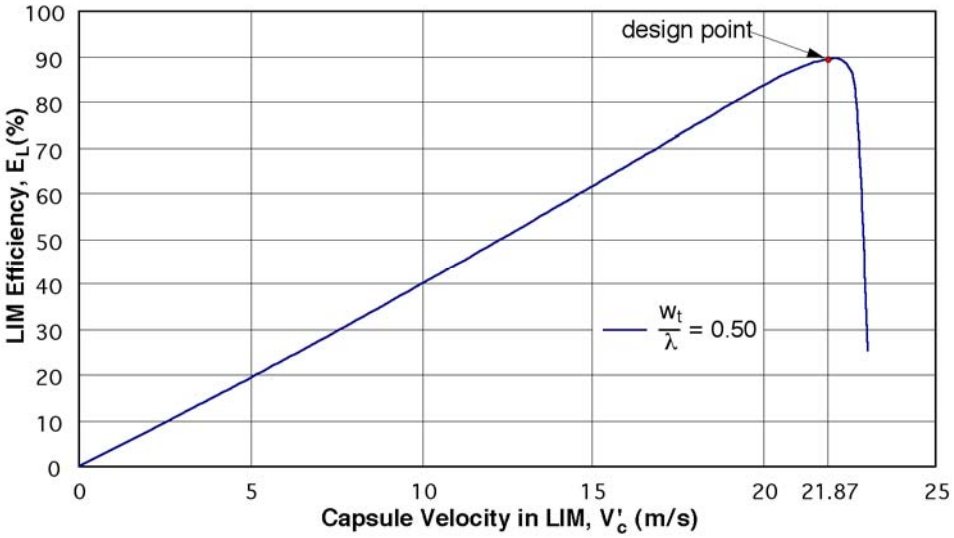

Figure III-6 LIM Unity Efficiency for $w_t/\lambda = 0.50$

From Figure III-6, it can be seen that the efficiency of the LIM motor, E_L, increases more or less linearly with increasing V_c' until the design velocity of 21.87 m/s is reached. With a slight further increase in V_c', the efficiency reaches a maximum and then decreases abruptly.

Shown in Figure III-7 is the LIM unit force, F_1, for $0 \leq V_c' \leq 23$ m/s. Note that the unit force is the thrust force generated by a single unit of LIM on the capsule passing through the LIM. The three curves correspond to: $w_t/\lambda = 0.25$, 0.50 and 0.75 as shown in the graph ledger.

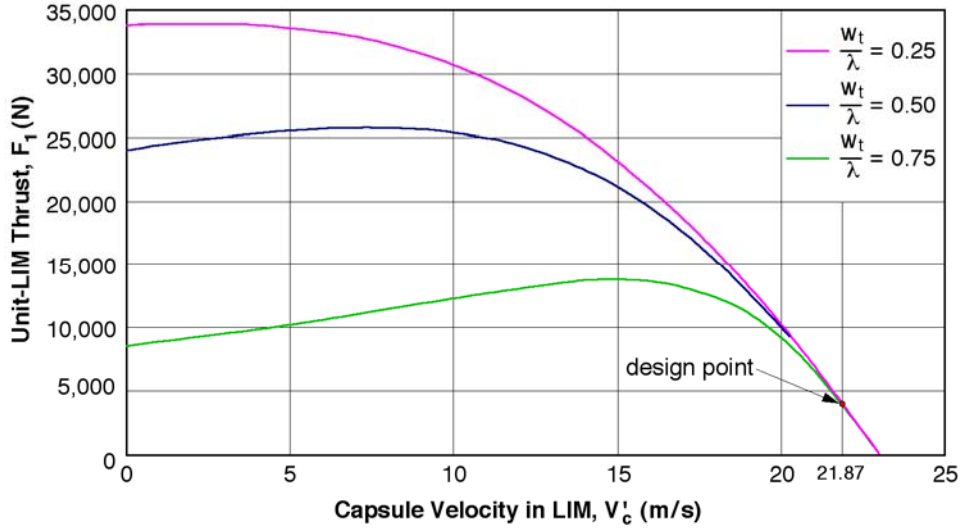

Figure III-7 LIM Unit Force versus Capsule Velocity

All three curves pass through the design point. However, for smaller values of V_c', the LIM unit forces for the three cases varies greatly. The case $w_t/\lambda = 0.25$ has a maximum value of F_1 approximately equal to 34,000 N at $V_c' = 2.5$ m/s, and a slightly less value at $V_c' = 0$. The other two cases have maximum values that are smaller than the first case and their maxima occur at larger V_c'. The LIM unit force at $V_c' = 0$ for the latter two cases are significantly lower than their maximum values. These three cases all develop $F_1 = 3{,}987$ N at $V_c' = 21.87$ m/s. It may appear that the upper curve $w_t/\lambda = 0.25$, is superior to the other two cases because of the large force it develops at small capsule velocities. Having large forces at small capsule velocity is good during system startup and restart. However, as shown in Figure III-8, the input power to the LIM unit is larger so there is additional current and power demand for this case should the LIM unit ever operate with low capsule velocities. Moreover, it is likely that this LIM unit would also be more expensive because the design must accommodate more current than the other two cases.

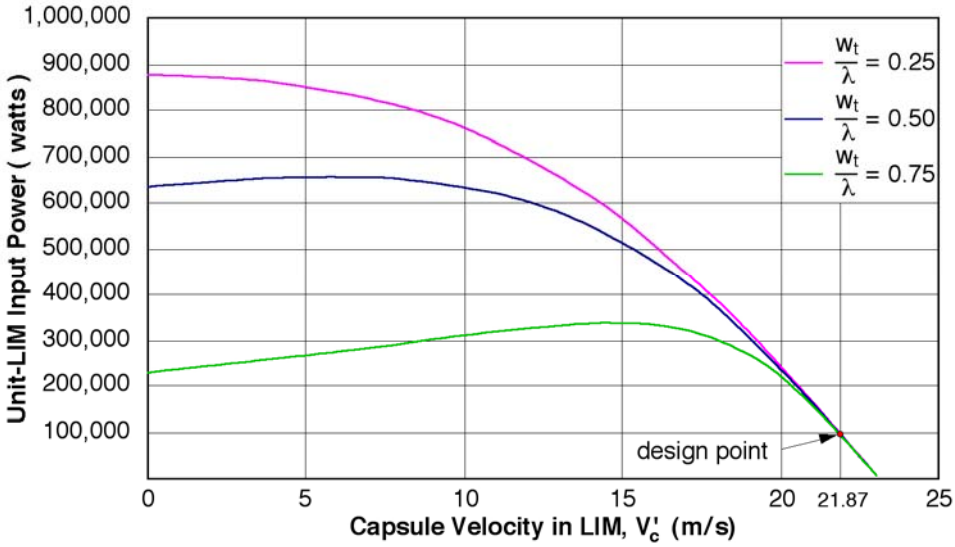

Figure III-8 Variation of LIM unit input power with capsule velocity

Based on the above study, it can be concluded that while the tooth width to tooth spacing, w_t/λ, does not have any significant effect upon LIM motor efficiency at least in the range studied here, it does have a strong effect on the LIM force and the LIM input power for capsule velocities less than the design velocity. At velocities smaller than the design value, smaller ratio of w_t/λ yields larger force but requires more power. What is the optimum value of w_t/λ will depend on many factors such as the need for startup, the cost of the LIM at lower values of w_t/λ, the possibility of overheating of the motor caused by capsule trains lodged inside a LIM in an accident, and other practical factors which must be considered carefully. More research is needed in the future on this issue to optimize the LIM design.

Appendix IV: Cost Model and Equations

IV-1. Cost Model

The general methodology used here for analyzing the cost and the cost effectiveness of the LIM-driven PCP is identical to that used in the past by the Principal Investigator for analyzing the transportation cost of coal by the coal log pipeline (CLP) technology [23, 24], and the transportation cost of biomass log fuel (BLF) by the pneumatic capsule pipeline (PCP) technology [25]. It is described as follows:

The cost model is based on a life-cycle cost analysis performed over the estimated economic life of the system, N years. The net-cash-flow approach is used which considers all the revenues (incomes) of a project as positive cash flow, and all costs (expenditures) as negative cash flow. During the life cycle (economic life) of the system, each cash flow is treated as a discrete payment (outlay of cash). Costs paid at the beginning of the project are the **initial costs**, and those paid subsequently are treated as annual outlays (**annual costs**). For simplicity, it is assumed that all the capital costs for constructing the LIM-driven PCP system, thereafter referred to simply as the "system", are encumbered at the beginning of the project. So, the capital cost and initial cost are treated as the same thing. All annual costs (expenses) are assumed to be paid at the end of each year--the end-of-year convention.

The **unit price**[1]**, U** (i.e., the price charged to customers for using the system to transport each tone of the minerals or mine wastes in **$/T**) is calculated based on the need to generate an **above-inflation rate of return, r,** for the owner of the system. To achieve this return rate, the after-tax cash flow equations for each year are first developed, treating the unit price as a variable with respect to time (years). These equations include the following:

The **after-tax cash flow (ATCF)$_n$** for any year **n** (n = 1, 2, 3 . . . N) is:

$$ATCF_n = BTCF_n - T_n \qquad \ldots\ldots\ldots\ldots\ldots\ldots \qquad (IV\text{-}1)$$

where **$BTCF_n$** is the before-tax cash flow for year **n**, and **T_n** is the corporate income tax that must be paid during year n.

The quantity **$BTCF_n$** is determined from:

$$BTCF_n = R_n - C_n \qquad \ldots\ldots\ldots\ldots\ldots\ldots\ldots \qquad (IV\text{-}2)$$

where **R_n** is the revenue for year **n**, and **C_n** is the cost for year **n**.

The corporal income tax, **T_n**, in Eq. IV-2 is calculated from

$$T_n = (BTCF_n - d_n)t \qquad \ldots\ldots\ldots\ldots\ldots\ldots\ldots\ldots \qquad (IV\text{-}3)$$

[1] Note that the terms "price" and "cost" depend on viewpoints: the payment that the seller receives from the customer is according to the **price**, which includes a profit to the seller. For the customer, what he pays the seller is a **cost** to himself.

where $\mathbf{d_n}$ is the depreciation which must be determined from the tax code, and **t** is the rate of corporate income tax, assumed to be 37% in this analysis. For simplicity, a "straight-line" or uniform depreciation over N_d years is used. Therefore,

$$d_n = d = \frac{C_c}{N_d} \qquad \text{(IV-4)}$$

where C_c is the capital cost, and N_d is the years of depreciation. The value of N_d must conform to government tax code. Note that when N_d (say, 20 years) is less than N (say, 30 years), Eq. IV-4 is valid only for the first N_d years. Thereafter, there will be no more depreciation, and $d_n = 0$ (zero) for the remaining years of the project's economic life.

Combining Eqs. IV-2, 3, and 4 yields

$$ATCF_n = (1\text{-}t)\,(R_n - C_n) + td_n \qquad \text{(IV-5)}$$

The present value of $ATCF_n$ is denoted as $\mathbf{ATCF_{np}}$. It can be calculated from

$$ATCF_{np} = \frac{ATCF_n}{(1+\delta)^n} = \frac{(1-t)\,(R_n - C_n) + td_n}{(1+\delta)^n} \qquad \text{(IV-6)}$$

The quantity δ in Eq.IV-6 is the inflation-adjusted discount rate which should be calculated from

$$\delta = r + I + rI \qquad \text{(IV-7)}$$

in which **r** is the above-inflation return rate, and **I** is the inflation rate.

The revenue $\mathbf{R_n}$ in Eqs.IV-5 & 6 is to be determined for each year in such a manner that the sum of the present value of $ATCF_n$ over the N years (from n =0 to n = N) is equal to the capital cost C_c, namely,

$$\sum_{n=0}^{N} ATCF_{np} = 0 \qquad \text{(IV-8)}$$

where n = 0, 1, 2, 3, . . . N. Note that year 0 refers to the beginning of the project when the capital cost C_c is incurred, which constitutes a negative cash flow. Equation IV-8 can be rewritten as

$$\left[\sum_{n=1}^{N} \frac{(1-t)(R_n - C_n) + td_n}{(1+\delta)^n}\right] = C_c \qquad \text{(IV-9)}$$

The revenue is assumed to be R_1 for the first year, and it is escalated at the rate of $\mathbf{e_r}$. Therefore, the revenue for the nth year becomes:

$$\begin{aligned} R_n &= (1 + e_r)\, R_{n-1} = (1 + e_r)^2\, R_{n-2} \\ &= (1 + e_r)^3\, R_{n-3} = \ldots\ldots\ldots \\ &= (1 + e_r)^n Ro \qquad (n = 1, 2, 3, \ldots N) \end{aligned} \qquad \text{(IV-10)}$$

Assuming that the quantity of minerals or mine wastes transported each year is **Q** (T/yr), the revenue generated each year, $\mathbf{R_n}$, becomes

$$R_n = QU_n \qquad \text{……..……} \qquad \text{(IV-11)}$$

where U_n is the price charged to the customer, during year n, for transporting unit weight of the mineral or mine waste, hereafter referred to simply as the **"unit price."**

If the present unit price is U_o, Eq.III-11 yields $R_o = QU_o$. Then, from Eq.IV-11 yields:

$$R_n = (1 + e_r)^n U_o Q \qquad \text{……} \qquad \text{(IV-12)}$$

Equation IV-12 can now be substituted into Eq. 10 to yield

$$\sum_{n=1}^{N} \frac{(1-t)\left[(1+e_r)^n U_o Q - C_n\right] + td_n}{(1+\delta)^n} = C_c \qquad \text{……} \qquad \text{(IV-13)}$$

Realizing that both Q and U_o in Eq.IV-13 are constant and do not vary with n, they can be factored out of the equation to yield

$$U_o = \frac{\left[\sum_{n=1}^{N} \frac{(1-t)C_n - td_n}{(1+\delta)^n}\right] + C_c}{Q\sum_{n=1}^{N} \frac{(1-t)(1+e_r)^n}{(1+\delta)^n}} \qquad \text{……} \qquad \text{(IV-14)}$$

Equation IV-14 can be reduced to

$$U_o = \frac{C_a}{Q} \qquad \text{……} \qquad \text{(IV-15)}$$

and

$$C_a = \frac{\left[\sum_{n=1}^{N} \frac{(1-t)C_n - \mathrm{td_n}}{(1+\delta)^n}\right] + C_c}{\sum_{n=1}^{N} \frac{(1-t)(1+e_r)^n}{(1+\delta)^n}} \qquad \text{……} \qquad \text{(IV-16)}$$

where C_a is the present value of the averaged annual cost, including both initial (capital) cost and annual (variable) costs. For simplicity, C_a will be referred to in this report as the **"annualized total cost (ATC)."**

Once U_o is determined, the unit price for any year n can be obtained from

$$U_n = (1+ e_r)^n U_o \qquad \text{……} \qquad \text{(IV-17)}$$

The annual cost C_n for year n in the foregoing equations is to be determined from

$$C_n = (1 + e_c)^n C_o \qquad (n = 1, 2, 3, \ldots N) \quad \ldots\ldots\ldots \qquad \text{(IV-18)}$$

where C_o is the present value of the annual cost, and e_c is cost escalation rate which is assumed to be the same as the general inflation rate I.

The present value of the annual cost, C_o, is determined from the present annual cost of various items including energy (electricity), fuel (gasoline and diesel), natural gas, salaries/wages, property tax, insurance, and other operations/maintenance costs, namely,

$$C_o = C_e + C_f + C_g + C_s + C_p + C_i + C_m \quad \ldots\ldots\ldots\ldots\ldots\ldots \qquad \text{(IV-19)}$$

where C_e is the energy cost, C_f is the fuel cost, C_g is the natural gas cost, C_s is the cost of salary and wages, C_p is the property tax cost, C_i is insurance cost, and C_m is the maintenance cost—all first-year costs based on current values. Note that corporate income tax is not included here since it has already been included before by using t in previous equations.

The property tax, C_p, and the insurance cost, C_i, for the present year are calculated from the capital cost C_c as follows:

$$C_p = e_p C_c \qquad \ldots\ldots\ldots\ldots\ldots\ldots\ldots\ldots\ldots\ldots\ldots\ldots \qquad \text{(IV-20)}$$

and

$$C_i = e_i C_c \qquad \ldots\ldots\ldots\ldots\ldots\ldots\ldots\ldots\ldots\ldots\ldots\ldots \qquad \text{(IV-21)}$$

where e_p and e_i are respectively the property tax rate and the insurance rate.

Finally, the capital cost, C_c, is determined from

$$C_c = 1.15\,(C_{tu} + C_{LIM} + C_{cap} + C_{in} + C_{out}) \quad \ldots\ldots\ldots\ldots\ldots\ldots \qquad \text{(IV-22)}$$

where C_{tu} is the capital cost of constructing the PCP tube (conduit), C_{LIM} is the cost of the LIM (linear induction motor) used for driving the PCP, C_{cap} is the cost of the capsules used for the system, C_{in} is the cost of the inlet station facilities, and C_{out} is the capital cost of the outlet station facilities. The factor 1.15 in Eq.IV-22 is for engineering – design, preconstruction survey and geotechnical data collection and interpretation. The engineering cost is estimated to be about 15% of the sum of the other capital cost items.

IV-2 Procedure for Cost Calculation

The procedure for calculating the unit price U_o is given as follows:

1. Determine C_o from Eq.IV-19 and C_c from Eq.IV-22. Both C_o and C_c are based on current market price.
2. The values of N, N_d, t, I, e_c and e_r are specified based on realistic assumptions.
3. The desired or required above-inflation return rate r is also specified, and the discount rate δ is calculated from Eq.IV-7.
4. C_n and d_n for each year are determined respectively from Eq.IV-18 and Eq.IV-4.
5. Equation IV-16 can then be used to calculate C_a and Eq. IV-15 can be used to calculate U_o.
6. Once U_o is determined, the unit price for any year n can be determined from Eq.IV-17.
7. The revenue for each year, R_n, can be determined from Eq.IV-12.

A computer program can be written based on the aforementioned procedure. The program can be written to print not only the value of U_o, but also values of C_n, R_n and U_n for each year in a tabular form. All the assumptions and input values should also be listed. The value of U_o obtained can then be compared with current price of transporting minerals and mine wastes by using other competing modes of transport such as rail or truck.

IV-3. Cost Assumptions

Common assumptions used for the cost analysis of this study, unless otherwise specified, are as follows:

(1) The general inflation rate, I, is 3%.
(2) The above-inflation return rate (return-on-investment), r, is 15%.
(3) The economic life of the project, N, is 20 yrs.
(4) Depreciation of capital is flat (constant) over 20 years ($N_d = 20$).
(5) The corporate income tax rate, t, is 37%
(6) The discount rate, δ, calculated from Eq. 8, is 0.1845.
(7) Present costs are based on Year 2005 values.
(8) All the cost items are inflated according to the same general inflation rate, I, of 3%.
(9) The revenue escalation rate, e_r, is the same as the general inflation rate, which is 3%.
(10) The property tax rate is equal to 2% of the total capital cost.
(11) The annual insurance cost is 0.5% of the total capital.
(12) The equity is 1.0. This means that all the money invested on the project (the capital cost) comes from the owner; no money is borrowed. Otherwise, interest rate would also enter the calculation.
(13) The cost figures are based on those discussed in Sec.5 Cost Analysis.

IV-4. Cost Details

(a) Capital Cost

Each of the capital cost item listed in Eq.IV-22 is the installed cost, which includes not only materials cost but also transportation of materials to the construction site, and labor to install. The installed cost of each of these cost items is separately determined as follows:

1. <u>Tube (Conduit) Cost, C_{tu}</u>

The cost of the tube is proportional to the length of the tube. If the cost per unit length, in \$/km (dollars per kilometer) is C_{tu1}, and the length of the tube is L, the total cost of the tube is

$$C_{tu} = LC_{tu1} \qquad \ldots\ldots\ldots\ldots\ldots\ldots\ldots\ldots \qquad \text{(IV-23)}$$

Note that L is the length of a single line tube, and C_{tu1} is the cost per unit length of a single line. Therefore, when twin lines are used, with a separate delivery line and a return line, the length L used in Eq.IV-23 must be double that of each single line.

The cost per unit length C_{tu1} consists of : (1) the cost of the tube shell (i.e., plain conduit of 1m x 1m cross section), estimated to be \$700,000/km for the concrete conduit, and \$1,400,000/km for the steel conduit; (2) the cost of the rails (ASCE Standard 60-lb, gage 24) in the tube, estimated at \$600,000/km; (3) the cost of land along the tube (assuming 10 m width and \$3,000 per acre), estimated to be \$7,400/km; and (4) gravel road of 5 m width along the tube right-of-way , estimated at \$300,000/km. Adding the foregoing parts together yields the total

construction cost of the tube, **C_{tu1}, to be $1.607 million per km for the concrete tube, and $2.307 million for the steel tube.**

2. LIM Cost, C_{LIM}

The cost of LIM is estimated from the rated power (input power) of the LIM used, which is determined from Fig.3.4.8 for the delivery line, and from Fig.3.4.15 for the return line. Note that the two figures are for a PCP of 10 km length. Since power consumed for a PCP is linearly proportional to length, the total power consumed for a PCP of any arbitrary length L is

$$P = \frac{LP_{in}}{10} \qquad \text{……} \qquad \text{(IV-24)}$$

where P is the total power (rated power) of the LIM for a PCP of length L. To be consistent with the values of P_{in} given in Figs.3.4.8 and 3.4.15, P and P_{in} are in Mw (megawatt). The PCP length L in the above equation is given in km. The value of P_{in} for any given case is to be determined from Fig.3.4.8 for the delivery line, and from Fig.3.4.15 for any return line.

Once the power of the LIM, P, is determined from Eq.IV-24, the cost of the LIM is estimated from

$$C_{LIM} = C_1 P = \frac{C_1 LP_{in}}{10} \qquad \text{……..} \qquad \text{(IV-25)}$$

where C_1 is the cost of the LIM in M$ (million dollars) per Mw (megawatt) of the LIM. For this analysis, it is assumed C_1= $0.8 million per Mw (i.e., $800/kw), which is approximately 5 times that of ordinary induction motors of large size. Using this assumption, Eq.IV-25 can be rewritten as

$$C_{LIM} = 0.08LP_{in} \qquad \text{……..…….} \qquad \text{(IV-26)}$$

where C_{LIM} is given in M$ (million dollars), L is given in km, and P_{in} is in Mw (megawatts).

3. Capsule Cost, C_{cap}

From Eq.3.3.29, the throughput of any PCP, T_h, can be calculated from

$$T_h = nW = \frac{W}{T} \qquad \text{……..} \qquad \text{(IV-27)}$$

where W is the weight of cargo carried by each capsule, n is the capsule injection rate, and T is the time interval of capsule injection. For the capsules used for transporting minerals or mine waste, it was assumed in **Sec.2.3. Capsule Design** that W is 8,000 lbs. Based on this value, and based on the assumption of continuous (around-the-clock and 365-days-a-year) operation, Eq.IV-27 can rewritten as

$$T_h = \frac{113.1}{T} \qquad \text{……..} \qquad \text{(IV-28)}$$

where T is in second, and T_h is in MTY (million tonnes per year)[2].

On the other hand, the number of capsules in each line of a PCP of length L is, from Eq.3.3.1,

$$N = \frac{L}{TV_c} \quad \text{…….} \quad \text{(IV-29)}$$

Substituting Eq.IV-28 into the above equation yields

$$N = 8.842\frac{LT_h}{V_c} \quad \text{……..……} \quad \text{(IV-30)}$$

Equation IV-30 can be used to calculate the number of capsules in each line of a length L in km, capsule velocity V_c in m/s, and throughput T_h in MTY. For a PCP system with twin lines operating simultaneously, the number of capsules given above should be doubled.

In addition to capsules in the line(s), there are additional capsules moving through the inlet station track and the outlet station track as shown in Figs.2.4.1 and 2.4.2. If the length of the rail track in each station is L_t, the average velocity of capsules moving through the station track is V_{ct}, and the capsule injection time interval is T, the number of capsules in the station at any given time is

$$N_t = \frac{L_t}{TV_{ct}} \quad \text{……} \quad \text{(IV-31)}$$

Substituting Eq.IV-28 into the above equation yields

$$N_t = 8.842\frac{L_t T_h}{V_{ct}} \quad \text{……..} \quad \text{(IV-32)}$$

From the foregoing, the total number of capsules needed for a twin-conduit PCP system including inlet and outlet stations is

$$N_{total} = 1.15(2N + 2N_t) = 20.34T_h(\frac{L}{V_c} + \frac{L_t}{V_{ct}}) \quad \text{……..} \quad \text{(IV-33)}$$

Note that the factor 1.15 in the above equation is to account for an extra 15% of capsules for use as spare, to replace damaged capsules or capsules pulled out of service for maintenance purpose. In Eq.IV-33, the quantity T_h is in MTY; L and L_t are lengths in km, and V_c and V_{ct} are capsule velocities in m/s. According to the design in Sec.2.4, the length L_t is approximately 0.3 km, and V_{ct} is approximately 2 m/s. Consequently, Eq.IV-33 reduces to

$$N_{total} = 20.34T_h(\frac{L}{V_c} + 0.15) \quad \text{……..} \quad \text{(IV-34)}$$

Once the total number of capsules for a given PCP system is determined from Eq.IV-34, the cost of the capsules becomes

$$C_{cap} = C_2 N_{total} \quad \text{…….} \quad \text{(IV-35)}$$

[2] "Tonnes" stands for metric tons, which is 1,000 kg, or 1.1 American tons.

Assuming that each capsule cost $8,000 to manufacture, combining the last two equations yields

$$C_{cap} = 0.1627 T_h (\frac{L}{V_c} + 0.15) \quad \ldots\ldots\ldots\ldots\ldots\ldots \quad \text{(IV-36)}$$

In Eq.IV-36, C_{cap} is the total capsule cost in M$ (million dollars) for a PCP system with twin conduits each having a length of L in km, a throughput of T_h in MTY, and a capsule velocity in the conduit, V_c, in m/s.

For PCP systems using a single conduit (the same conduit) for both the delivery and return line, the above equation is modified to read:

$$C_{cap} = 0.1627 T_h (\frac{L}{2V_c} + 0.15) \quad \ldots\ldots\ldots\ldots\ldots\ldots \quad \text{(IV-36)}$$

4. <u>Inlet Station, C_{in}</u>

The inlet station cost includes the following components:

Land: From Fig.2.4.2, assume that the inlet station requires a land area of 200m x 200m, approximately. This is equivalent to about 10 acres. At the assumed price of $3,000 per acre, which is conservative for mine land, the land cost for the inlet terminal is about $30,000.

Building: Assume that the terminal needs a building of 20,000 sq.ft. At $80 per sq.ft., the building cost at the inlet station is about $1,600,000.

Rail Track: Depending on throughput, the inlet station may use 2 to 5 parallel tracks. The track length L_t for one track is, from Fig.2.4.2, approximately 0.3 km. Therefore, for n tracks (n = 2, 3, 4 or 5), the total length of the track for the inlet is 0.3n (km). Assuming the cost is $600,000 per km, the track cost for n tracks is $180,000 times n.

Rail switching equipment: $200,000.

Loading equipment: The loading equipment consists of hoppers and conveyor belts to feed minerals (or mine wastes) into capsules. The cost is determined from $C_{load} = 3T_h$, where T_h is throughput in MTY and C_{load} is in M$ (million dollars).

Rotary push arm: The rotary push arm for moving capsules along the track in the inlet station, shown in Fig.2.4.3, is estimated at $1.2 million.

Automatic control equipment: The automatic control equipment for the entire PCP system, with the SCADA located at the inlet, is estimated to cost $0.4 million to install.

Substation: The cost of the substation (i.e., transformer station) to bring adequate power to the inlet station, not only for running the LIM but also for running the substation equipment and buildings, is based on the power needed there. The power is to be calculated from Eq.IV-24 for the LIM of the delivery line, to be designated as P_{del}, plus the power for running station equipment and building, P_{eb}. The latter is estimated to be 0.5 Mw, which is believed to be conservative. Thus, the total power needed at the inlet station is

$$P_{del} = \frac{L(P_{in})_{del}}{10} + 0.5 \quad \ldots\ldots\ldots\ldots\ldots\ldots\ldots\ldots \quad \text{(IV-37)}$$

As it is the case with Eq.IV-24, the power terms in Eq.IV-37 are in Mw, and L is in km.

The cost of the substation is estimated by assuming the average cost to be $300,000 per Mw. Using this assumption, the cost for the substation at the inlet is

$$C_{sub} = 0.3\left[\frac{L(P_{in})_{del}}{10} + 0.5\right] \qquad \text{(IV-38)}$$

Vehicles: Assuming that the inlet station needs two pick up trucks and two forklifts, the cost for assumed to be $100,000.

Finally, summing up all the foregoing cost components of the inlet station yields the total cost for the inlet station as follows:

$$C_{in} = 3.68 + 3T_h + 0.18n + 0.03L(P_{in})_{del} \qquad \text{(IV-39)}$$

In the above equation, C_{in} is in M$ (million dollars), T_h is throughput in MTY, n is the number of rail tracks at the inlet, L is the conduit length in km, and $(P_{in})_{del}$ is the power in Mw obtained from Fig.3.4.8. Note that n=2 for throughput less than 5 MTY, n=3 for throughput between 5 and 10 MTY, n=4 for throughput between 10 and 25 MTY, and n=5 for throughput between 25 and 50 MTY.

5. Outlet Station, C_{out}

The outlet station needs the same amount of land and only one-third of the building needed for the inlet station. It needs the same amount of rail track and rail switching equipment as needed at the inlet station. No loading equipment is needed, but the unloading facility/equipment is expected to cost $1.5T_h$ in million dollars. The cost for the rotary arm to move capsules within the station is expected to be the same as for the inlet, i.e., $1.2 million. Since the SCADA is located at the inlet station, the need for automatic control equipment at the outlet station is less than that for the inlet, estimated to be only $100,000. Similar to the inlet, the cost of the substation is

$$C_{sub} = 0.3\left[\frac{L(P_{in})_{ret}}{10} + 0.5\right] \qquad \text{(IV-40)}$$

where $(P_{in})_{ret}$ is the input power of the LIM for the return line given in Mw, obtained from Fig.3.4.15.

Based on the foregoing, the total cost of the outlet station, C_{out}, can be determined from

$$C_{out} = 2.21 + 1.5T_h + 0.18n + 0.03L(P_{in})_{ret} \qquad \text{(IV-41)}$$

In the above equation, C_{out} is in million dollars, T_h is in MTY, n is the number of tracks as discussed for the inlet, and $(P_{in})_{ret}$ is the LIM power of the return line found from Fig.3.4.15.

6. Total Capital Cost, C_c

Once the individual components of the capital cost are obtained from the foregoing analysis, the total capital, C_c, can be determined from Eq.IV-22.

(b) Operation/Maintenance (O/M) Cost

The operation/maintenance (O/M) costs include the energy cost C_e, the fuel cost C_f, the cost of natural gas for heating buildings C_g, the cost of salaries and wages C_s, the property tax C_p, the insurance cost C_i, and the maintenance cost C_m. They are separately evaluated as follows:

1. Energy Cost, C_e

The electrical energy used by the LIM-driven PCP system, E, includes the energy used by the LIM of the **delivery** line E_{LIMD}, the energy used by the LIM of the **return** line E_{LIMR}, and the energy used for other purposes such as lighting the inlet and outlet station and running miscellaneous electrical equipment and appliances, E_{oth}, namely,

$$E = E_{LIMD} + E_{LIMR} + E_{oth} \quad \ldots\ldots\ldots\ldots\ldots\ldots \quad \text{(IV-42)}$$

where E_{LIMD} is determined from Fig.4.3.1, E_{LIMR} is determined from Fig.4.3.2, and E_{oth} is assumed to be a flat number of 800,000 kwh.
Assuming that the cost of electricity is 10 cents per kwh, from Eq.IV-42 the annual cost of energy (electricity) is:

$$C_e = 10^{-7} (E_{LIMD} + E_{LIMR} + E_{oth}) \quad \ldots\ldots\ldots\ldots\ldots\ldots \quad \text{(IV-43)}$$

In the above equation, C_e is in million dollars, and the three Es are in kwh.

2. Fuel Cost, C_f

The annual cost of fuel for driving the two pickups and two forklifts are estimated to be $20,000. Thus, C_f = $0.02 million.

3. Natural Gas Cost, C_g

The annual cost of natural gas for heating the two terminal stations is estimated at $40,000. Thus, C_g = $0.04 million.

4. Sallary and Wages, C_s

The number of workers for each system is somewhat dependent on the throughput – larger throughputs will require more workers taking care of the system and so forth. For the throughput of 10 MTY, it is assumed that proper operation of the system will require the use one manager, two engineers, 4 technicians, 24 laborers (8 in each shift), and 4 clerks. Assuming that the annual salary (including fringe benefits) for the manager is $150,000, for each engineer is $120,000, for each technician is $100,000, for each laborer is $80,000, and for each clerk is $60,000, the total annual cost of salary for the 10 MTY system is then C_s = $2.95 million.

Assuming that when the system throughput is increased to 50 MTY, the number of technicians and laborers will be doubled, whereas the number of the manager, engineers and clerks will remain the same. Thus, at 50 MTY the total cost for salaries will be $5.27. Using the salary costs estimated for these two throughputs (10 and 50 MTY) as data points, and assuming a linear relationship between salary and throughput, the following equation is derived and will be used for estimating the total salaries/wages for the system for any

throughput between 1 and 50 MTY:

$$C_s = 0.058T_h + 2.37 \quad \text{……..} \qquad \text{(IV-44)}$$

where T_h is throughput in MTY and C_s is salary cost in million dollars.

5. Property tax, C_t

The annual proper tax is assumed to be 2% of the total capital cost, namely, $C_p = 0.02\ C_c$.

6. Insurance, C_i

The annual cost of insurance is estimated at 0.5% of the total capital cost, namely, $C_i = 0.005\ C_c$.

8. Maintenance Cost, C_m

Since the salary part of the cost already included the salary for maintenance workers (technicians and laborers), the maintenance cost here is for materials only and replacement of parts. It is estimated to be 5% of the capital cost. Therefore, $C_m = 0.05\ C_c$.

9. Annual Total O/M Cost, C_o

Summing up all the individual components of the annual O/M costs yields the annual total O/M cost as follows:

$$\mathbf{C_o = C_e + 0.075C_c + 0.058T_h + 2.43} \quad \text{…….} \qquad \textbf{(IV-44)}$$

where C_e is given by Eq.IV-43, and C_c by Eq.IV-22.